Nile Decision Support Tool
River Simulation and Management

Burundi
Congo
Egypt
Eritrea
Ethiopia
Kenya
Rwanda
Sudan
Tanzania
Uganda

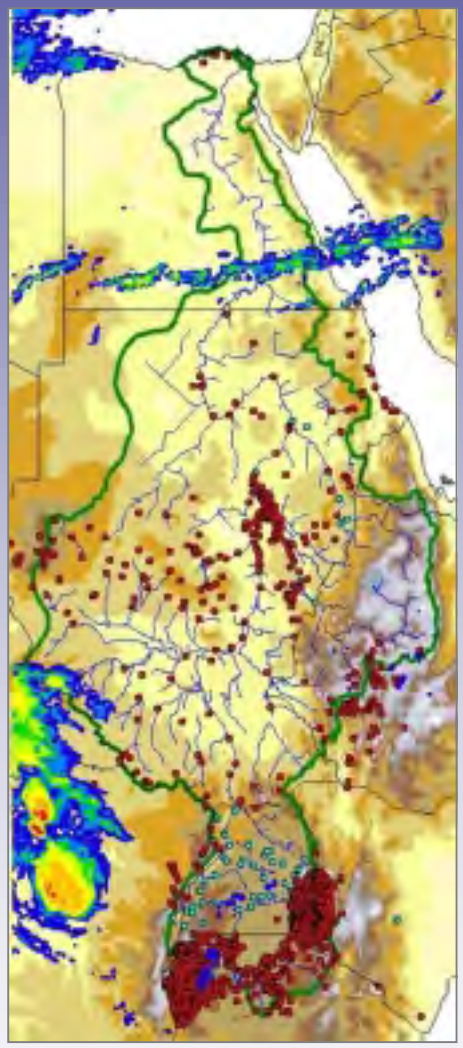

Developed collaboratively by

The Nile Basin Nations,

The Georgia Water Resources Institute at the Georgia Institute of Technology,

and

The Food and Agriculture Organization of the United Nations

June 2003

Nile Decision Support Tool (Nile DST)
River Simulation and Management

Report developed by

Huaming Yao
Senior Research Engineer

Aris Georgakakos
Project Director

Georgia Water Resources Institute
School of Civil and Environmental Engineering
Georgia Institute of Technology

In collaboration with

The Nile Basin Nations

and

The Food and Agriculture Organization (FAO)
of the United Nations
Nile Basin Water Resources Project (GCP/INT/752/ITA)

June 2003

Acknowledgements

This report and associated software were developed by the Georgia Water Resources Institute (GWRI) at the Georgia Institute of Technology as part of the Nile Basin Water Resources Project (GCP/INT/752/ITA). This project was funded by the Government of Italy and was executed for the Nile Basin nations by the Food and Agriculture Organization (FAO) of the United Nations.

The GWRI Director and project staff are grateful to the Nile Basin nations (Burundi, Congo, Egypt, Eritrea, Ethiopia, Kenya, Rwanda, Sudan, Tanzania, and Uganda), their focal point institutions, their Project Steering Committee (PSC) members, and their National Modelers for entrusting us to work with them in this important basin-wide project. The development of databases, models, technical reports, software, and user manuals are key but not the only project accomplishments. Even more important are the evolving contributions relating to people and the difference the project is poised to make in data and information sharing, developing a common knowledge base for policy debates, and long term capacity building.

GWRI is also grateful to the Government of Italy and to FAO for sponsoring this project and for providing dependable logistical and technical support through the FAO offices in Rome and Entebbe.

It is our hope that the Nile DST effort will contribute in some positive way to the historic process of the Nile Basin nations to create a sustainable and peaceful future.

Aris Georgakakos
GWRI Director
Atlanta, June 2003

Disclaimer and Copyright Notice

Table of Contents

Chapter	Page No.
1. Overview	1-1
2. System Description and Data	2-1
2.1 Nile River Hydrology Overview	2-1
2.2 System Data Summary	2-6
3. River Routing Models	3-1
3.1 The Reach from Pakwatch to Mongala	3-1
3.2 The Reach from Mongala to Malakal	3-8
3.3 The Reach from Malakal to Melut	3-16
3.4 The Reach from Melut to Mogren	3-22
3.5 The Reach from Mogren to Dongola	3-22
3.6 River Reaches on the Blue Nile and Atbara River	3-33
4. Inflow Forecasting	4-1
5. Decision Model and Reservoir Regulation Rules	5-1
5.1 System Dynamics	5-1
5.2 State Augmentation	5-9
5.3 Performance Index	5-13
5.4 Control Method	5-16
5.5 Heuristic Reservoir Regulation Rules	5-17
5.5.1 Reservoir Release-Elevation Rule	5-17
5.5.2 Reservoir Release-Elevation Rule (Simplified)	5-22
5.5.3 Target Reservoir Elevation Rule	5-23
5.5.4 Target Release Rule	5-24
5.5.5 Regional Coordination Rule	5-25
5.5.6 Customized Regulation Rules	5-26

Table of Contents Cnt'd

Chapter	Page No.
6. Scenario Assessment	6-1
6.1 Scenario Assessment Examples	6-3
7. Conclusion and Further Work	7-1
References	7-3
Appendix A: Reservoir Data	A-1
A.1 Elevation versus Storage Relationships	A-2
A.2 Rating Curves at Various Locations	A-9
Appendix B: Hydro Turbine Characteristic Curves and Hydro Power Data	B-1
B.1 Hydro Turbine Curves	B-2
B.2 Hydro Power Data	B-6
Appendix C: Statistics of Net Basin Supply and Tributary Inflows	C-1
C.1 Historical Record Periods and Annual Average Values	C-2
C.2 10-day Historical Inflow Sequences	C-3
C.3 Annual Historical Average Inflow Sequences	C-10
Appendix D: Mathematical Background	D-1
D.1 ELQG Control Method	D-2
D.2 Artificial Neural Networks	D-8
Appendix E: Operating Rules for Reservoirs in Sudan and Ethiopia	E-1

River Simulation and Management

Chapter 1

Introduction and Overview

The Nile River Basin is spread over ten countries covering an area of about 3.1 million km^2, or approximately 10 percent of the African continent. The river discharge per unit drainage area is relatively small, and almost all of the Nile water is generated from 20 percent of the basin, while the remainder is in arid or semi-arid areas. The Nile Basin encompasses five main regions (Figure 1): (**a**) the Equatorial Lake sub-basin within the countries of Uganda, Tanzania, Kenya, Rwanda, Burundi, and Congo, (**b**) the Sudd, the Bahr el Ghazal, and the Sobat River Basin (in Sudan and Ethiopia), (**c**) the White Nile (in Sudan) connecting the Sudd with the Blue Nile, (**d**) the Blue Nile and Atbara Rivers draining parts of Ethiopia, Eritrea, and Sudan, and (**e**) the Main Nile flowing through Northern Sudan and Egypt. Each region has distinct hydrologic features, water use requirements, and development opportunities.

The Nile River Simulation and Management (Nile RSM) module is a tool developed to assess the benefits and tradeoffs associated with various basin wide water development and management options. The guiding principles for the development of this module are outlined below:

- The *data of the Nile RSM should be shared and agreed upon* by the Nile Basin nations;

- The Nile RSM should be based on *sound and current scientific and engineering approaches* able to handle the Nile Basin size, natural complexity, and range of development and management options; It should also include functionalities useful for users of varying technical backgrounds and experience, from novice to advanced;

- The Nile RSM should be a *neutral* decision support tool; Thus, its overriding purpose should be to objectively assess the benefits and tradeoffs associated with various water development and sharing strategies that may interest the Nile Basin partners individually or as an interdependent community of nations;

- The Nile RSM should be *sustainable and adaptable* as future needs arise; The implications of this are twofold: First, the Nile RSM should be based on *widely supported* computational technology and should be *expandable* to incorporate new data and applications; Second, *effective technology and know-how building* mechanisms should be implemented during the Nile RSM development as well as for the long term.

The Nile RSM is designed to support regional (sub-basin) and basin-wide *planning* purposes. Its function is to process the data and quantify the response of the basins for alternative hydrologic, water use, and development/management scenarios. To this end, the Nile RSM includes models that fall under the categories of (**a**) river and reservoir simulation, (**b**) system optimization, and (**c**) scenario assessment. The model purpose, methodology, and application range are discussed in the chapters that follow.

The report is organized in seven chapters and four appendices. Chapter 2 reviews reservoir characteristics and other system data. Chapter 3 describes the forecasting models for the net basin supplies and tributary inflows. Chapter 4 takes up the development of routing models for the various river reaches from Lake Albert to the High Aswan Dam. Chapter 5 synthesizes the elements of the simulation model and incorporating it within the decision model. It also elaborates on the underlying mathematical details of the optimization scheme, as well as on simpler reservoir regulation rules. Chapter 6 discusses several applications of the decision system designed to (**1**) test its validity and (**2**) present examples of scenario investigations pertaining to the Equatorial Lake regulation, the construction of hydro power facilities in Ethiopia, and the implications of the Jonglei Canal. Lastly, Chapter 7 summarizes the conclusions and includes several recommendations for further developments. The appendices include various system characteristics and supporting mathematical material.

The Nile RSM is part of the Nile DST software package. Software usage is described in a series of separate documents.

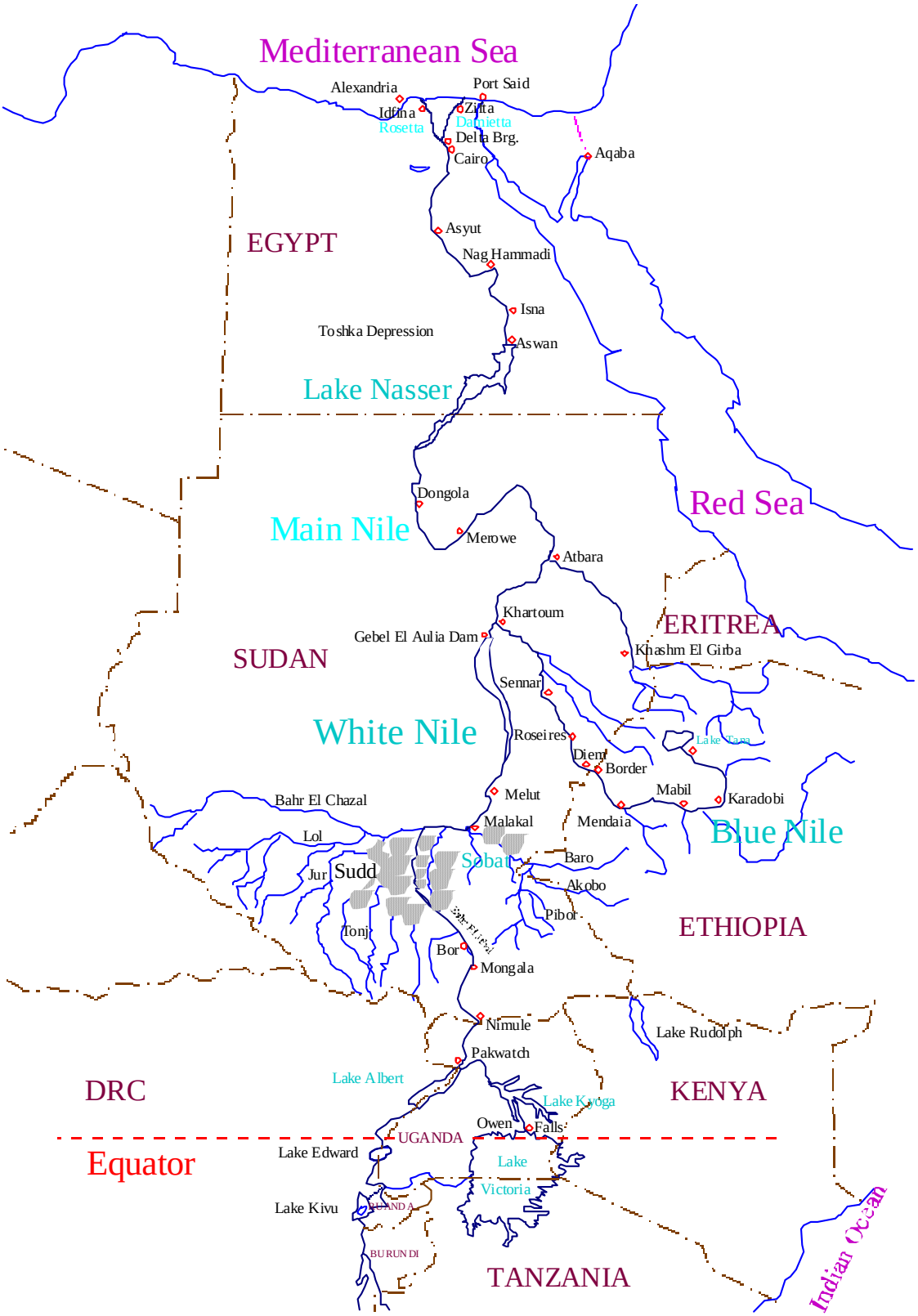

Figure 1.1: A Map of the Nile Basin

Chapter 2

System Description and Data

The purpose of this section is to provide background on the Nile river system and its water resources development and management potential. To this end, Section 2.1 provides a basin wide overview; Section 2.2 summarizes various system data and information.

2.1 Nile River Hydrology Overview

Equatorial Lake Region

The Equatorial Lake region encompasses Lakes Victoria, Kyoga, and Albert and their drainage basins. The lakes are connected through the Victoria and Kyoga Niles and form a cascade containing vast quantities of water. The combined lake storage capacity (within the historical fluctuation range) is 260 billion cubic meters (bcm), 215 bcm of which pertain to Lake Victoria. Lake Victoria has a drainage basin of about 263,000 square kilometers (including 69,000 square kilometers of lake area) and contributes almost 90% of the total equatorial lake outflow. The bi-modal rainfall pattern over the lake plateau (with a higher peak in April-May and a lesser peak in October-November) and the dampening storage effect of Lake Victoria give rise to a seasonally uniform lake outflow. Over the 1905-1977 time frame, annual lake outflow (at the exit of Lake Albert) has varied from a maximum of 64.6 bcm per year to a minimum of 10.8 bcm per year with an annual average of 28.4 bcm. However, for the last 14 years of this record (1963-1977), average lake outflow nearly doubled (to about 49 bcm per year). Lake levels and outflows continue to be considerably higher than those recorded during the first sixty years of the twentieth century.

Lake Victoria is regulated by the Owen Falls hydroelectric Dam, while Lakes Kyoga and Albert are presently unregulated. Kyoga is situated 100 kilometers downstream from Victoria and is 100 meters lower in elevation. Albert (Mobutu Sese Seco) is situated 200 kilometers downstream from Kyoga and is 410 meters lower in elevation. Notwithstanding environmental

concerns, the steep topography of the Victoria and Kyoga Niles is conducive to hydroelectric development. In addition to Owen Falls and its extension, other potential hydroelectric sites could raise the total generation capacity to 2300 MW.

Food production in the Equatorial Lake region is primarily based on rain-fed agriculture. However, the water master plans of the Equatorial Lake Nations also include large scale irrigated agricultural developments. In this regard, consumptive water use could potentially approach 5 to 10 bcm per year over the next 40 to 50 years, especially in view of a rapidly rising population.

Sudd, Bahr el Chazal, and Sobat

Exiting Lake Albert, the Nile flows north to Nimule at the Ugandan-Sudanese border. From here, it changes name from Albert Nile to Bahr el Jebel, receives the contribution of several tributaries known as Torrents, reaches Mongala, and soon thereafter enters the Sudd. Over the 1913 to 1971 time period, the flow at Mongala varied from a 64 bcm per year maximum to a 15.3 bcm per year minimum, with a 31 bcm per year average. Most of the water comes from Lake Albert with the Torrents contributing an average of 4.8 bcm per year. Much like the Sudd rainfall, the flow of the Torrents is highly seasonal occurring from May to November.

Below Mongala, the river enters the Sudd swamps, spills over its banks, and inundates the adjacent flood plains. The extent of the flooded area varies with flow, but in the 1979-1980 period it was estimated to be 30,000 square kilometers (Sutcliffe and Parks, 1999). In the Sudd, evaporation exceeds rainfall by about 1300 millimeters per year, causing most of the spilled water to evaporate. At Malakal, where the river and its bifurcations emerge from the Sudd, only half of the Mongala flow remains. Specifically, over the 1913-1971 time period, the flow at Malakal averaged 15.2 bcm per year. The percent reduction of the flow increases in wet years and decreases in dry years. From 1963 to 1971 the average annual flow at Mongala was 55.02 bcm, while the flow at Malakal was 21.4 bcm, representing a 61% reduction.

The seasonal cycle of wetland flooding and drying is a key element of the ecology and the

economy of the Sudd. Howell et al. (1988) and Sutcliffe and Parks (1999) explain that the swamps are either permanent wetland areas (i.e., wetlands that remain flooded throughout the year) or seasonal wetland areas (i.e., wetlands that are flooded during the rainy season and uncovered during the dry season, from December to April). Seasonal swamps are most valuable to the local economy as they support cattle grazing during the dry season. In 1979-1980 nearly half of the wetlands were seasonal swamps. Permanent wetland areas are habitats of a rich diversity of plant and animal life.

The Jonglei Canal was first proposed (Garstin, 1904) as a water conservation project to reduce evaporation in the Sudd and augment the Nile flow. In Phase II of the project, the Canal would divert up to 43 million cubic meters per day from Bahr el Jebel at Bor, before significant over bank spillage would occur, by-pass the swamps, and discharge into the Sobat River immediately before its junction with the White Nile. From a water conservation standpoint, the canal benefit would depend on its operating rule (partitioning the flow between the Bahr el Jebel and Jonglei) as well as on the flow regulation exercised by Lake Albert. From the standpoint of the local population, the canal should support and enhance Sudd's cattle grazing potential.

The Bahr el Ghazal and its tributaries (Bahr el Arab, Lol, Jur, Tonj and others) drain an area of more than 500,000 square kilometers. As in the Sudd, rainfall over the basin occurs between March and October and generates seasonal runoff (June to November) averaging 11 to 14 bcm per year. Over bank spillage occurs extensively in the basin over a variable wetland area ranging from 4,000 to 17,000 square kilometers (Sutcliffe and Parks, 1999). Wetland evaporation is so significant that when the river joins Bahr el Jebel at Lake No, its flow contribution is minimal (0.4 bcm per year).

Water conservation projects have also been proposed for the Bahr el Ghazal river basin. The potential water benefits from these projects are estimated at 5 to 8 bcm per year (UNDP, 1981, Fahmy and Fahmy, 1981), but these estimates are based on insufficient data. As in the Sudd, the seasonal wetlands of the Bahr el Ghazal enable cattle grazing during the dry season and are

crucial for the survival of the local population.

Below Lake No, the river is known as the White Nile and flows eastward until it joins the Sobat River, a few kilometers upstream of Malakal. Sobat's main tributaries, Baro, Akobo, and Pibor, drain portions of Ethiopia and southern Sudan, and contribute an average of 13.7 bcm per year (as estimated by the 1913 to 1971 flow record) to the White Nile. Sobat's rainfall is seasonal from April to October and so is its streamflow (from June to November). Before joining Pibor, Baro spills an average of 2.8 bcm per year to the adjacent Machar Marshes (Jonglei Investigation Team, 1954). Water conservation projects have been proposed to minimize spillage and augment the flow of the White Nile. However, the impacts of the conservation projects for the local population are not fully understood.

White Nile

From Malakal, the White Nile flows north toward Khartoum, a distance of approximately 840 kilometers, on a very mild channel slope with no significant additions to flow. The Gebel el Aulia Dam dominates this part of the basin. The dam is located 40 kilometers upstream of the confluence with the Blue Nile, but its backwater effects (on river stage and flow) extend 600 kilometers upstream to Melut. The reservoir has a storage capacity of 3.5 bcm and its principal purpose is to raise the river stage and facilitate the pumping of irrigation water. Evaporation losses are estimated at 3.5 bcm per year, and current irrigation withdrawals amount to 1.5 bcm per year. Significant backwater effects occurred even before the construction of the Gebel el Aulia Dam, especially during the Blue Nile flood season. During such times, surface debris has been seen to float down the Blue and up the White Nile for several kilometers (Hurst, 1950). Because of this peculiar river response, evaporation losses cannot be fully avoided by modifying the reservoir operating rules. An estimated lower limit for the evaporation losses is 1.7 to 2 bcm per year.

Blue Nile and Atbara

The Blue Nile originates from Lake Tana far up in the Ethiopian highlands and spirals down

toward Sudan in deep gorges. The distance from Lake Tana to the Ethiopian-Sudanese border (Diem) is 900 river-kilometers, and the elevation drop is nearly 1300 meters. At the border, the river enters the Sudanese plains and flows toward Khartoum for another 700 kilometers of mildly sloped terrain. The climate of the Ethiopian plateau is influenced by the migration of the Inter-tropical Convergence Zone (ITCZ) which produces heavy rains from June to September and dry conditions for the rest of the year. As a result, the Blue Nile is highly seasonal with most flow occurring from July to October. At Diem the river averages 50 bcm per year, but during exceptionally wet or dry years, it may exceed 70 bcm or fall below 30 bcm per year. Below Diem, Dinder and Rahad add another 4 bcm to the annual flow, but reservoir evaporation and channel conveyance losses detract 2.5 to 3 bcm.

With the exception of two relatively small Sudanese reservoirs (Roseires and Sennar) and a hydroelectric weir below Lake Tana, no other regulation projects exist along the Blue Nile. However, the topography of the basin in Ethiopia can support a series of major hydroelectric and storage projects (U.S. Bureau of Reclamation Study, 1964). The characteristics of these projects (i.e., Lake Tana, Karadobi, Mabil, Mendaia, and Border) and those of Roseires and Sennar are summarized later in this Chapter. Full hydropower development in Ethiopia could create 62 bcm of combined reservoir storage and 5700 MW of hydroelectric power capacity. The benefits and implications of such projects are important for Ethiopia and all Nile Basin Nations.

Presently, large scale irrigation takes place only in Sudan below Sennar (at the Managil and Gezira irrigation developments) using an estimated 15.3 bcm of water per year. In fact, the primary purpose of Roseires and Sennar is to secure and divert this quantity to the irrigation areas. By contrast, food production in Ethiopia relies mainly on rain-fed agriculture. However, significant expansion of irrigated lands is possible in both countries, and extensive water withdrawals could develop in the near future.

The last tributary of the Nile is the Atbara River which drains parts of Ethiopia (north of Lake Tana), Eritrea, and Sudan. Atbara contributes an average flow of 12 bcm per year in a highly

seasonal pattern similar to that of the Blue Nile. The river provides water for irrigation (at 1.5 bcm annually) and energy generation through the Khashm el Girba reservoir.

Main Nile

The Main Nile encompasses the reaches from Khartoum to Wadi Halfa (1500 kilometers), Lake Nasser (400 kilometers), and the Egyptian Nile from Aswan to the Mediterrannean Sea (1200 kilometers). In this part of the basin, rainfall is minimal and evaporation losses are high. The reach from Khartoum to Wadi Halfa averages 2.5 bcm of water losses per year, while the evaporation losses at Lake Nasser are estimated at 10 bcm per year. The average inflow to Lake Nasser is 84 bcm per year, but in this century, actual inflow has varied from a 125 bcm per year high to a 40 bcm per year low. The marked inflow variability underscores the importance of Lake Nasser as an over year storage reservoir. The 106 bcm of active lake storage (between 147 and 178 meters) provides much-needed security against severe droughts. When water levels exceed 178 meters, the Toshka spillway diverts water to the desert to avoid downstream flooding and channel erosion.

The old Aswan Dam is located six kilometers downstream of the High Aswan Dam and provides diurnal flow regulation. The power stations of the two dams have a combined power capacity of 2721 MW. At present, Egypt uses 55.5 bcm of water per year, primarily for irrigation. The water is delivered to farms through an elaborate network of irrigation canals. However, as with all Nile Basin Nations, water demands continue to rise.

2.2 System Data Summary

The Nile River Simulation and Management (Nile RSM) Module includes several existing and planned reservoirs across the Nile basin. Table 2.1 lists the elevation range and active storages (billion cubic meters, bcm) for all reservoirs currently in the system. Most reservoirs have hydroelectric generation units, the number and capacities of which are shown on Table 2.2.

Table 2.1: Reservoir Elevation Ranges and Active Storages

Reservoir	Min Level (m)	Max Level (m)	Active Storage (bcm)
Victoria	1133.08	1136.28	215.55
Kyoga	1030.31	1034.11	14.91
Albert	618.75	623.97	29.86
Gebel el Aulia	372	377	3.35
Tana	1783.8	1787.57	11.50
Karadobi	1041	1156	29.93
Mabil	837.8	910.6	10.96
Mendaia	724.81	743.6	5.37
Border	563.43	575	4.47
Roseires	467	481	2.66
Sennar	415	421.7	0.76
Khasm el Girba	450	473	1.25
High Aswan Dam	147	178	105.96

Table 2.2: Hydroelectric Plant Generation Capacities

Reservoir	Number of Units	Total Capacity (MW)
Victoria	10+5	410
Kyoga	0	0
Albert	0	0
Gebel elAulia	0	0
Tana	4	100
Karadobi	12	1356
Mabil	12	1200
Mendaia	12	1620
Border	14	1400
Roseires	7	250
Sennar	2	15
Khasm el Girba	5	13
HAD/OAD	12+13	2721

Other reservoir data, including elevation versus storage curves and hydro turbine characteristics are included in Appendices A and B.

Inflows are key inputs to the hydro system. The available common period of the historical records is from 1912 to 1977. Table 2.3 reports the monthly inflow means in mcm/day; the associated standard deviations are included in Table 2.4. The annual inflows at all locations are plotted in Figure 2.1. Other inflow statistics and graphs of 10-day inflow sequences are included in Appendix C.

Table 2.3: Historical Monthly Mean Inflows (mcm/day)

	Jan	Feb	Mar	Apr	May	Jun	Jul	Aug	Sep	Oct	Nov	Dec
Victoria	27.92	77.26	174.71	403.53	283.03	-54.41	-142.95	-74.67	-48.64	3.68	122.67	124.50
Kyoga	-15.57	-14.33	-8.68	3.30	7.63	0.67	1.66	4.59	7.10	5.12	-2.17	-8.14
Albert	-9.33	-9.48	-3.07	12.68	18.07	7.24	11.71	21.28	21.38	23.98	24.31	3.47

Torrents	0.89	0.58	1.09	5.40	15.28	13.85	18.55	30.08	29.93	23.62	13.82	4.52
Sobat	30.96	14.41	8.82	8.08	13.30	28.58	41.57	51.32	59.13	64.31	65.86	55.51
Tana	2.40	1.65	1.25	1.03	1.60	4.54	17.37	41.39	34.58	18.21	7.40	3.92
Karadobi	8.91	6.14	4.66	3.84	5.94	16.90	64.57	153.89	128.59	67.72	27.52	14.57
Mabil	5.06	3.48	2.64	2.18	3.37	9.59	36.64	87.31	72.96	38.42	15.61	8.27
Mendaia	7.69	5.30	4.02	3.31	5.13	14.59	55.75	132.86	111.02	58.46	23.76	12.58
Border	4.90	3.38	2.56	2.11	3.27	9.30	35.54	84.71	70.78	37.27	15.15	8.02
Dinder	0.00	0.00	0.00	0.00	0.00	0.00	10.74	33.48	36.25	12.94	1.82	0.36
Rahad	0.00	0.00	0.00	0.00	0.00	0.00	3.19	10.86	12.73	7.77	0.94	0.07
Khashm Girba	0.62	0.23	0.03	0.11	0.23	2.29	52.18	179.20	114.85	26.11	5.67	1.82

Table 2.4: Historical Monthly Inflow Standard Deviations

	Jan	Feb	Mar	Apr	May	Jun	Jul	Aug	Sep	Oct	Nov	Dec
Victoria	143.88	135.18	157.14	189.49	171.18	129.69	106.92	88.80	102.86	87.47	220.54	183.85
Kyoga	11.69	10.36	9.19	12.91	16.32	16.14	11.83	11.77	20.07	21.63	24.43	21.43
Albert	10.40	11.85	14.41	15.10	15.43	14.31	11.19	13.58	18.02	20.21	24.79	14.94
Torrents	1.64	1.03	1.53	5.99	12.03	10.90	10.78	16.18	20.40	18.83	13.76	7.09
Sobat	23.92	14.55	10.44	6.70	7.71	7.91	5.81	5.17	5.88	6.68	9.71	19.20
Tana	0.78	0.74	0.74	0.61	1.18	2.03	8.92	8.67	9.78	8.31	2.68	1.23
Karadobi	2.90	2.75	2.74	2.26	4.38	7.55	33.17	32.25	36.35	30.90	9.95	4.56
Mabil	1.65	1.56	1.56	1.28	2.49	4.29	18.82	18.30	20.62	17.53	5.64	2.58
Mendaia	2.50	2.38	2.37	1.95	3.79	6.52	28.64	27.85	31.38	26.68	8.59	3.93
Border	1.60	1.51	1.51	1.24	2.41	4.16	18.26	17.75	20.01	17.01	5.48	2.51
Dinder	0.00	0.00	0.00	0.00	0.00	0.00	8.24	12.70	14.36	11.78	1.90	0.47
Rahad	0.00	0.00	0.00	0.00	0.00	0.00	2.82	3.01	3.07	5.51	1.11	0.14
Girba	1.14	0.87	0.14	0.73	1.18	5.32	40.27	70.03	66.79	18.62	4.37	1.65

Table 2.5 lists the net evaporation rates of the other reservoirs used in this study. For the Equatorial Lakes, the net basin supplies incorporate rainfall and evaporation losses; therefore, net evaporation rates are zero.

Table 2.5: 10-day Net Evaporation Rate (mm/day)

10-day	Gebel Aulia	Tana	Karadobi	Mabil	Mendaia	Border	Roseires	Sennar	Girba	HAD
1	5.60	4.32	4.32	4.32	4.32	4.32	5.60	5.60	4.90	5.75
2	5.60	4.32	4.32	4.32	4.32	4.32	5.60	5.60	4.90	5.75
3	5.60	4.32	4.32	4.32	4.32	4.32	5.60	5.60	4.90	5.75
4	6.40	4.64	4.64	4.64	4.64	4.64	7.30	7.30	5.60	4.92
5	6.40	4.64	4.64	4.64	4.64	4.64	7.30	7.30	5.60	4.92
6	6.40	4.64	4.64	4.64	4.64	4.64	7.30	7.30	5.60	4.92
7	7.10	3.19	3.19	3.19	3.19	3.19	7.80	7.80	6.37	3.40

8	7.10	3.19	3.19	3.19	3.19	3.19	7.80	7.80	6.37	3.40
9	7.10	3.19	3.19	3.19	3.19	3.19	7.80	7.80	6.37	3.40
10	7.50	2.57	2.57	2.57	2.57	2.57	8.27	8.27	6.72	4.95
11	7.50	2.57	2.57	2.57	2.57	2.57	8.27	8.27	6.72	4.95
12	7.50	2.57	2.57	2.57	2.57	2.57	8.27	8.27	6.72	4.95
13	7.40	2.55	2.55	2.55	2.55	2.55	8.32	8.32	6.04	6.27
14	7.40	2.55	2.55	2.55	2.55	2.55	8.32	8.32	6.04	6.27
15	7.40	2.55	2.55	2.55	2.55	2.55	8.32	8.32	6.04	6.27
16	7.30	0.07	0.07	0.07	0.07	0.07	7.93	7.93	4.57	7.92
17	7.30	0.07	0.07	0.07	0.07	0.07	7.93	7.93	4.57	7.92
18	7.30	0.07	0.07	0.07	0.07	0.07	7.93	7.93	4.57	7.92
19	6.40	-4.97	-4.97	-4.97	-4.97	-4.97	4.06	4.06	-5.54	8.88
20	6.40	-4.97	-4.97	-4.97	-4.97	-4.97	4.06	4.06	-5.54	8.88
21	6.40	-4.97	-4.97	-4.97	-4.97	-4.97	4.06	4.06	-5.54	8.88
22	5.90	-5.90	-5.90	-5.90	-5.90	-5.90	2.61	2.61	-9.54	9.93
23	5.90	-5.90	-5.90	-5.90	-5.90	-5.90	2.61	2.61	-9.54	9.93
24	5.90	-5.90	-5.90	-5.90	-5.90	-5.90	2.61	2.61	-9.54	9.93
25	6.50	-1.23	-1.23	-1.23	-1.23	-1.23	5.40	5.40	-0.69	10.80
26	6.50	-1.23	-1.23	-1.23	-1.23	-1.23	5.40	5.40	-0.69	10.80
27	6.50	-1.23	-1.23	-1.23	-1.23	-1.23	5.40	5.40	-0.69	10.80
28	6.20	3.65	3.65	3.65	3.65	3.65	5.89	5.89	4.42	9.93
29	6.20	3.65	3.65	3.65	3.65	3.65	5.89	5.89	4.42	9.93
30	6.20	3.65	3.65	3.65	3.65	3.65	5.89	5.89	4.42	9.93
31	6.10	4.73	4.73	4.73	4.73	4.73	6.27	6.27	4.42	8.91
32	6.10	4.73	4.73	4.73	4.73	4.73	6.27	6.27	4.42	8.91
33	6.10	4.73	4.73	4.73	4.73	4.73	6.27	6.27	4.42	8.91
34	5.40	4.74	4.74	4.74	4.74	4.74	5.90	5.90	4.30	6.97
35	5.40	4.74	4.74	4.74	4.74	4.74	5.90	5.90	4.30	6.97
36	5.40	4.74	4.74	4.74	4.74	4.74	5.90	5.90	4.30	6.97

Irrigation withdrawals refer to water taken out of the river and lake system and not available for downstream users. Where unavailable, the seasonal evapotranspiration pattern is used to determine the 10-day distribution of annual withdrawals. This distribution is different from location to location and is an input model parameter. The withdrawal pattern is specified as a fraction of the annual volume for each 10-day period. A typical distribution for selected locations is shown in Table 2.6.

Table 2.6: Sample 10-day Water Withdrawal Distributions

10-day	Gebel Aulia	Girba	HAD	Karadobi	Malakal	Sennar	Victoria
1	0.05	0.02	0.01	0.04	0.03	0.02	0.03
2	0.04	0.02	0.01	0.04	0.03	0.02	0.03

3	0.05	0.02	0.02	0.04	0.03	0.03	0.03
4	0.04	0.01	0.02	0.04	0.03	0.02	0.03
5	0.04	0.01	0.02	0.04	0.03	0.02	0.03
6	0.03	0.01	0.02	0.04	0.02	0.02	0.02
7	0.05	0.01	0.02	0.04	0.03	0.01	0.03
8	0.04	0.01	0.02	0.04	0.03	0.01	0.03
9	0.05	0.01	0.03	0.04	0.03	0.02	0.03
10	0.00	0.01	0.03	0.04	0.03	0.00	0.03
11	0.00	0.01	0.03	0.04	0.03	0.00	0.03
12	0.00	0.01	0.03	0.04	0.03	0.00	0.03
13	0.00	0.02	0.03	0.05	0.03	0.00	0.03
14	0.00	0.02	0.03	0.05	0.03	0.00	0.03
15	0.00	0.02	0.04	0.05	0.03	0.01	0.03
16	0.00	0.04	0.04	0.00	0.03	0.02	0.03
17	0.00	0.04	0.04	0.00	0.03	0.02	0.03
18	0.00	0.04	0.04	0.00	0.03	0.02	0.03
19	0.00	0.03	0.04	0.00	0.03	0.04	0.03
20	0.00	0.03	0.04	0.00	0.03	0.04	0.03
21	0.00	0.03	0.05	0.00	0.03	0.04	0.03
22	0.00	0.04	0.04	0.00	0.03	0.05	0.03
23	0.06	0.04	0.04	0.00	0.03	0.05	0.03
24	0.05	0.05	0.04	0.00	0.03	0.05	0.03
25	0.05	0.05	0.03	0.00	0.03	0.05	0.03
26	0.04	0.05	0.03	0.00	0.03	0.05	0.03
27	0.04	0.05	0.03	0.00	0.03	0.05	0.03
28	0.05	0.04	0.02	0.04	0.03	0.05	0.03
29	0.04	0.04	0.02	0.04	0.03	0.05	0.03
30	0.05	0.05	0.02	0.04	0.03	0.06	0.03
31	0.04	0.03	0.02	0.04	0.03	0.03	0.03
32	0.04	0.03	0.02	0.04	0.03	0.03	0.03
33	0.04	0.03	0.02	0.04	0.03	0.03	0.03
34	0.05	0.03	0.02	0.04	0.03	0.03	0.03
35	0.04	0.03	0.02	0.04	0.03	0.03	0.03
36	0.02	0.03	0.02	0.04	0.03	0.03	0.03

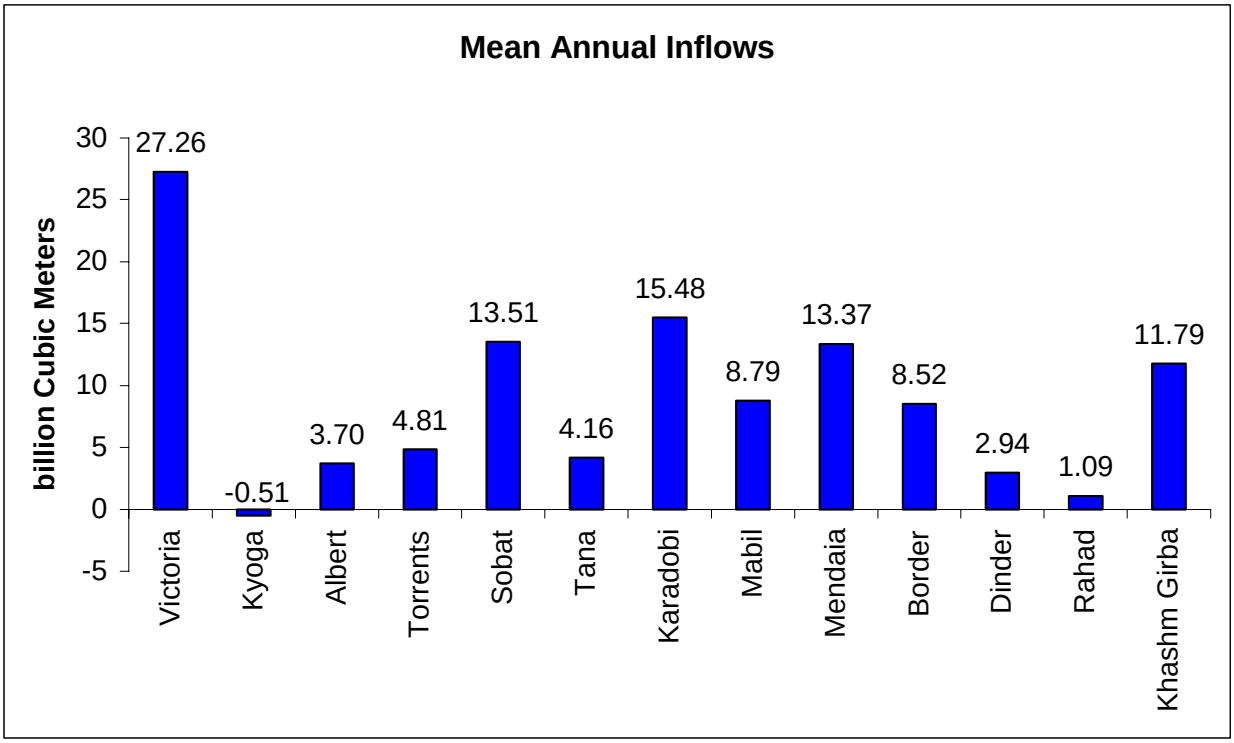

Figure 2.1: Mean Annual Inflows

Chapter 3

River Routing Models

This Chapter describes the development of river routing models for the various reaches of the White and Main Nile from Pakwatch (Lake Albert exit) to Dongola (HAD entrance). No routing models are developed for the river reaches on the Blue Nile because of the current unavailability of historical data. The models are of two types, one based on linear regression methods and another based on neural network theory. Both neural network and regression models fall in the "black box" category. Physically-based models are another alternative, but have not been considered in this work due to the long river extent and the limited availability of longitudinal and cross-sectional data. Assessment of model performance is conducted via comparisons with historical data. The routing model time resolution is 10 days.

3.1. The Reach from Pakwatch to Mongala

This reach (see Figure 1.1) receives the outflow from Lake Albert and discharges at Mongala after accepting significant contributions from several Torrents in Sudan. It is a fairly short reach, about 300 km long, with a peculiar hydrologic behavior: The outflow at Mongala is the inflow at Pakwatch augmented by the Torrent contribution during the wet season. If the flow is below 100 mcm per day, the flow at Mongala records a water gain over the combined Pakwatch-Torrent flow input; however, when the flow is high, water is lost.

The 10-day historical flows from 1958 to 1967 at Pakwatch, Torrents, and Mongala are shown in Figure 3.1. Correlation analysis indicates that the flow at Mongala depends mainly on (1) the flow at Pakwatch, (2) the flows of the Torrents during the same ten-day period, and (3) the flow of the previous 10-day period at Mongala.

A linear regression model was developed and has the following form:

$$Q_{Mngl}(k) = 0.1630749\ Q_{Pkwtch}(k) + 0.3295462\, Q_{Trnt}(k) + 0.7385824\, Q_{Mngl}(k-1) + 7.317859 + \varepsilon_1(k),$$

where $Q_{Mngl}(k)$ and $Q_{Mngl}(k-1)$ are the flows during periods k and (k-1) at Mongala, $Q_{Pkwtch}(k)$ is the flow during period k at Pakwatch, and $Q_{Trnt}(k)$ is the flow during period k from the Torrents. $\varepsilon_1(k)$ is a white random process representing model errors.

The performance of the model is evaluated by comparing the predicted with the actual values at Mongala over the historical period (Figure 3.2). The blue line represents the actual series while the red line represents model predictions. The figure shows that model predictions and actual values correspond fairly well both on the high as well as the low flows. The scatter plot of the simulated versus observed flows is shown in Figure 3.3, which indicates a very good correspondence over the full range of flow. Figure 3.4 shows the error sequence. It shows that the regression residuals are fairly uncorrelated, with a lag-1 correlation coefficient of about 0.3. The error mean is 0 (mcm/d), and the error standard deviation is 6.3 million cubic meters per day, mcm/d, which represents 5% of the mean flow value and compares favorably to the 12.24 mcm/d reported in *Panattoni et al., 1978*. The correlation coefficient between predicted and actual values is 0.99

Other regression formulations were also examined. The regression statistics are summarized in Table 3.1. The number of Pervious Periods Used in the table indicates how many terms are used in the regression as input variables for the selected parameter. For example, a value of 1 for Pakwatch indicates one term is used in the regression model, namely, the flows of the current period. Clearly, the formulation presented above provides the best fit and includes the smallest number of terms.

Table 3.1: Routing Model Statistics for the Pakwatch-Mongala Reach

Model Name	Previous Periods Used			Statistics		
	Pakwatch	Torrents	Mongala	Error Mean	Error STD	Correlation Coef.
REG100	1	0	0	0.00	22.63	0.87
REG110	1	1	0	0.00	12.09	0.96
REG101	1	0	1	0.00	7.87	0.99
REG111	**1**	**1**	**1**	**0.00**	**6.63**	**0.99**

A neural network model was also developed for comparison purposes. The neural network has a structure of three layers, one output node, three hidden nodes, and three input nodes (Figure 3.5). The first input represents the inflow at Pakwatch, the second represents the inflow from the Torrents, and the third represents the flow of the previous period at Mongala. The model provides the flow of the current 10-day period at Mongala. The network was trained using 359 historical data pairs. After 20,000 iterations the training procedure converges to its optimal parameter values representing network weights, biases, and error means and standard deviations (Table 3.2).

A detailed account of the application of neural network and regression theory to hydrologic models can be found in *Georgakakos et al., 1995b*, and will not be duplicated here. The error standard deviation is 4.86 million cubic meters per day (or 4% of the mean flow), while the error mean is 2.46 (mcm/d). The correlation coefficient between the predicted and actual values is 0.9952.

As indicated by the error statistics, both models exhibit good performance, but the regression model is much simpler, and is adopted for use within the Nile RSM.

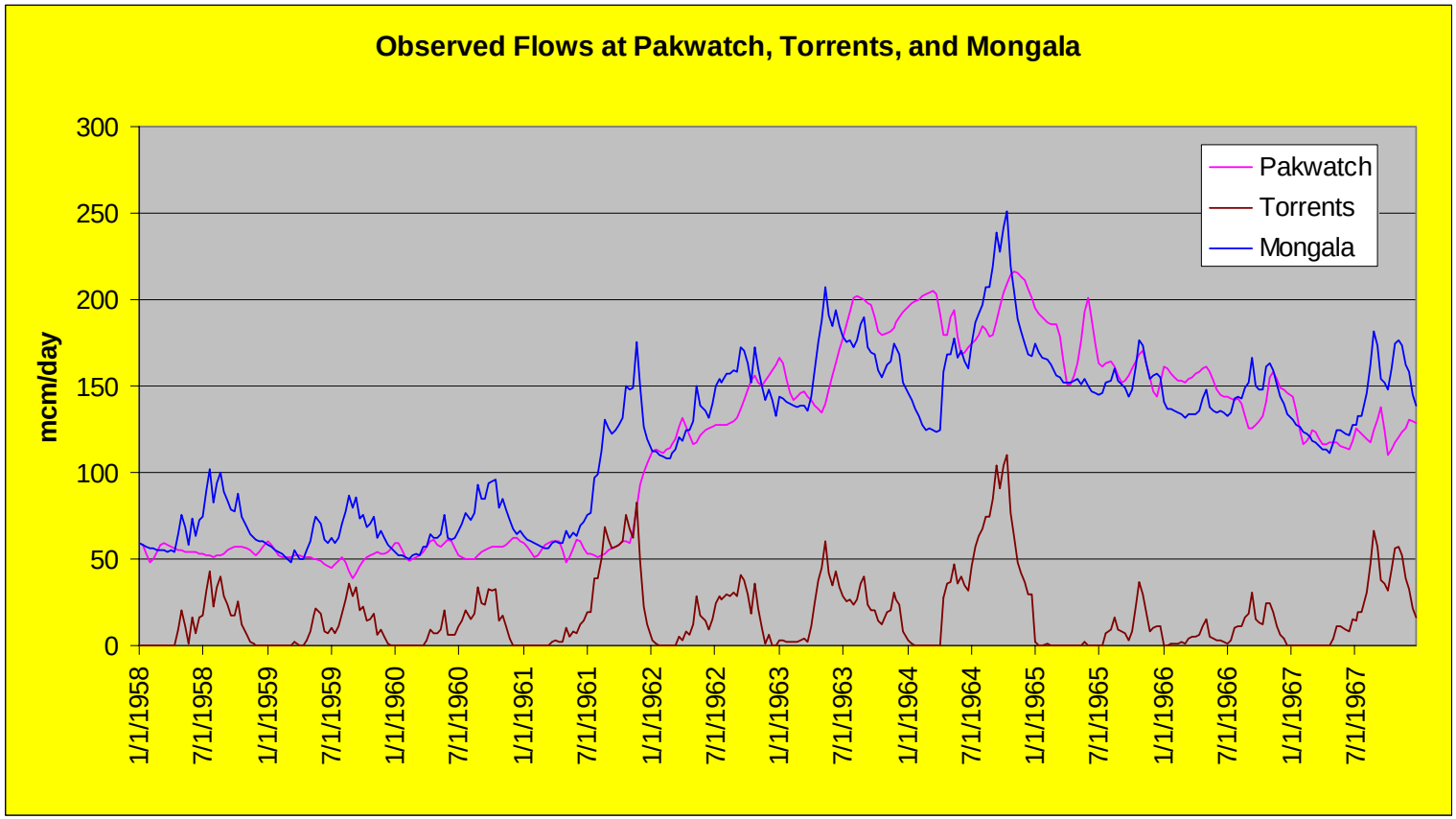

Figure 3.1: Historical Flow Sequences at Pakwatch, Torrents, and Mongala.

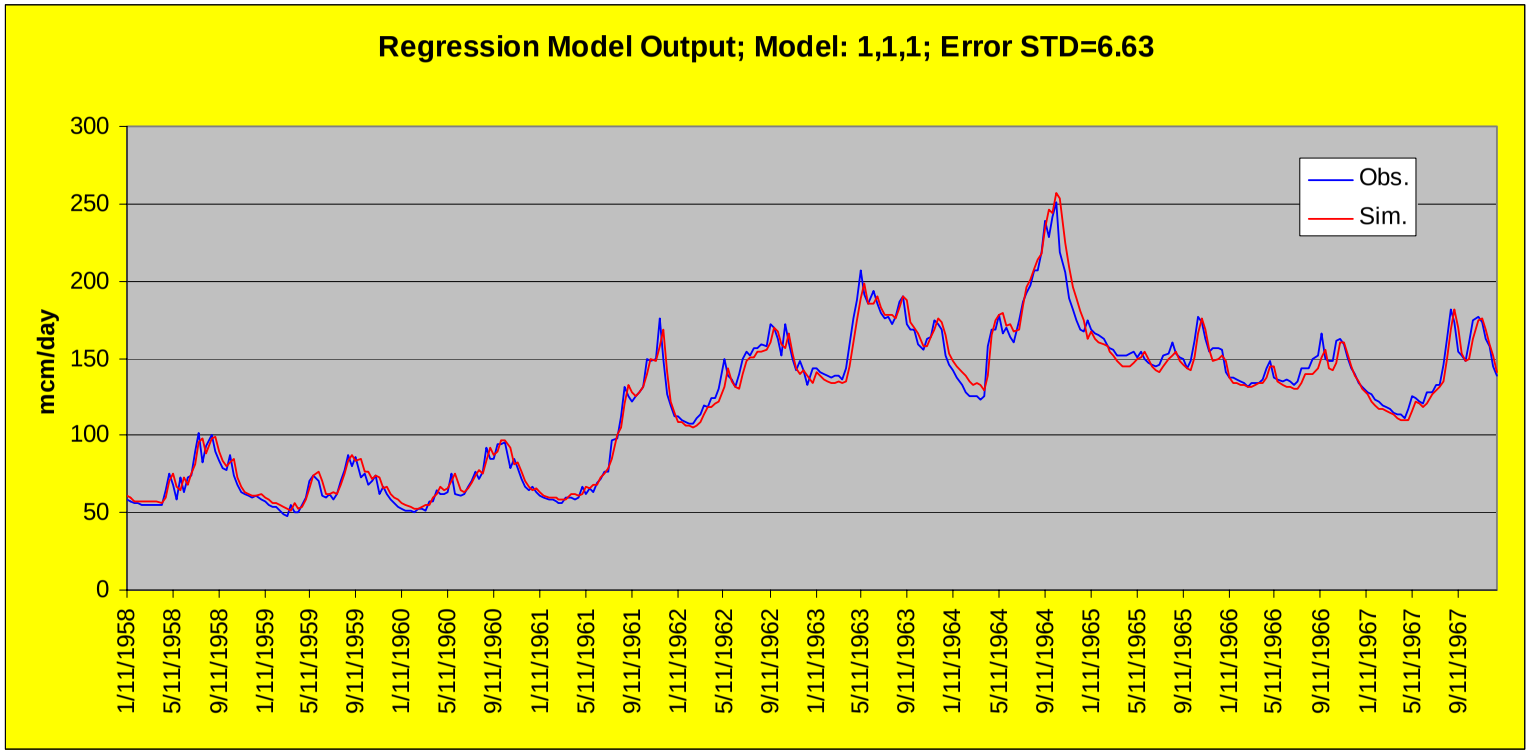

Figure 3.2: Regression Model Results

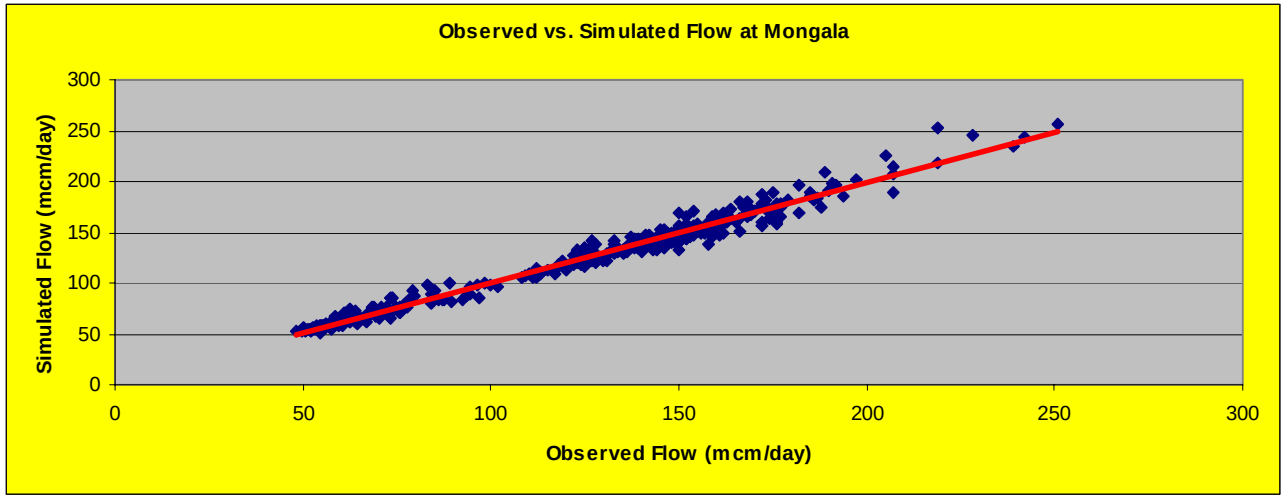

Figure 3.3: Regression Model Results for Mongala

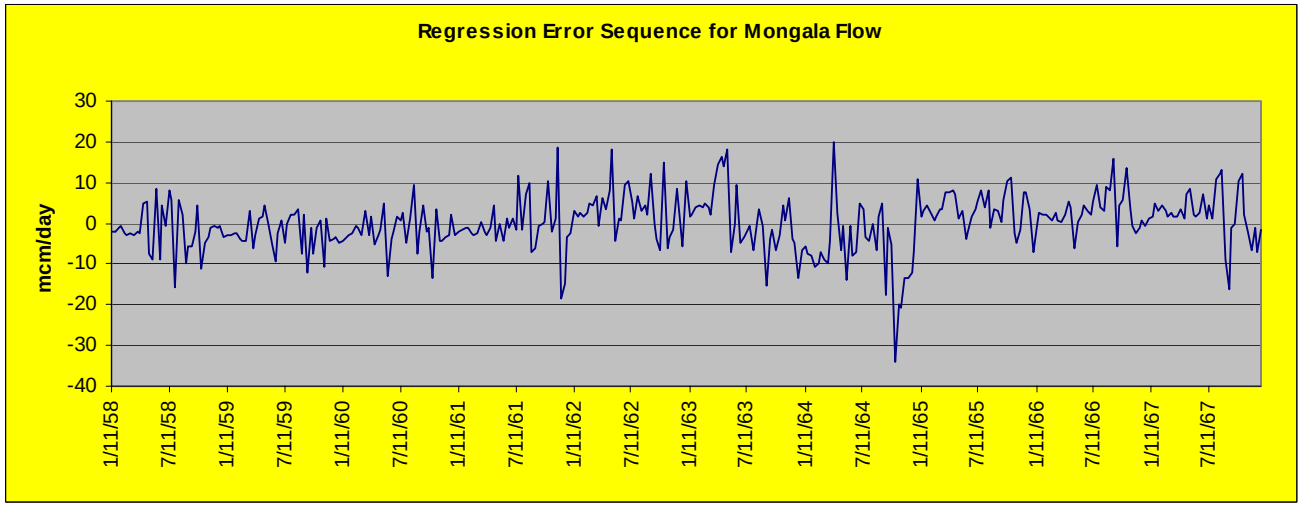

Figure 3.4: Regression Errors for Mongala Flow

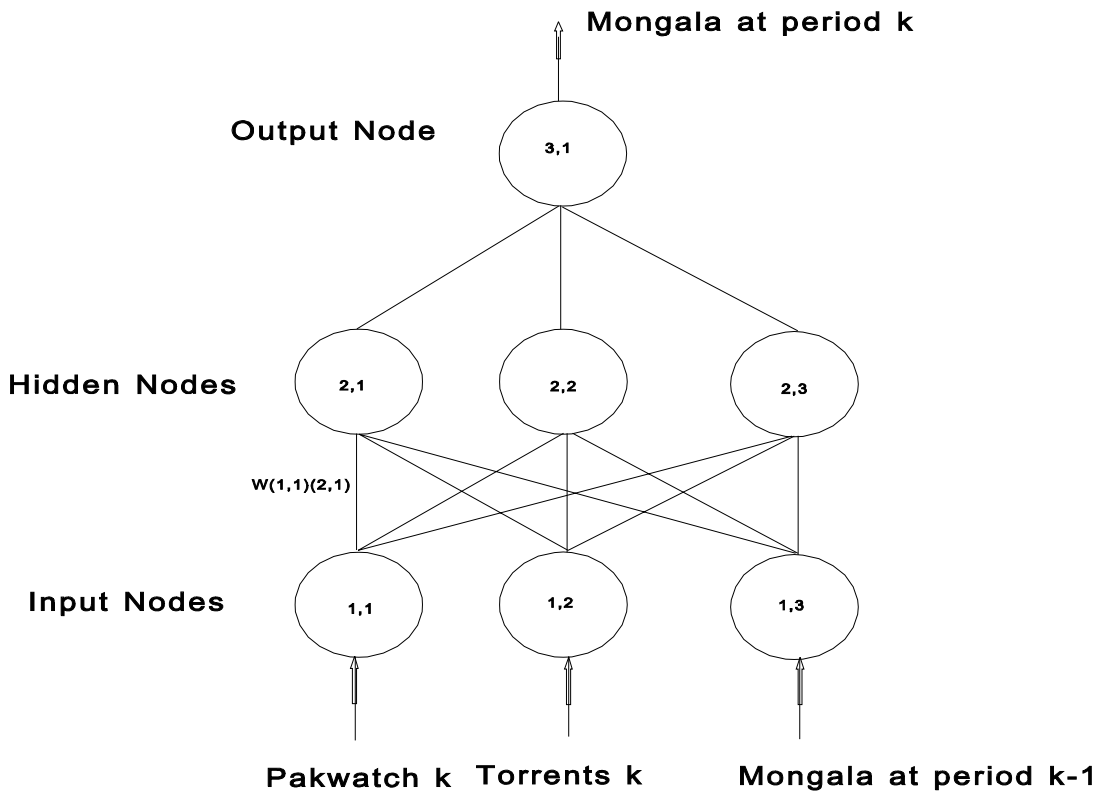

Figure 3.5: NN Structure for Mongala Flow

Table 3.2: Neural Network Parameters from Pakwatch to Mongala

Weights(W)	(2,1)	(2,2)	(2,3)	(3,1)	Bias
(1,1)	-0.690028	8.532247	2.627826		
(1,2)	6.685845	5.013562	-2.686717		
(1,3)	3.049544	-2.210577	-4.749204		
(2,1)				8.170815	-6.511251
(2,2)				1.855178	-2.365463
(2,3)				-3.804214	-0.562214
(3,1)					-0.956839

* Qmax=251.00 Qmin=0.00 B=0.05 A=0.95

3.2. The Reach from Mongala to Malakal

After Mongala, the river enters a region of very mild slopes and extensive swamps (Sudd). In this area, evaporation losses are high, especially during the rainy season when most of the river's water overflows into the surrounding wetlands. The Sobat River joins the White Nile just upstream Malakal. Following *Panattoni et al., 1978,* an essential step in the development of routing models for this reach is to represent the water losses. Then, inflow at Malakal would simply be the inflow at Mongala minus the losses plus the inflow of Sobat. This river reach is also depicted in Figure 1.1.

The contemporaneous historical ten-day flow data from 1912 to 1975 for Mongala, Sobat and Malakal are plotted in Figure 3.6. Several regression formulations were examined. The corresponding statistics are reported in Table 3.3. The model with two terms from Mongala and one term from Sudd Loss has the best statistics and is most parsimoneous. The formulation corresponding to this model is given by:

$$Q_{Lss}(k) = 0.9926\,Q_{Mngl}(k) - 0.9522\,Q_{Mngl}(k-1) + 0.9435\,Q_{Lss}(k-1) - 1.0379 + \varepsilon_2(k),$$

where $Q_{Lss}(k)$ is the water loss of period k, and $Q_{Mngl}(k)$ is the flow of period k at Mongala.

The simulated series from the regression model and the actual series are plotted on Figure 3.7. The scatter plot of the simulated versus observed flows is shown in Figure 3.8, which indicates a very good correspondence over the full range of the flow. Figure 3.9 shows the regression error sequence, which indicates that the regression error appears to be white. The lag-1 error correlation coefficient is less than 0.23. The error standard deviation is 2.08 mcm/day (or 2.3% of the Malakal flow) and a correlation coefficient (simulated versus observed) of 0.9974. By comparison, the standard error reported in *Panattoni et al., 1978,* is 6.546 mcm/day.

Table 3.3: Routing Model Statistics for Malakal Flows

Model Options	Mongala	Sud Loss	Error Mean	Error STD	Correlation Coef.
REG10	1	0	0.00	6.54	0.97
REG11	1	1	0.00	5.47	0.98
REG21	**2**	**1**	**0.00**	**2.08**	**1.00**
REG22	2	2	0.00	2.07	1.00
REG31	3	1	0.00	2.08	1.00

A significant water project proposed for this reach is the construction of the Jonglei Canal which, at the completion of its second phase, would have the capacity to pass approximately 43 mcm/day from Jonglei to Malakal. Since the decision system is to be used as a planning and assessment tool, there is a need to simulate the hydrologic regime at the Sudd after the construction of this Canal. This is a difficult task, particularly because of the limited information regarding the operation rules of the Canal and its hydraulic characteristics. It was, thus, decided to adopt the following approach. If Mongala flow is less than the natural "safe" flow level of 30 mcm/day, all flow passes through the natural channel. If there is flow in excess of 30 mcm/day, the extra water passes through the Jonglei Canal until the canal capacity is reached. If the water flow is in excess of the 73 mcm/day (natural "safe" flow threshold plus Jonglei Canal capacity), the extra flow passes again through the natural channel and is subject to the losses predicted by the previous regression equation.

As before, a neural network model (Figure 3.10) with three layers, one output node, three hidden nodes, and three input nodes is developed. The first input represents the flow of the current period k at Mongala, the second represents the inflow of the previous period k-1 at Mongala, and the third input represents the loss of the previous period k-1 at Malakal. The output is the flow loss of the current period k at Malakal.

The neural network parameters and statistics are summarized in Table 3.4. The error standard deviation is 2.046 mcm/day (again, approximately 2% of the average Malakal flow), the error mean is 0.023 mcm/day, and the correlation coefficient between estimated and actual values is 0.9973. Overall, there is a very good correspondence between the estimated and observed values.

However, in view of the comparable performance of the regression and neural network models and the fewer parameters of the regression model, it is selected as the Nile RSM routing model for this reach.

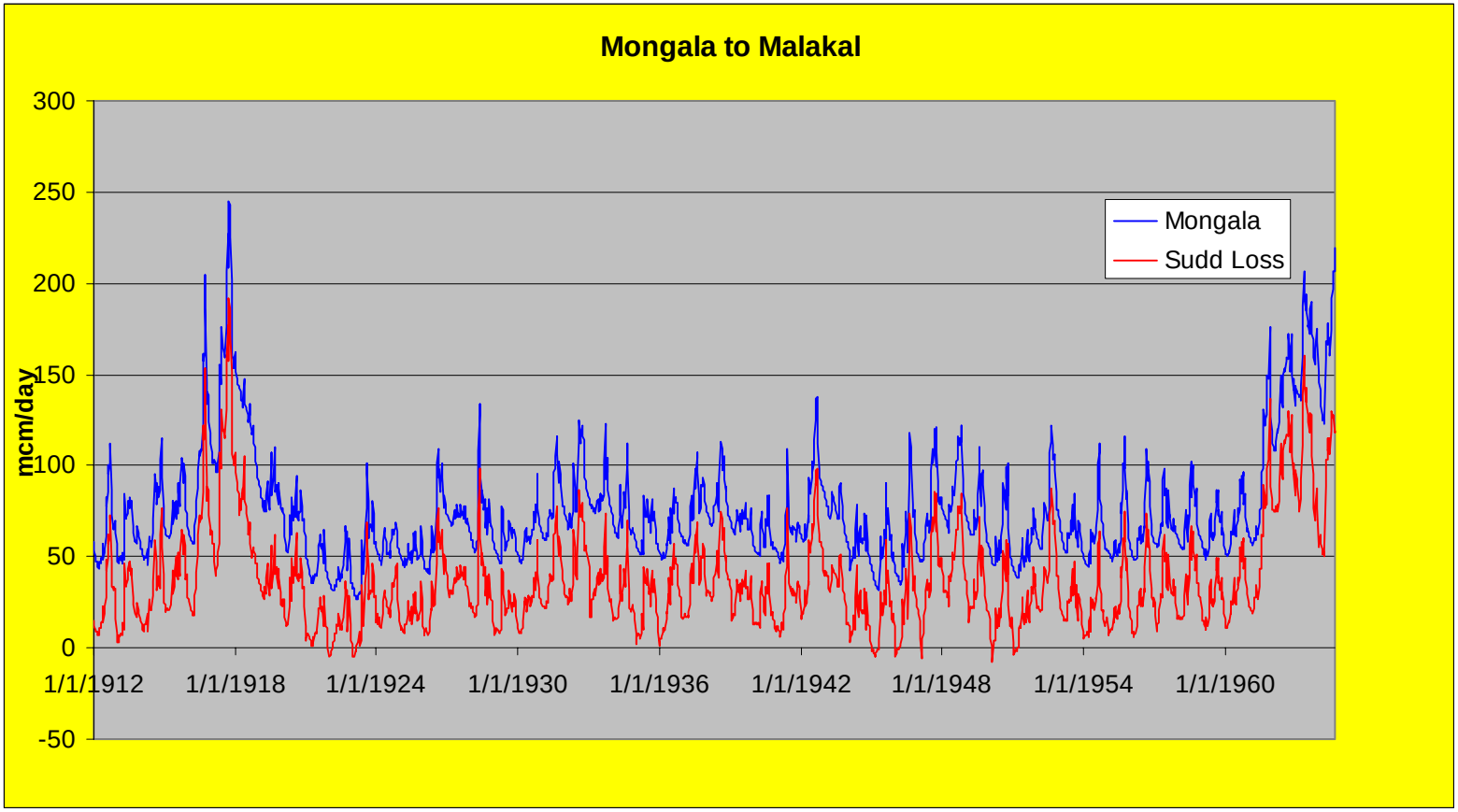

Figure 3.6: Historical Flows at Mongala

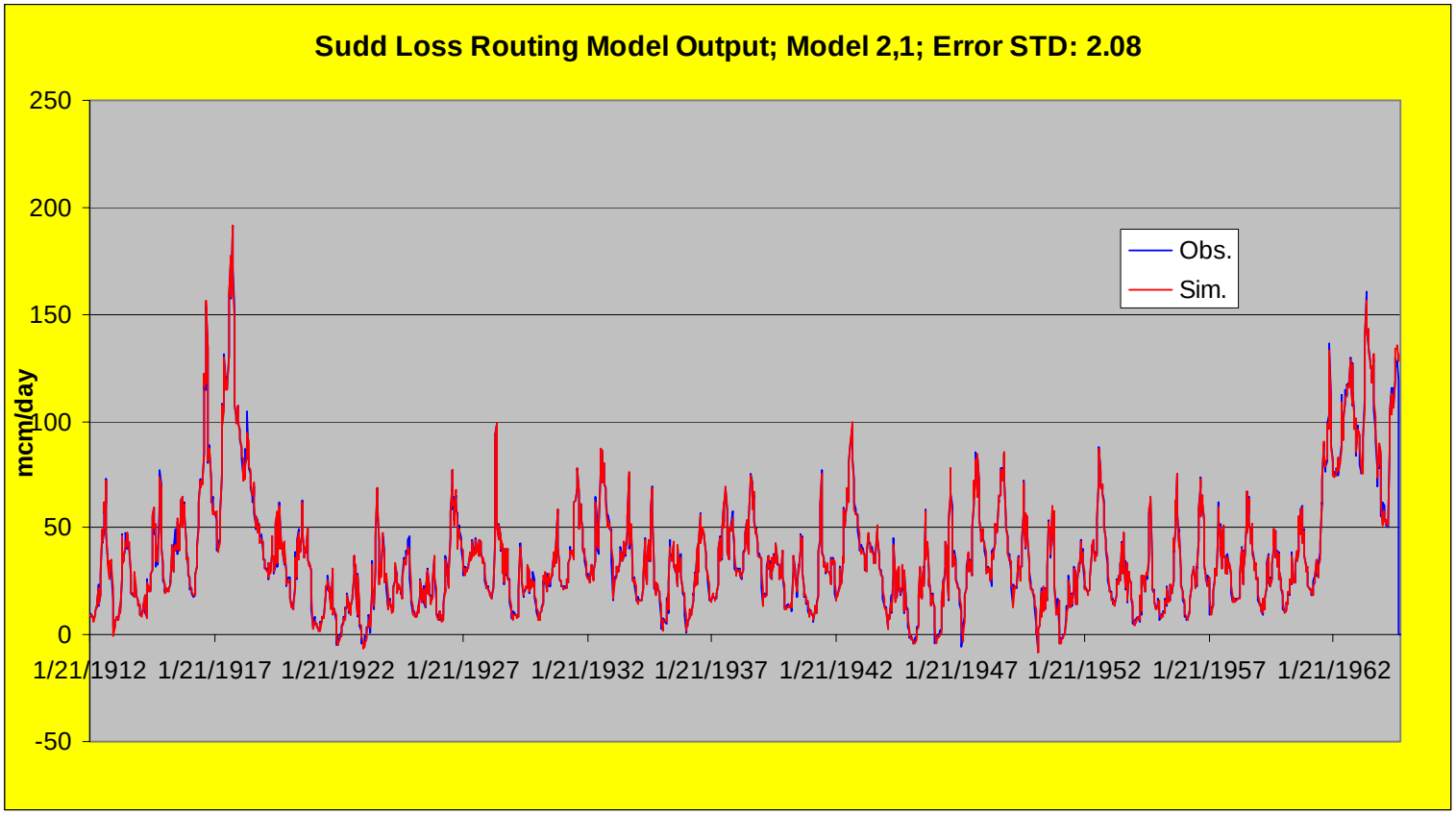

Figure 3.7: Routing Model Results

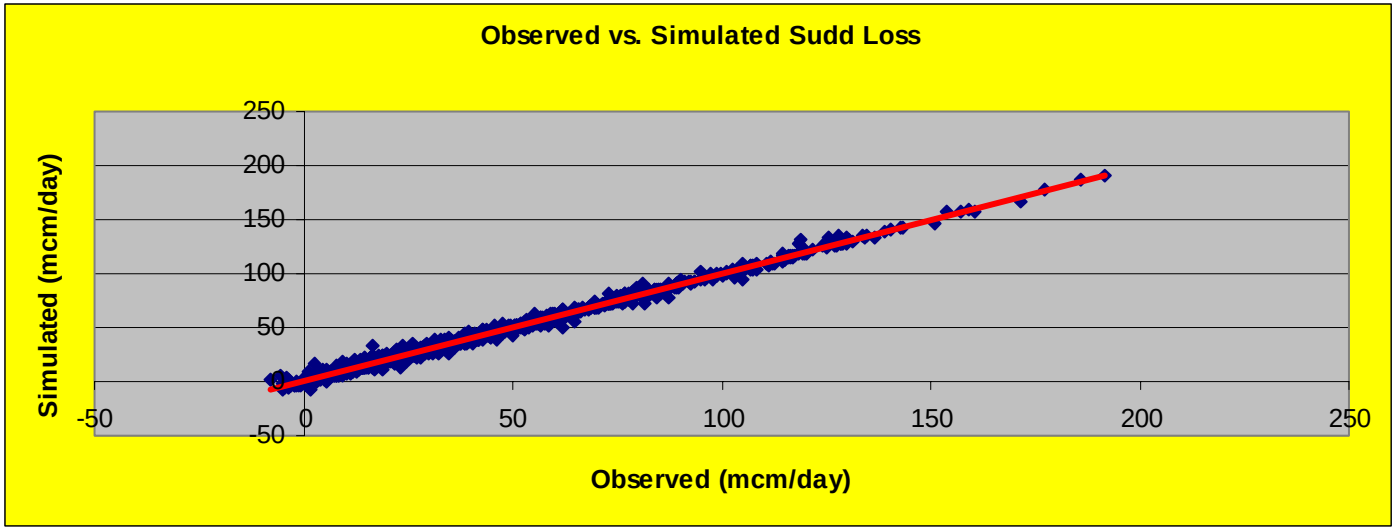

Figure 3.8: Routing Model Results for Sudd Loss

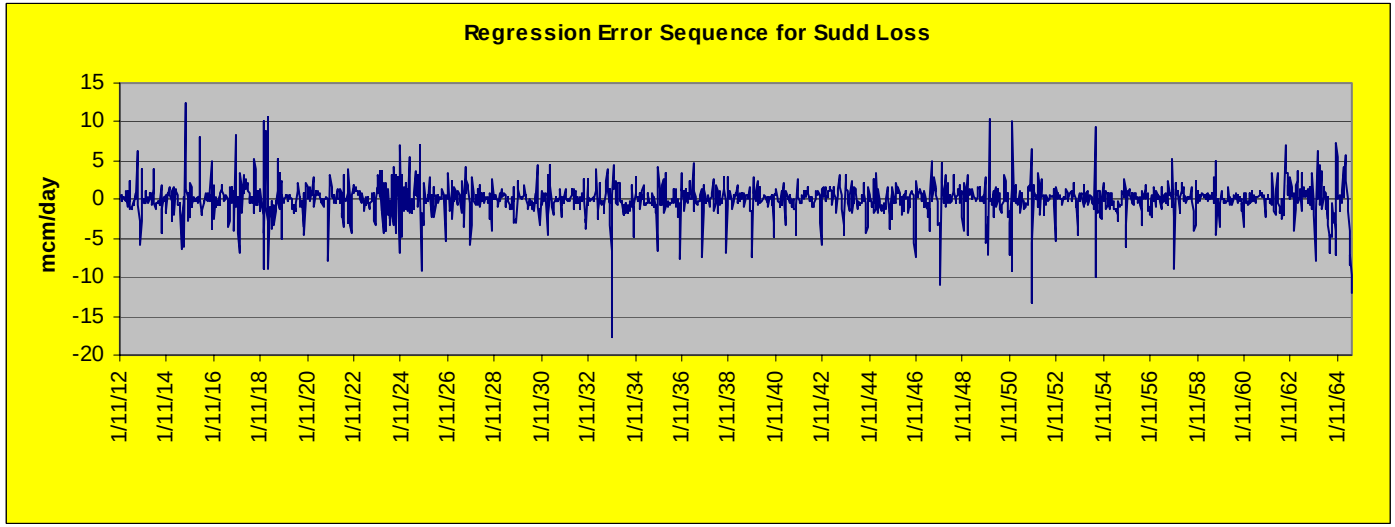

Figure 3.9: Regression Errors for Sudd Loss

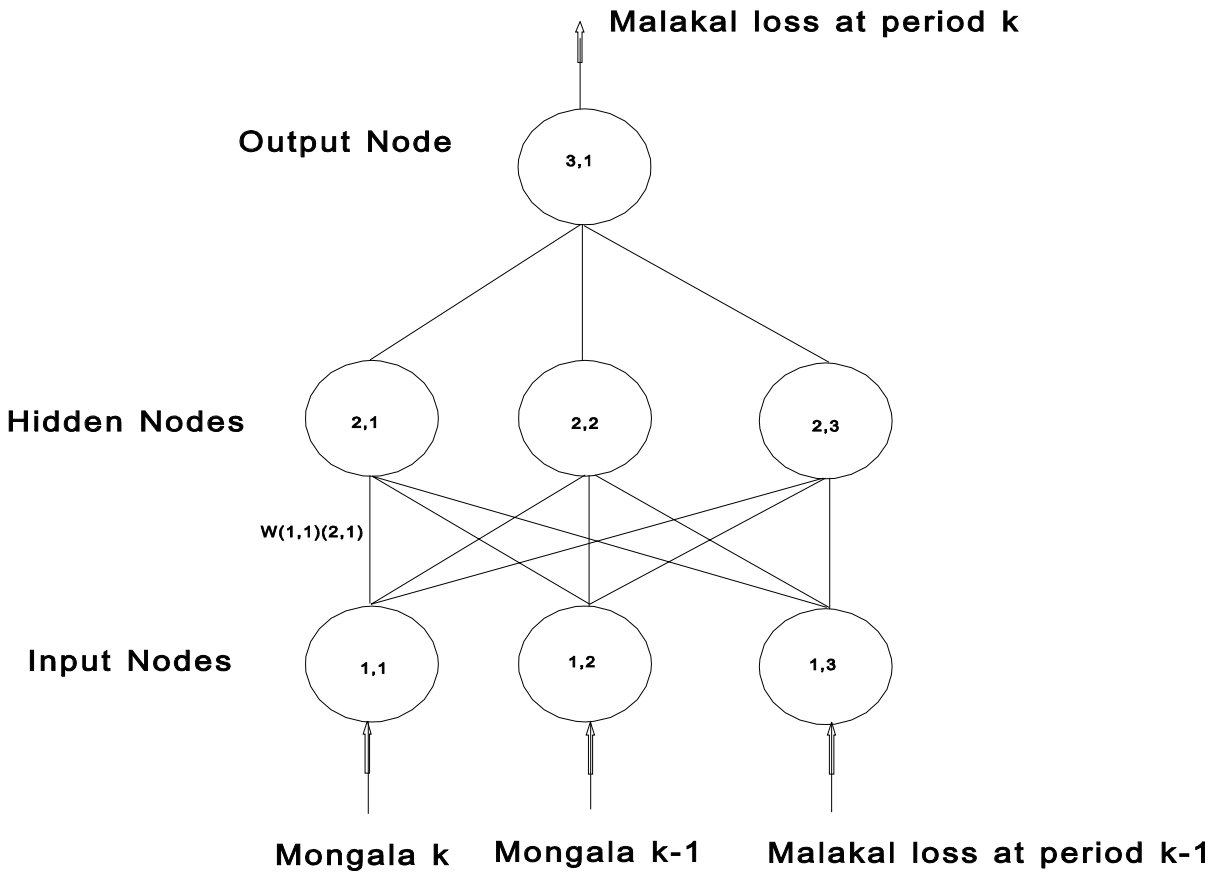

Figure 3.10: NN Structure for Sudd Loss

Table 3.4: Neural Network Parameters from Mongala to Malakal

Weights(W)	(2,1)	(2,2)	(2,3)	(3,1)	Bias
(1,1)	-3.650269	-4.511335	-8.607306		
(1,2)	2.165485	6.138326	8.283106		
(1,3)	-1.855476	-6.308887	-8.461061		
(2,1)				-3.412888	-0.270654
(2,2)				-3.365039	3.276706
(2,3)				-8.392963	-1.266964
(3,1)					2.937189

* Qmax=245.00 Qmin=-8.0 B=0.05 A=0.95

3.3. The Reach from Malakal to Melut

This is a short reach with no significant tributaries. Correlation analysis shows that the flow at Melut mainly depends on the discharge at Malakal and the flow of the previous period at Melut. The map of this river reach is shown in Figure 1.1.

The contemporaneous historical ten-day flow data from 1948 to 1977 for Malakal and Melut are plotted in Figure 3.11. Several regression formulations were examined. The corresponding statistics are reported in Table 3.5. The model with two terms from Malakal and one term from Melut exhibits good performance and has the smallest number of terms. The formulation corresponding to this model is given by:

$$Q_{Mlt}(k) = 0.7871429\, Q_{Mlkl}(k) - 0.6410149\, Q_{Mlkl}(k-1) + 0.859542\, Q_{Mlt}(k-1) - 0.4866521 + \varepsilon_3(k) ,$$

where $Q_{Mlt}(k)$ is the flow of period k at Melut, $Q_{Mlkl}(k)$ is the flow of period k at Malakal, and $\varepsilon_3(k)$ is a random error term.

The simulated series from the regression model and the actual series are plotted on Figure 3.12. The scatter plot of the simulated versus observed flows is shown in Figure 3.13, which indicates a very good correspondence over the full range of the flow. Figure 3.14 shows the regression error sequence. The lag-1 error correlation coefficient is 0.23. The error standard deviation is 2.36 mcm/day (2.6% of the average flow at Melut) and a correlation coefficient (between simulated and observed values) of 0.9974.

Table 3.5: Routing Model Statistics for Melut Flows

Model Name	Previous Periods Used			Statistics	
	Malakal	Melut	Error Mean	Error STD	Correlation Coef.
REG10	1	0	0.00	6.11	0.98
REG11	1	1	0.00	3.04	0.99
REG21	**2**	**1**	**0.00**	**2.36**	**1.00**
REG22	2	2	0.00	2.16	1.00
REG31	3	1	0.00	2.22	1.00

The neural network model is shown on Figure 3.15 and has two input, two hidden, and one output nodes. The first input represents the flow at Malakal while the second represents the flow of the previous period at Melut. The output is the flow of the current period at Melut. The network parameters weights, biases, and the mean error and its standard deviation are given in Table 3.6. The correspondence is good with an estimated error standard deviation of 2.44 mcm/day and an error mean of -0.0033 mcm/day. The correlation coefficient between the estimated and the actual values is 0.996.

In view of the comparable performance of the regression and neural network models and the fewer parameters of the regression model, it is selected as the Nile RSM routing model for this reach.

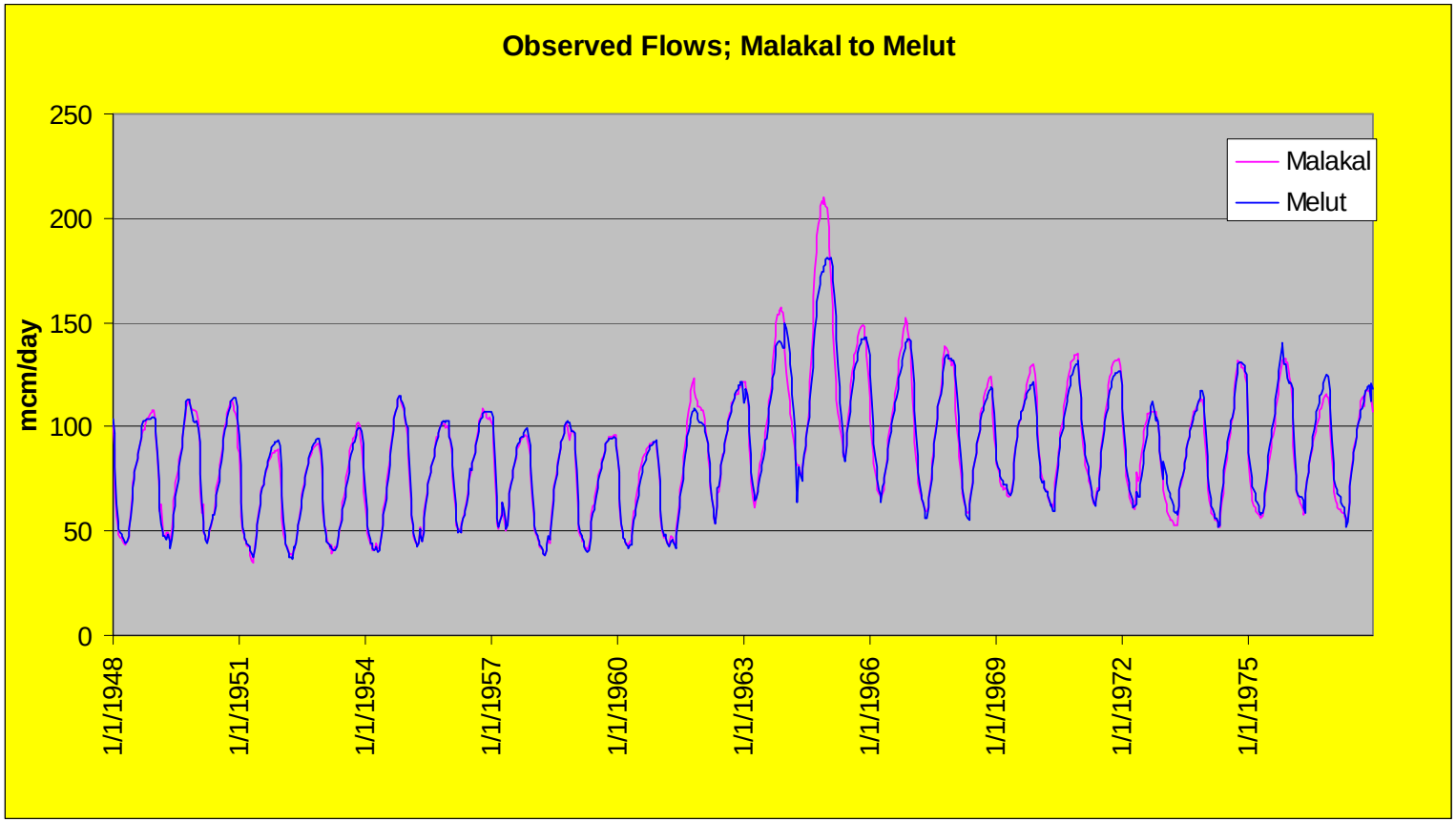

Figure 3.11: Historical Flows at Malakal and Melut

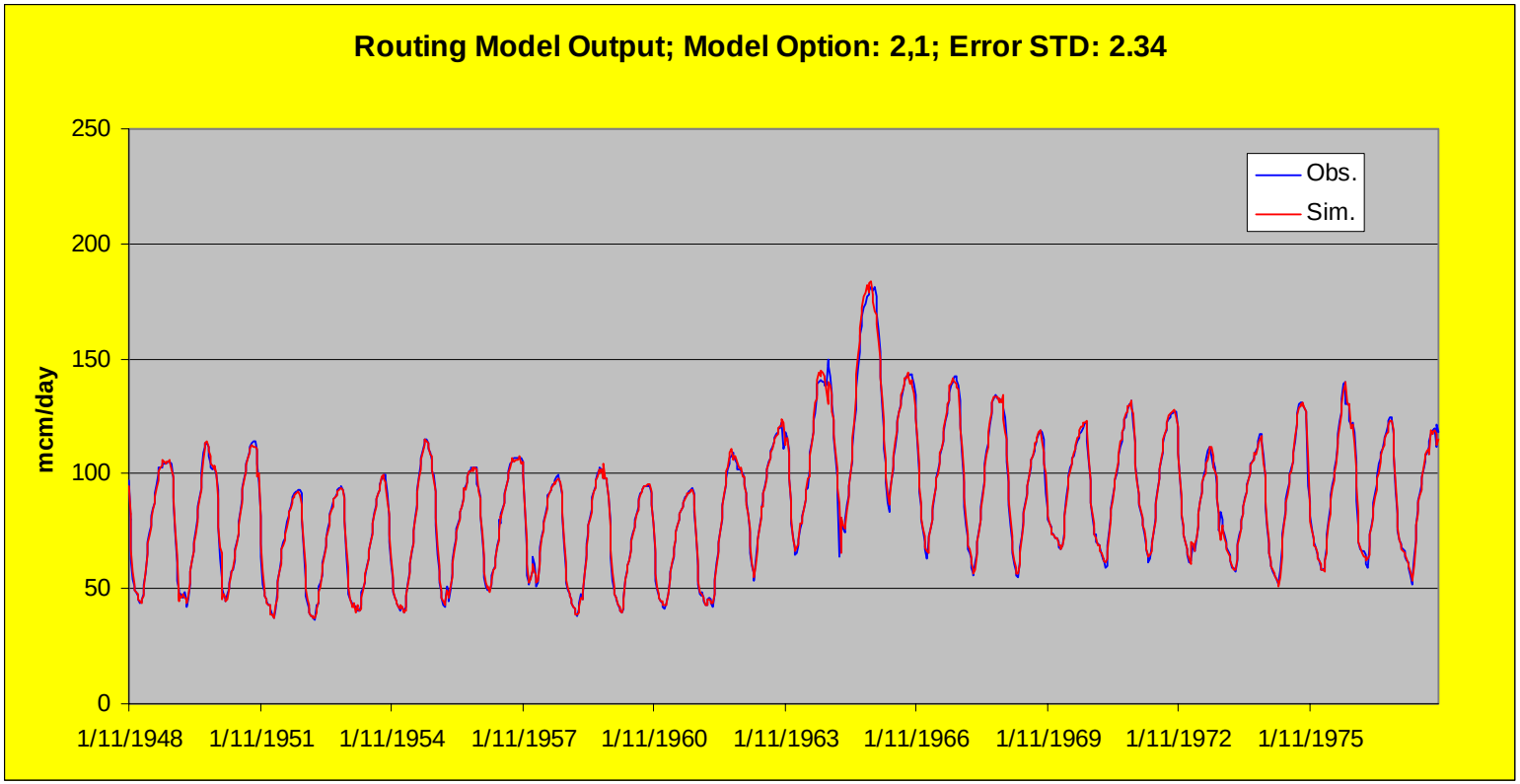

Figure 3.12: Routing Model Results

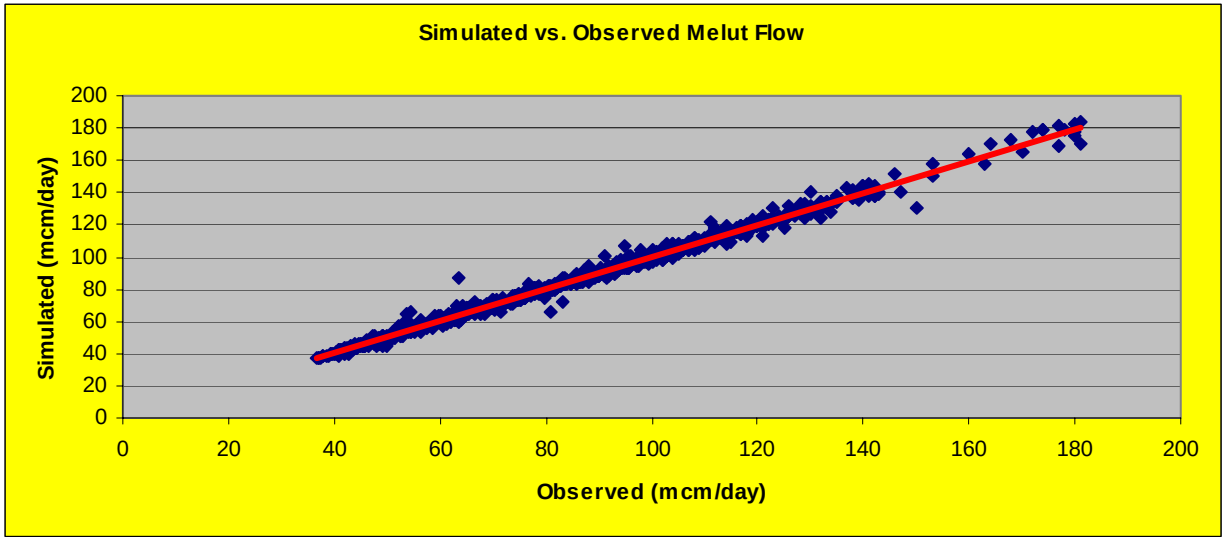

Figure 3.13: Routing Model Results for Melut

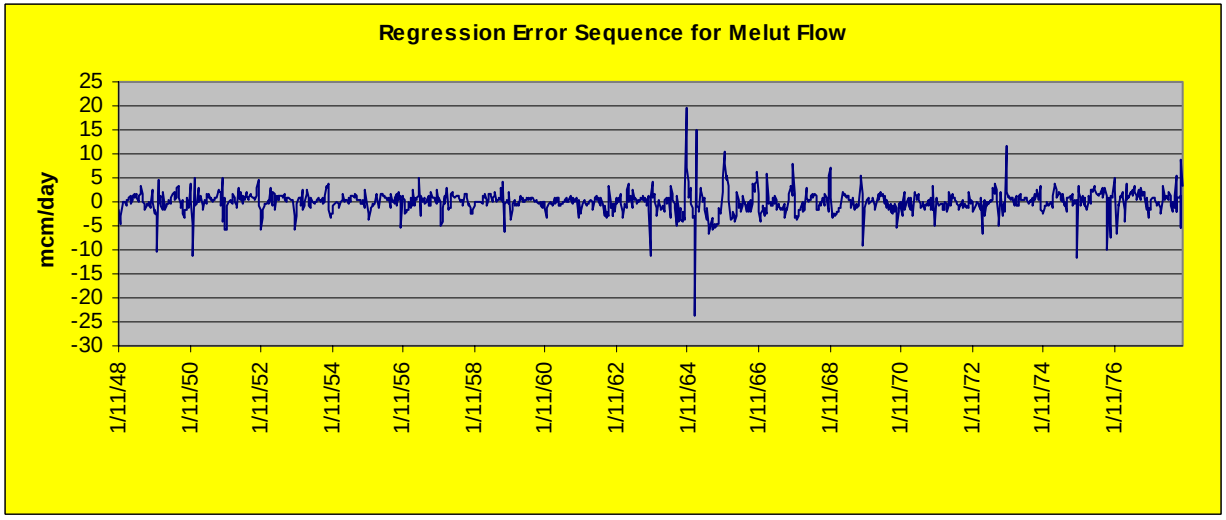

Figure 3.14: Regression Errors for Melut Flows

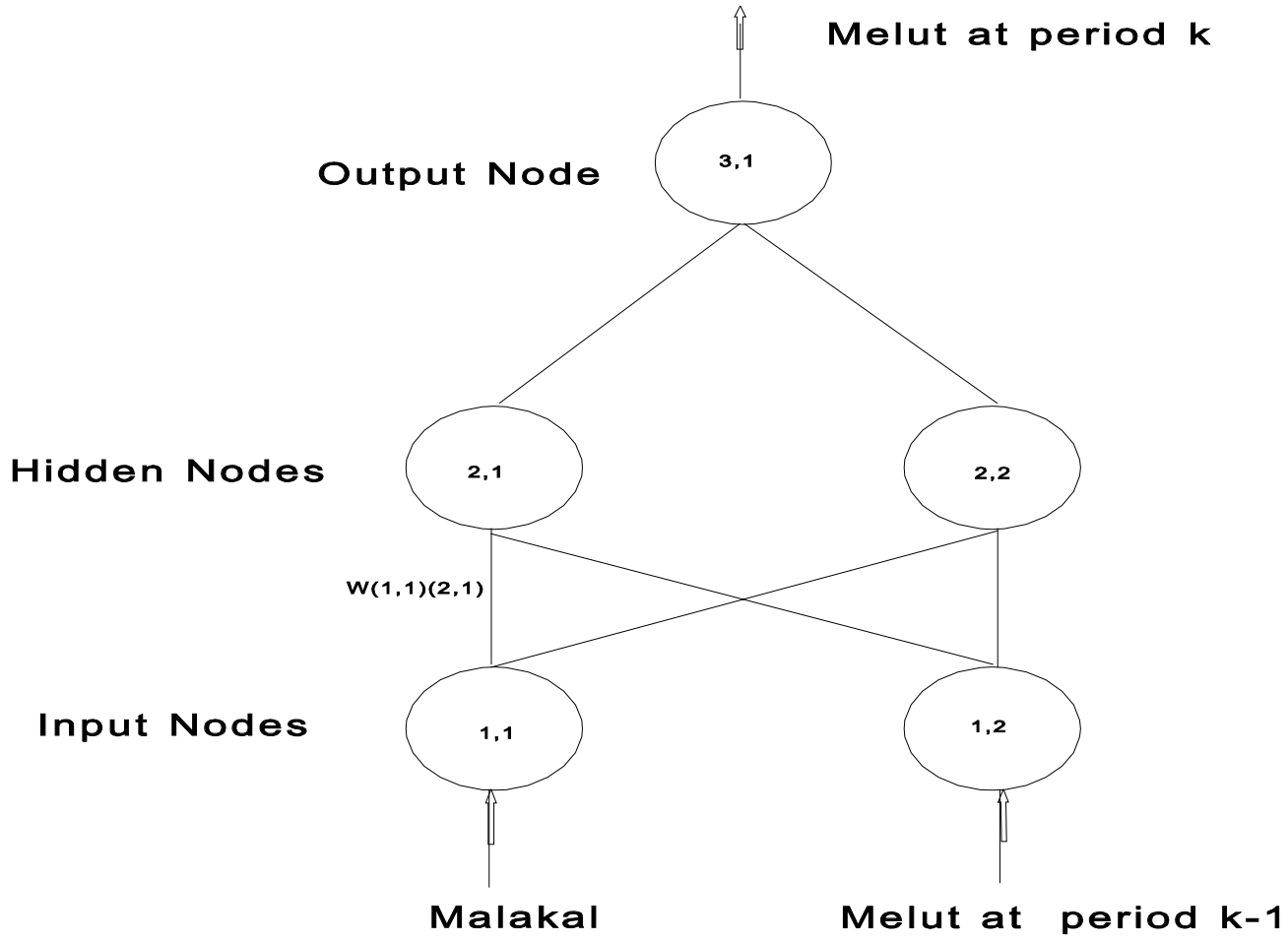

Figure 3.15: NN Structure for Melut Flow

Table 3.6: Neural Network Parameters for the Reach from Malakal to Melut

Weights(W)	(2,1)	(2,2)	(3,1)	Bias
(1,1)	-4.631851	-0.889161		
(1,2)	-1.854314	-5.572766		
(2,1)			-6.598139	-0.273720
(2,2)			-2.635438	4.603583
(3,1)				2.284771

* Qmax=210.00 Qmin=34.5 B=0.05 A=0.95

3.4. The Reach from Melut to Mogren

This reach includes the Gebel El Aulia reservoir and is dominated by backwater effects extending several hundred kilometers upstream. As the operation rules of Gebel Aulia affect the transport of water through this reach, it is herein handled as a reservoir rather than a routing reach. The modeling philosophy is discussed in the following chapter.

3.5. The Reach from Mogren to Dongola (HAD Entrance)

This reach extends for over 1500 km and receives input from three major tributaries: The White Nile, Blue Nile, and the River Atbara. A map of this river reach is shown in Figure 1.1. The contemporaneous historical ten-day flow data from 1912 to 1982 for the White Nile at Mogren, the Blue Nile at Khartoum, and the River Atbara at Atbara are plotted in Figure 3.16.

Several regression formulations were examined. The corresponding statistics are reported in Table 3.7. The model with three terms for Mogren, three terms for Khartoum, two terms for Atbara, and two terms for Dongola has the best statistics. The formulation

corresponding to this model is given by:

$$Q_{HAD}(k) = \sum_{i=1}^{i=3} a_i \quad Q_{GA}(k-i+1) + \sum_{i=1}^{i=3} b_i \quad Q_{Blnl}(k-i+1)$$
$$+ \sum_{i=1}^{i=2} c_i \quad Q_{Atbr}(k-i+1) + \sum_{i=1}^{i=2} d_i \quad Q_{HAD}(k-i) \quad + \quad e \quad + \quad \varepsilon_5(k) \quad ,$$

where $Q_{HAD}(k)$ is the flow during period k at the entrance of the High Aswan Dam, $Q_{GA}(k)$ is flow at the exit of Gebel El Aulia (flow at Mogren), $Q_{Blnl}(k)$ is the flow of the Blue Nile at Khartoum, $Q_{Atbr}(k)$ is the flow at Atbara, and

$a_1 = 0.1997$, $a_2 = 0.3788$, $a_3 = -0.06165$,
$b_1 = 0.2892$, $b_2 = 0.6043$, $b_3 = -0.3851$,
$c_1 = 0.4438$, $c_2 = 0.0874$,
$d_1 = 0.4636$, $d_2 = 0.03330$,
$e = -5.7570$.

The simulated series from the regression model and the actual series are plotted on Figure 3.17. The scatter plot of the simulated versus observed flows is shown in Figure 3.18, which indicates a very good correspondence over the full range of the flow. Figure 3.19 shows the regression error sequences. The lag-1 error correlation coefficient is 0.25. The error standard deviation is 24.15 mcm/day (approximately 10% of the average Dongola flow) and a correlation coefficient of 0.9946.

Table 3.7: Routing Model Statistics for Dongola Flows

Models	Previous Periods Used				Statistics		
	Mogren	Khartoum	Atbara	Dongola	Error Mean	Error STD	Correlation Coef.
REG0001	0	0	0	1	0.00	76.13	0.95
REG0002	0	0	0	2	0.00	56.04	0.97
REG1110	1	1	1	0	0.00	56.41	0.97
REG1111	1	1	1	1	0.00	30.07	0.99
REG2222	2	2	2	2	-0.01	25.93	0.99
REG3322	**3**	**3**	**2**	**2**	**0.01**	**24.15**	**0.99**
REG3333	3	3	3	3	0.01	23.06	1.00
REG4422	4	4	2	2	-0.03	24.09	0.99
REG4433	4	4	3	3	0.01	22.98	1.00

A neural network model was also developed for this reach. Its structure is shown in Figure 3.20. It includes three layers, 10 input nodes, 10 hidden nodes, and one output node. The first three inputs represent the current and two previous flows at Mogren, the next three inputs represent the current and two previous flows at Khartoum, nodes 7 and 8 represent the current and previous flows at Atbara, and the last two input nodes represent the two previous flows at Dongola. (Prior to the construction of the High Aswan Dam, flow records were kept at Wadi Halfa.)

Table 3.8 lists the neural network weights, biases, mean error and standard deviation. The simulated error standard deviation is 22.38 mcm/day, and the error mean is -0.0033 mcm/day. The correlation coefficient between the estimated and the actual values is 0.9954. In view of the comparable performance of the regression and neural network models and the fewer parameters of the regression model, it is selected as the Nile RSM routing model for this reach.

For a river reach with 1500 km long, the time lag of the routing model is an important issue. Our simulations indicate that the regression model can correctly predict the peak and low flows with no time delays. Figure 3.21 provides an example of the comparison between the predicted and the observed peak and low flows.

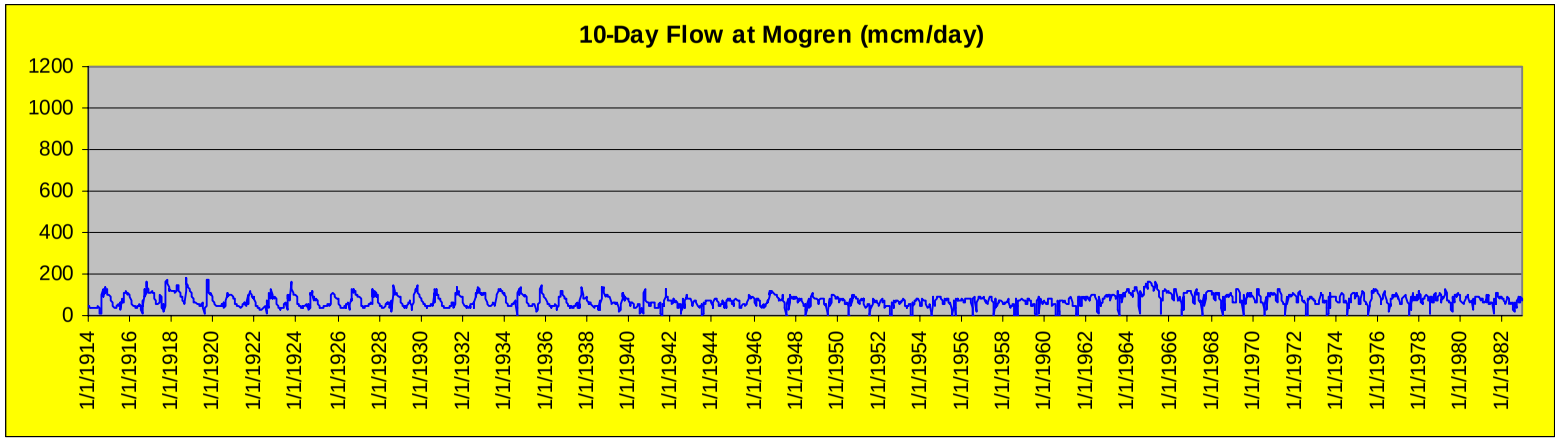

Figure 3.16 A: Historical Flow at Mogren

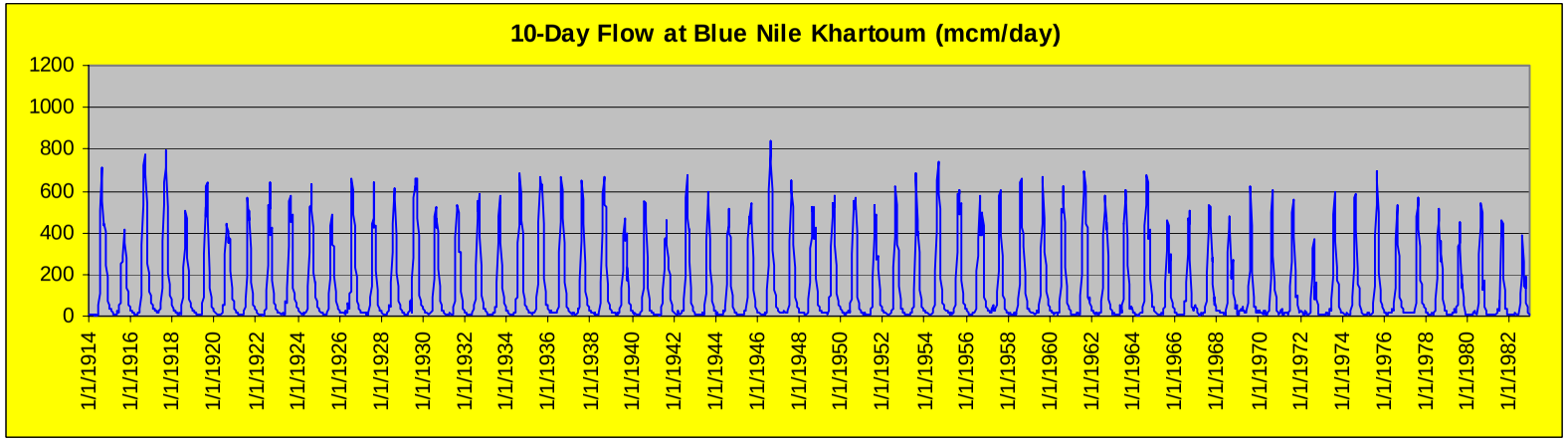

Figure 3.16 B: Historical Flow at Khartoum

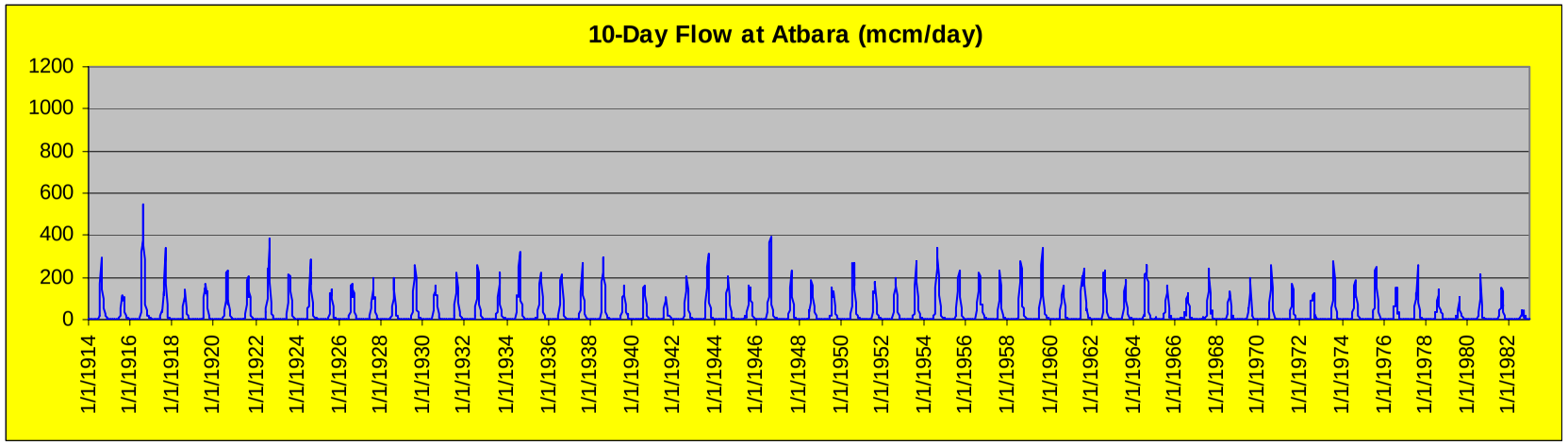

Figure 3.16 C: Historical Flow at Atbara

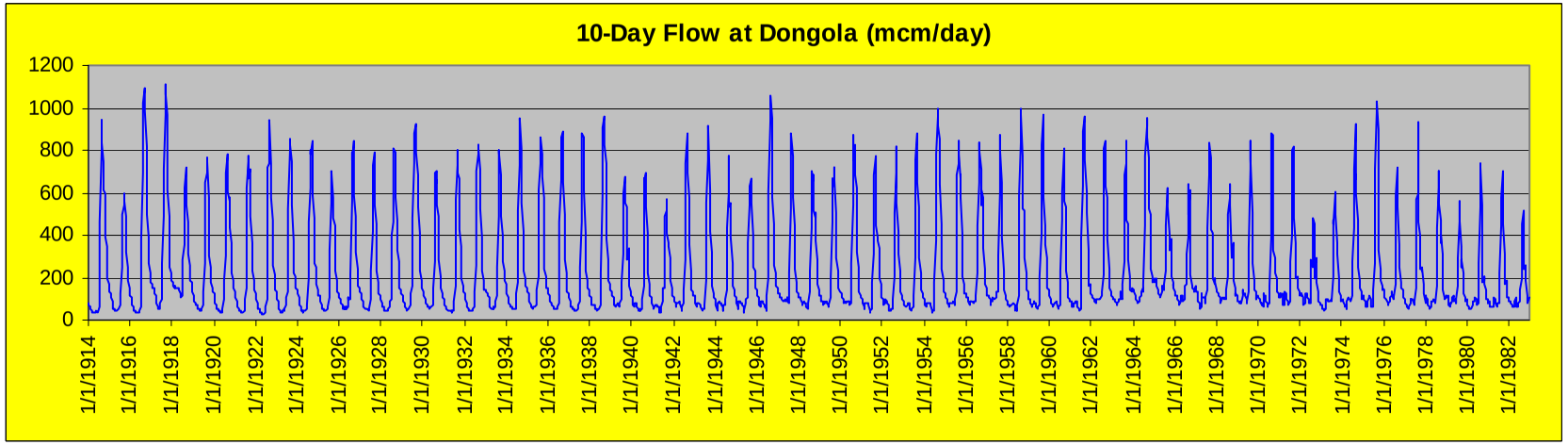

Figure 3.16 D: Historical Flow at Dongola

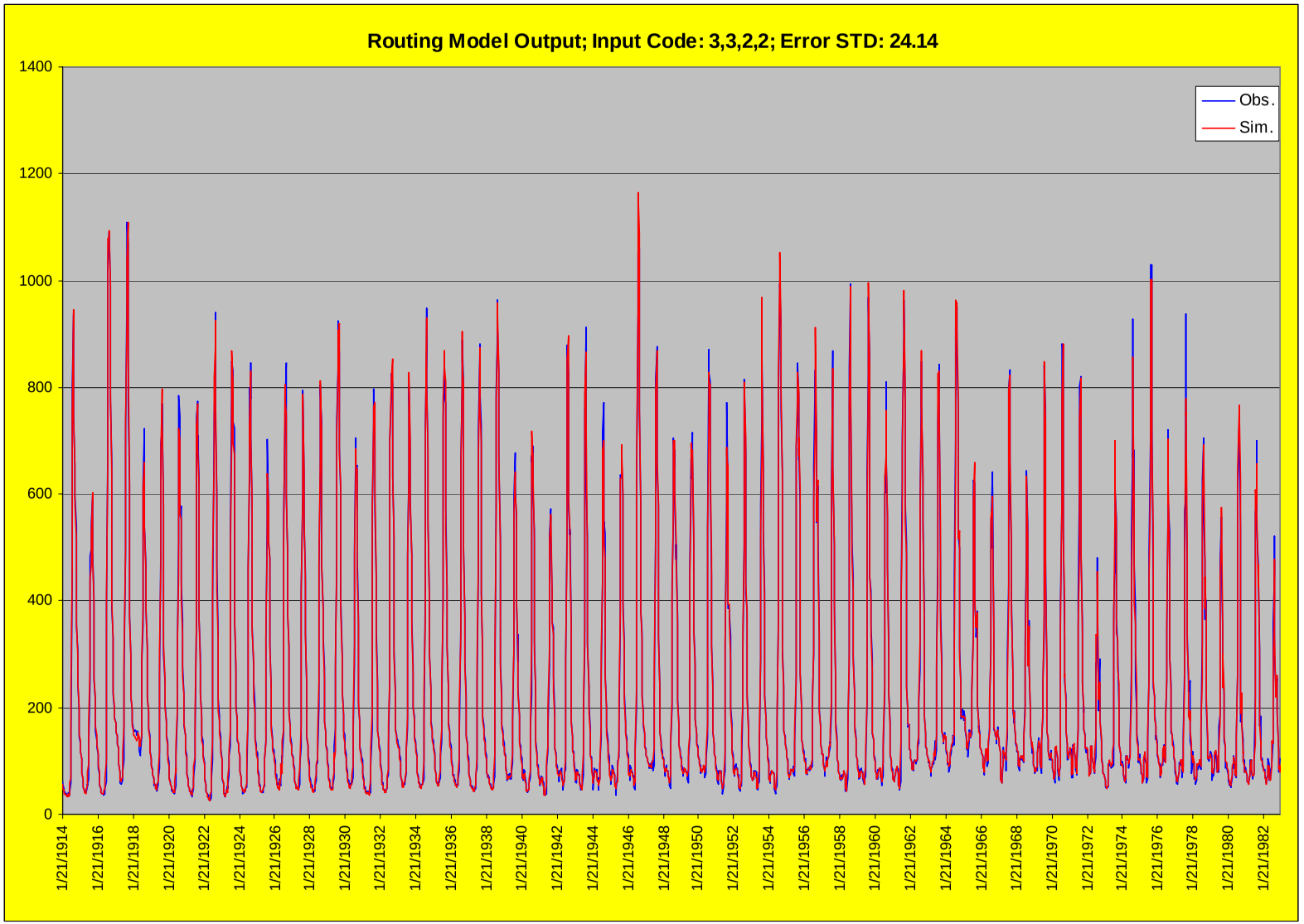

Figure 3.17: Routing Model Results

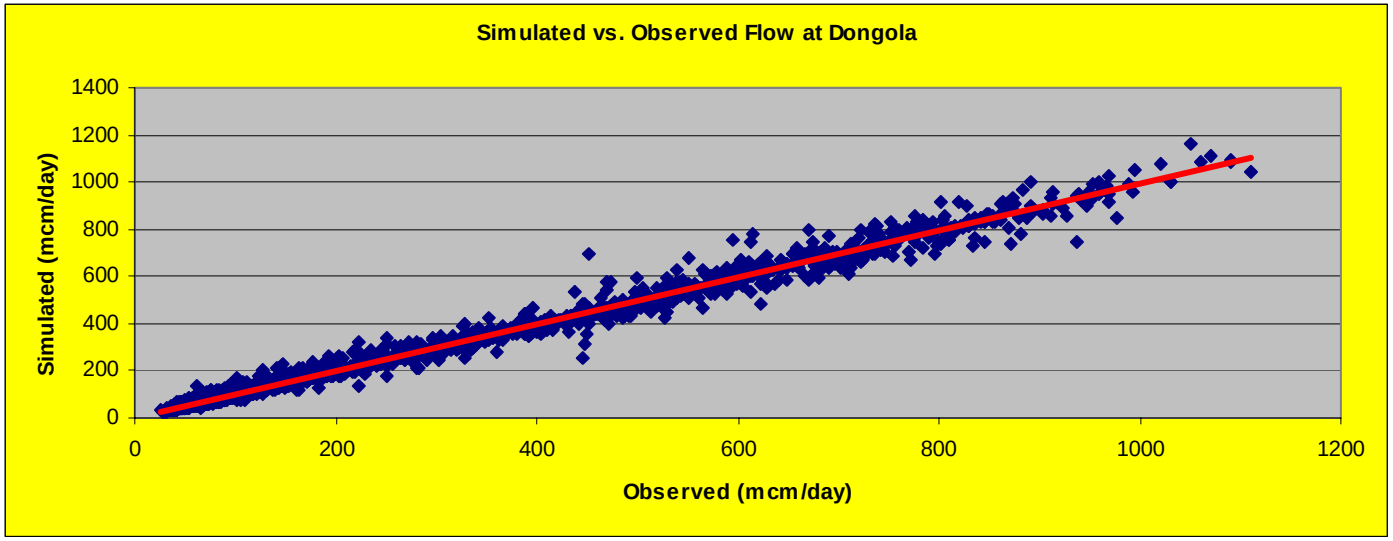

Figure 3.18: Routing Model Results for Dongola

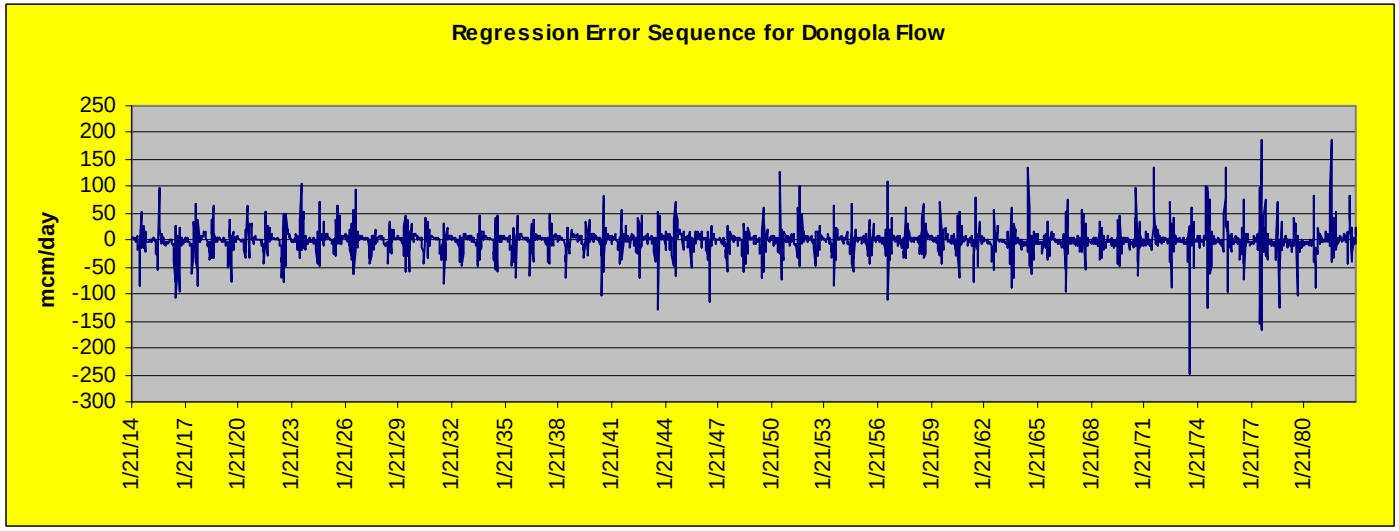

Figure 3.19: Regression Errors for Dongola Flows

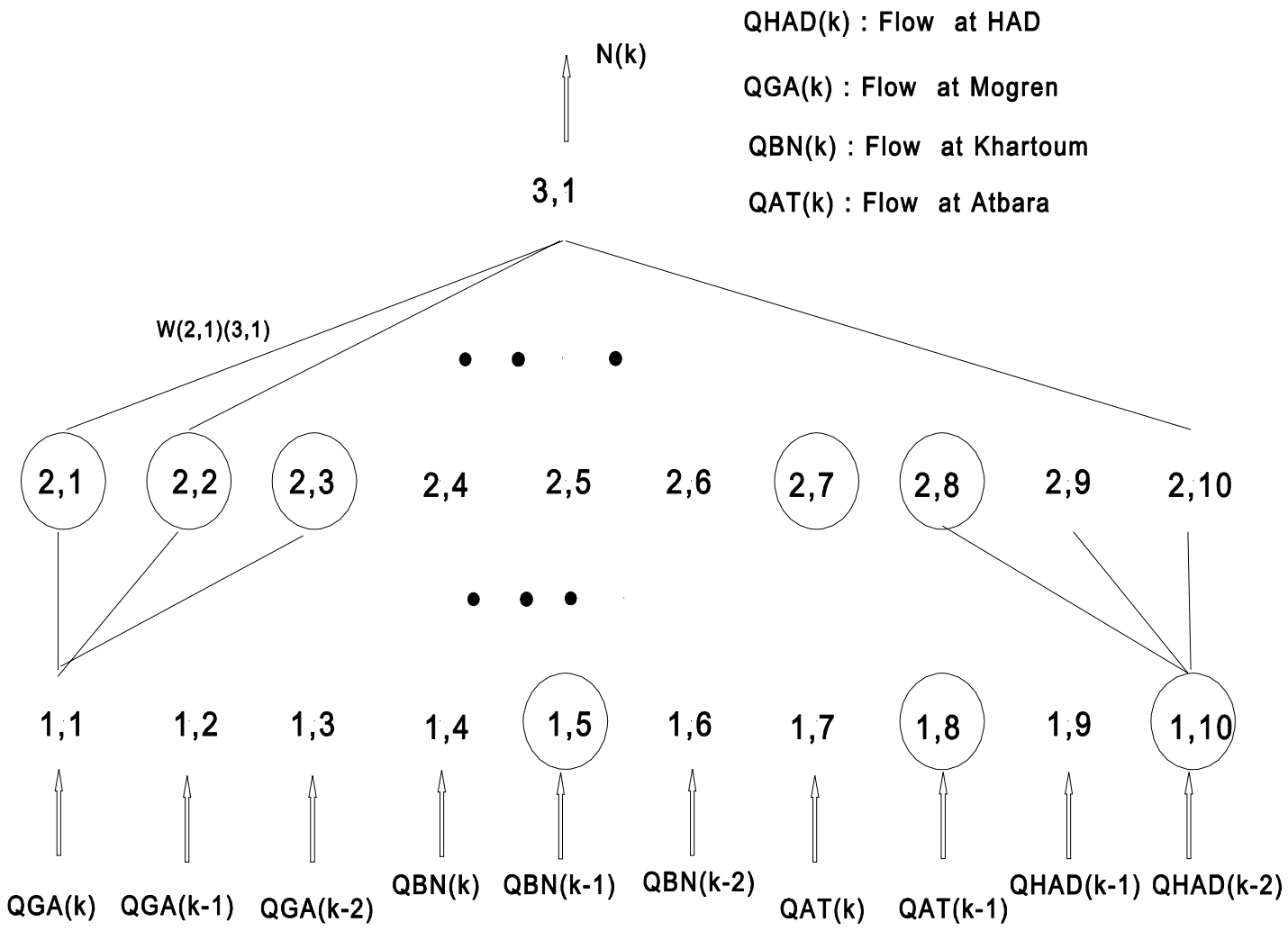

Figure 3.20: NN Structure for Dongola Flow

Table 3.8: Neural Network Parameters for Mogren to HAD Entrance (Dongola)

W11,2i: 0.654499 0.117191 0.514672 0.835771 0.966232 0.598246 0.523984 0.732781 0.676616 1.004078

W12,2i: 0.813969 -0.098443 0.671252 0.540097 1.964983 1.195523 -0.019517 0.387023 -0.167187 1.218853

W13,2i: -0.158198 0.872295 0.364230 0.499504 1.288583 -0.137989 0.306230 0.002583 0.883989 0.619411

W14,2i: 0.998708 0.124562 0.006615 0.227429 1.681282 0.678426 0.185383 0.276222 -0.130141 0.721485

W15,2i: 1.012546 -0.008714 0.254643 0.742249 2.987751 0.915004 -0.076600 0.088551 -1.256892 1.227850

W16,2i: -1.006575 0.659955 -0.052903 0.787232 -0.646748 -0.201073 1.329358 0.006017 0.866375 -0.062988

W17,2i: 0.653663 0.673194 0.124524 0.588006 0.936612 1.605673 0.671292 0.784672 -0.496346 0.779228

W18,2i: 1.029457 0.873996 0.812746 0.840638 1.088094 1.156331 0.386051 0.303183 -0.207640 0.442760

W19,2i: 0.633326 -0.061278 0.435673 0.309702 3.805823 0.425833 -0.021741 -0.114784 -0.892685 0.398388

W110,2i -0.233417 0.737724 0.227550 0.412316 0.526150 0.587421 0.823954 0.097402 -0.339623 -0.003044

W21,31: 2.097514

W22,31: -0.642028

W23,31: 0.676885

W24,31: -0.550764

W25:31: 4.491103

W26,31: 2.594411

W27,31: -1.509434

W28,31: 0.411534

W29,31: -2.140229

W210,31: 2.158591

Bias(2,i): -1.602930 0.085739 -1.018929 0.332149 -0.373749 -2.696098 0.676730 -0.544122 1.391811 -2.256349

Bias(3,1): -3.169648

Mean Error: 0.008616 Error Std.: 22.381780

Qmax=1110.000000 Qmin=0.000000 B=0.050000 A=0.950000

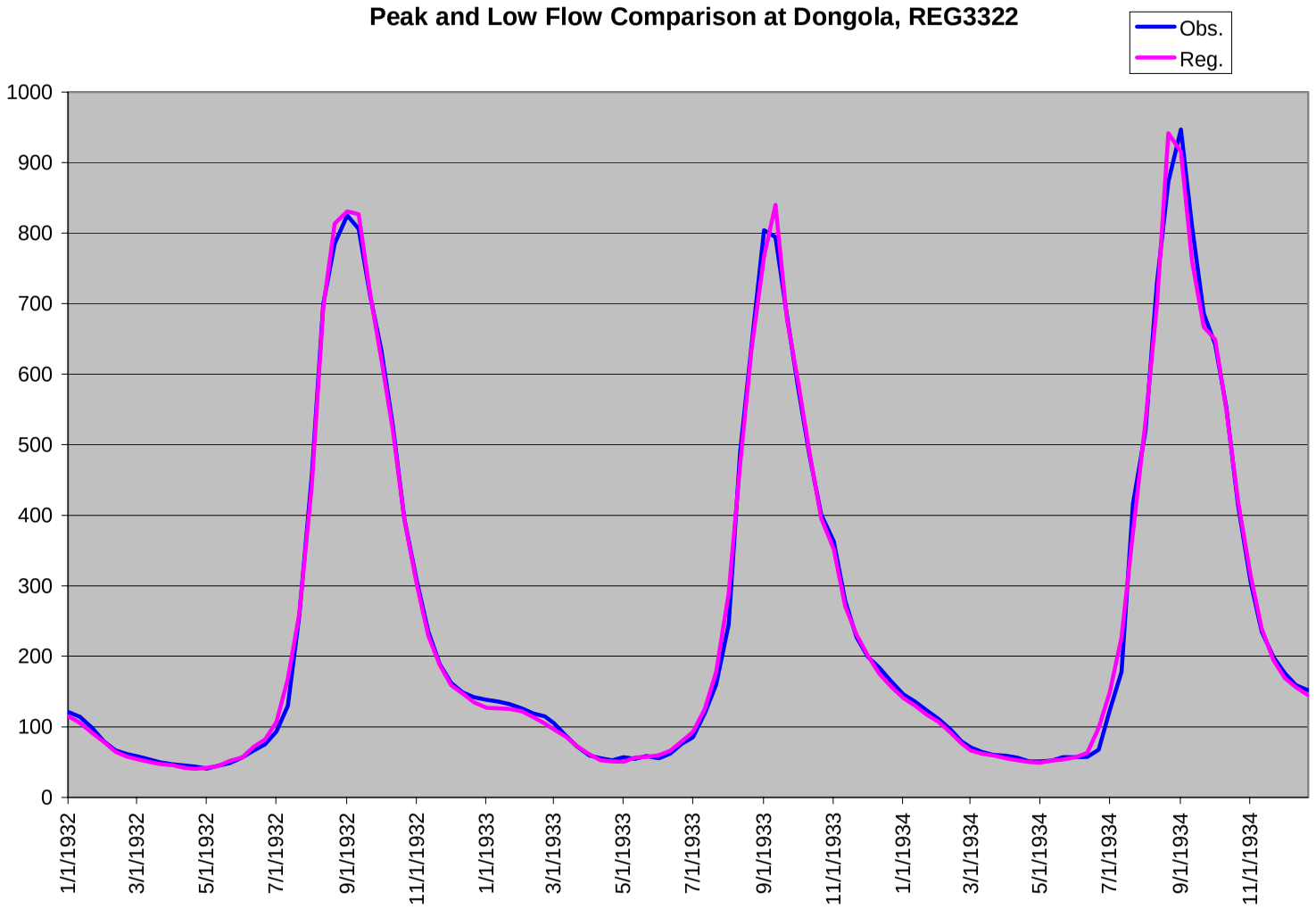

Figure 3.21: Peak and Low Flow Comparison at Dongola

3.6. River Reaches on Blue Nile and Atbara River

No routing models are developed for Blue Nile and Atbara river reaches because of the unavailability of long historical records. However, in the Nile RSM simulation model, a water transmission coefficient β is assigned to each reach. This coefficient is used as follows: Assume the flow at the beginning of a river reach is W_1. Then the flow at the end of the reach W_2 is computed from

$$W_2(k) = \beta W_1(k) + I(k) - D(k) \ ,$$

where I(k) is local inflow, and D(k) is withdrawal, if any. The water transmission coefficient is user specifiable. A recommended value is 1% reduction of flow for every 100 km river length.

Chapter 4

Inflow Forecasting

Inflow forecasts are critical in river basin management. Accurate, multi-lead forecasts translate into concrete benefits such as more energy generation, more effective drought mitigation, and better flood protection. Indeed, high inflow forecasts when reservoirs are nearly full necessitate higher turbine releases, more energy generation, and less spillage. Similarly, during droughts, inflow forecasting would determine whether to continue to release as usual or to reduce releases, sustaining water supplies longer.

This section describes the inflow forecasting model developed as part of the Nile DST. The model generates probabilistic forecasts with long lead times. Such forecasts are used to derive probabilistic sequences for key variables such as reservoir elevations, releases, and energy generation, and thus affect the selection of optimal policies.

The forecasting model is called historical analog (HA) inflow forecasting model. The central premise of this model is that streamflows materialize as a result of a nonlinear, deterministic, and chaotic hydro-meteorological process orbiting around an unknown attractor. Although the attractor is not easily definable, this hypothesis leads to the following scenario: If the process is presently at a certain point in its orbit, its future position can be reasonably inferred by observing the movement it experienced on similar occasions in the past. It is noted that a process point may not just simply be the inflow value at a particular time period, but it may include a number of previous inflows, depending on the dimensionality of the unknown attractor.

The HA forecasting model can also be corroborated from a different angle. Streamflows are the result of the rainfall-runoff process, and the values they have over a certain time period, to a certain extent, reflect the existing soil moisture and surface storage conditions in the drainage basin. Thus, even under two different climatic scenarios (of rainfall, evaporation, etc.), a basin initially tends to respond in a similar fashion until a time when it Aforgets@ its initial hydrologic

conditions and moves on to a different state. This, in fact, is the underlying notion for the Extended Streamflow Prediction (ESP) approach to streamflow forecasting.

Motivated by the above intuitive concepts, the HA forecasting model Asearches@ into the historical record and selects several inflow traces which, at some time in the past, have started from conditions similar to those of the current inflow sequence. Each one of these traces is a possible future realization of the inflow process, and all together constitute a set on which to base probabilistic, multi-lead forecasts.

The procedure of the HA model is described herein through an example. Suppose that we are presently at April 1st, and the previous periods= inflows have been W_1, W_2,...,W_n , where subscript A1@ represents the preceding period (last day in March), A2@ the day before that, etc. n is a parameter called analog corridor length. W_1, W_2,...,W_n are the most recent flows at the beginning of the forecasts. The next step is to retrieve all inflow traces of the same month and date as the W_1, W_2,...,W_n from the historical record and compute their Euclidian distance, E_j ,from the current sequence within the corridor:

$$E_j = \sum_{i=1}^{n} (W_i - W_i^j)^2$$
$$j = 1, 2, ..., m$$

where m is the total number of years of the historical record; W_i^j is the historical flow of year j which has the same calendar date as W_i; and E_j is the norm measuring the distance of the current flows W_i and W_i^j. A small value of E_j means that W_i and W_i^j are similar and close. This implies that it is very likely that the flows following the corridor period will be close and similar. The flows following W_i^j are known (in the historical record) and can be used as the forecasts of the flows following W_i. For the generation of multiple forecast traces, we rank the E_j's from smallest to largest, and select the flows in the record following W_i^j in the top portion of the ranked list. Figure 4.1 depicts the HA concept with two forecasting traces selected.

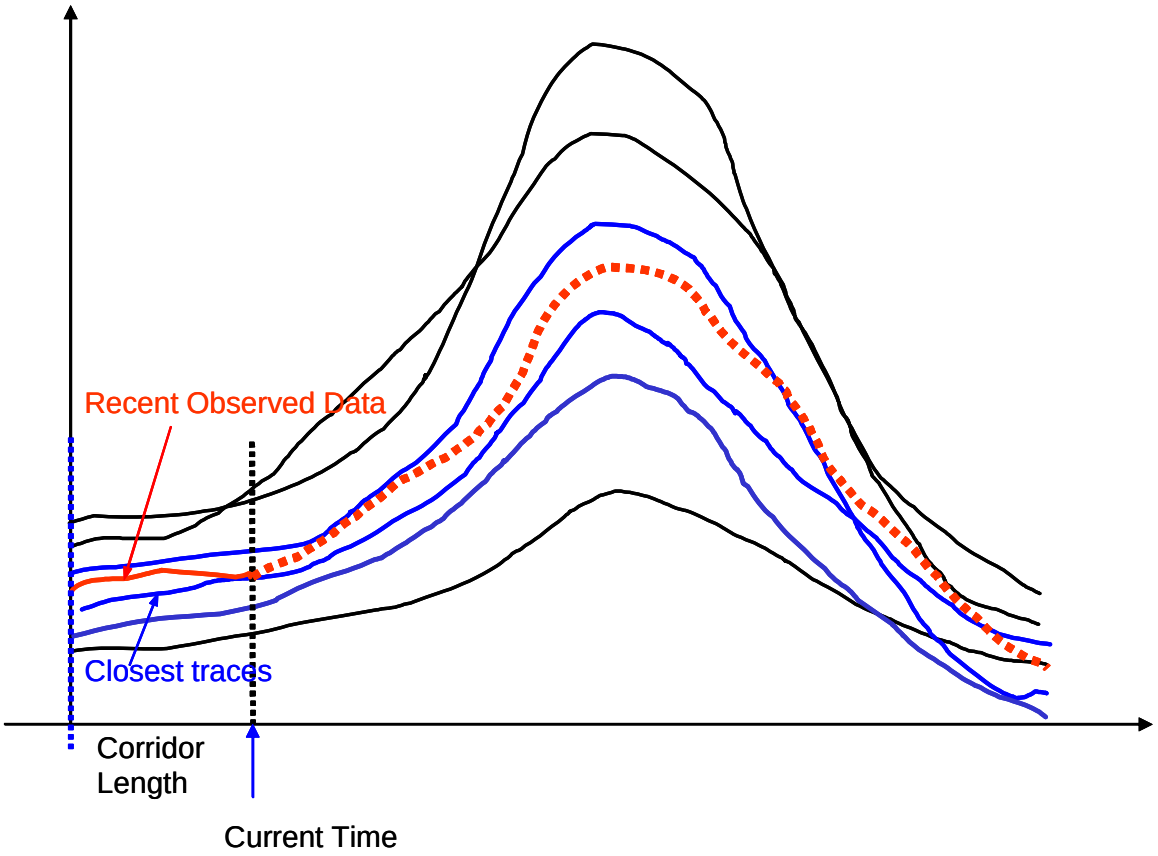

Figure 4.1: Historical Analog Selection Scheme

The HA model has two parameters: the analog corridor length and the number of traces. The length of the analog corridor is related to the Amemory@ of the basin, namely, the time period influenced by the current hydrologic conditions. Three to five months have been found to be appropriate and are currently used in the Nile DST. The number of the generated traces depends on the available data records and the requirements for statistical significance. It is recommended that one third of the total record be used, which implies 20 traces. Calibration of these two parameters can be done through retrospective simulations with the historical records. For detailed information on parameter calibration and simulation, the reader is referred to Yao and Georgakakos, 2001.

The application of the above procedure to multi-site inflow situations is straight forward. To apply the forecasting model, we need long concurrent records for all locations. As an example, a model application is shown for the period from January 1, 1960 to December 21, 1960. The corridor length is five 10-days, the number of forecasted traces is 20, and the forecasting horizon is 12 months. Figures 4.3 ad to 4.4 show the forecasted 10-day inflow traces at selected locations. The observed historical sequences are also plotted in the same chart with thicker red lines. The results show that the observed sequences stay within the range of the forecasted traces over most of the forecast horizon.

The effectiveness of the forecasting model is assessed via two simulation statistics: forecast reliability and relative uncertainty range. Reliability is defined as the percentage of time that the observed data is within the range of the forecast traces. The relative uncertainty range is the average ratio of the forecast range to the corresponding historical inflow range. Clearly, the higher the reliability and the smaller the relative uncertainty range, the better the forecasting model. Simulation study shows that the Historical Analog model exhibits 80% reliability for all locations through out different months of a year, while the relative uncertainty range varying from 0.1 to 1, with average value about 0.5. Overall, the model shows good forecast skill and reliability.

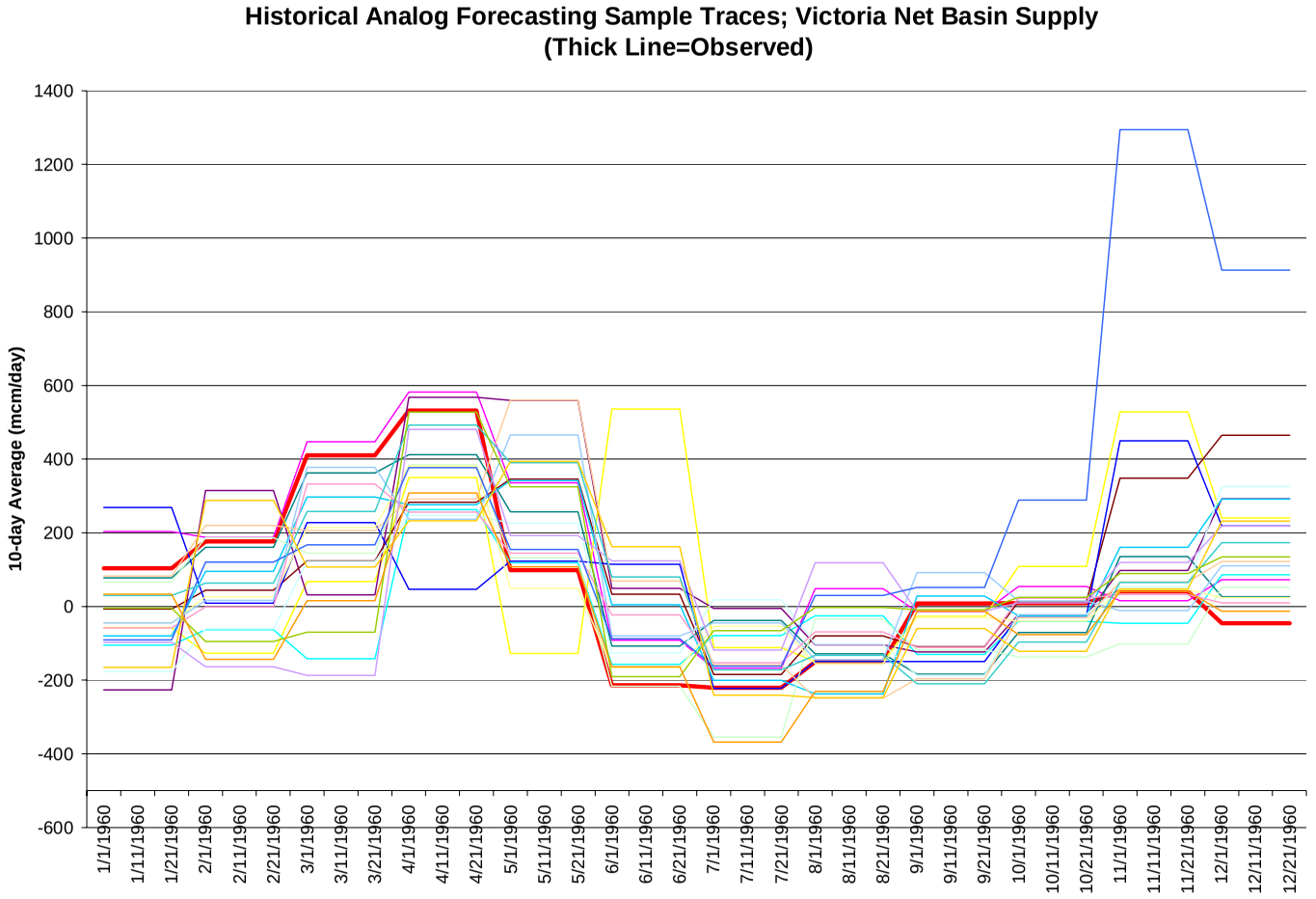

Figure 4.2: HA Forecasting Sample Traces for Victoria Net Basin Supply

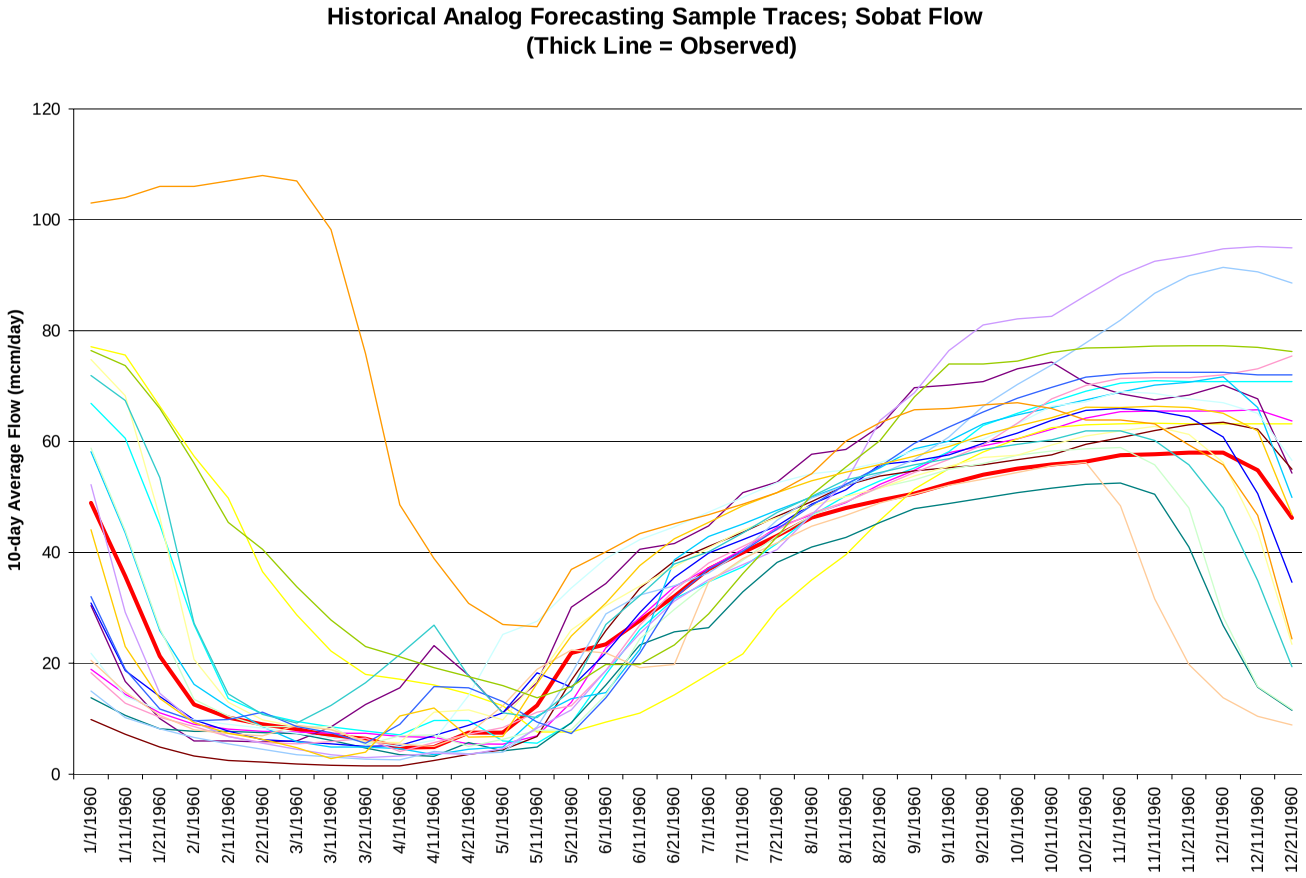

Figure 4.3: HA Forecasting Sample Traces for Sobat Flows

Chapter 5

Decision Model and Reservoir Regulation Rules

5.1. System Dynamics

The system dynamics are a set of equations which describe the response of the various system elements (reservoirs and routing reaches) to various inflow and release scenarios. The dynamics of the reservoirs are modeled by water balance equations, while that of the routing reaches by the routing equations discussed in Chapter 3. These equations are assembled below.

Equatorial Lakes (Victoria, Kyoga, and Albert):

The water balance equations of the equatorial lakes are given by:

$$S_V(k+1) = S_V(k) + W_V(k) - R_V(k) - D_V(k)$$
$$S_K(k+1) = S_K(k) + W_K(k) + R_V(k) - R_K(k) - D_K(k)$$
$$S_A(k+1) = S_A(k) + W_A(k) + R_K(k) - R_A(k) - D_A(k)$$
$$k = 1,2,3,\ldots, N$$

where the subscripts V, K, A respectively pertain to quantities of Lakes Victoria, Kyoga, and Albert; S(k) is the storage at the beginning of period k, R(k) is the release during period k; W(k) is the net basin supply during period k; D(k) is a water demand during period k; k is the time interval corresponding to ten days; and N is the time horizon of the decision model.

Lake Albert Exit (Pakwatch) to Mongala:

$$Q_{Mngl}(k) = \frac{a_1}{U_F(k)} R_A(k) + a_2 Q_{Trnt}(k) + a_3 Q_{Mngl}(k-1) + a_4 + \varepsilon_1(k) ,$$

where $Q_{Mngl}(k)$ is the average daily flow at Mongala in million cubic meters (mcm/d) during time period k, $R_A(k)$ is the release of Lake Albert (billion cubic meters per period), $Q_{Trnt}(k)$ is the daily average flow of the Torrents (mcm/d), $\varepsilon_1(k)$ is the model error presumed (previous chapter) to be

a white, normal sequence with mean zero and variance 6.33^2 $(mcm/day)^2$, U_F is a unit conversion factor equal to the number of days in each period k (usually 10 or 11, but also 9 or 8 in the last period of February) divided by 1000 (conversion of bcm to mcm), a_1 =0.1630749, a_2 = 0.3295462, a_3 = 0.7385824, and a_4 =7.317859.

Mongala to Malakal:

$$Q_{Lss}(k) = b_1\ Q_{Mngl}(k) + b_2\ Q_{Mngl}(k-1) + b_3\ Q_{Lss}(k-1) + b_4 + \varepsilon_2(k)$$

where $Q_{Lss}(k)$ is the daily average loss (mcm/d) in this reach during time period k, $Q_{Mngl}(k)$ is the flow at Mongala as defined previously, and b_1, b_2, b_3, b_4, are regression coefficients:

$$\left\{ \begin{array}{l} b_1 = 0.9926 \\ b_2 = 0.9522 \\ b_3 = 0.9435 \\ b_4 = 1.0379 \end{array} \right\},$$

Lastly, $\varepsilon_2(k)$ is a normal, white, zero-mean, random process with a variance of 2.07^2 $(mcm/d)^2$.

Flow at Malakal:

$$Q_{Mlkl}(k) = Q_{Mngl}(k) + Q_{Sbt}(k) - Q_{Lss}(k),$$

where $Q_{Mlkl}(k)$ is the daily average flow at Malakal (mcm/d), $Q_{Mngl}(k)$ and $Q_{Lss}(k)$ are the flow at Mongala and the Sudd loss defined earlier, and $Q_{Sbt}(k)$ is the daily average discharge of the Sobat River (mcm/d). The rating curve at Malakal is provided in the appendix.

Flow at Melut:

$$Q_{Mlt}(k) = c_1\ Q_{Mlkl}(k) + c_2\ Q_{Mlkl}(k-1) + c_3\ Q_{Mlt}(k-1) + c_4 + \varepsilon_3(k)$$
$$= c_1\ Q_{Mngl}(k) + c_1\ Q_{Sbt}(k) - c_1\ Q_{Lss}(k) + c_2\ Q_{Mlkl}(k-1) + c_3\ Q_{Mlt}(k-1) + c_4 + \varepsilon_3(k)\ ,$$

where $Q_{Mlt}(k)$ is the daily average flow at Melut (mcm/d), $\varepsilon_3(k)$ is a normal white random sequence with mean zero and variance 2.36^2 $(mcm/d)^2$, $c_1 = 0.7871429$, $c_2 = -0.6410149$, $c_3 = 0.859542$, and $c_5 = -0.4866521$. The rating curve at Melut is reported in the appendix.

Gebel El Aulia Reservoir:

The response of the Gebel El Aulia reservoir is complicated by the very mild slope of the White Nile in this region, and as a result, a water balance equation of the kind used for the Equatorial Lakes is not adequate. To model the backwater effects extending over 600 Km upstream, we used the transfer function approach described by *Panattoni et al., 1978*. They define the net inflow of the Gebel El Aulia reservoir as follows:

$$I_{GA}(k) = Q_{Mlt}(k)\ U_F\ -\ [\,S_{GA}(k+1)\ -\ S_{GA}(k)\,]\ -\ e_{GA}(k)\ A_{GA}(k)\ -\ D_{GA}(k)\ ,$$

where $I_{GA}(k)$, $S_{GA}(k)$, $e_{GA}(k)$, $A_{GA}(k)$, $d_{GA}(k)$ represent the net inflow, storage, evaporation rate, surface area, and water withdrawal of the Gebel El Aulia reservoir, $Q_{Mlt}(k)$ is the flow at Melut, and U_F is the unit conversion factor. And then, they derive the relationship between the net inflow and reservoir outflow. The most significant terms of this transfer function correspond to the present and previous ten-day period associations of these two variables, while the rest are at least one order of magnitude less and, most likely, represent a noise of the particular data used in the estimation process. Based on these observations, the following relationship between Gebel El Aulia net inflow and outflow is established:

$$R_{GA}(k) = 0.48\ \ I_{GA}(k)\ +\ 0.52\ \ \ I_{GA}(k-1)\ .$$

Finally, combining the above equations and solving for the storage at time (k+1), results in the following dynamical equation for the Gebel El Aulia storage:

$$S_{GA}(k+1) = -\frac{0.04}{0.48} S_{GA}(k) + \frac{0.52}{0.48} S_{GA}(k-1) - \frac{1}{0.48} R_{GA}(k) - R_{GA}(k)$$
$$- \frac{0.52}{0.48} D_{GA}(k-1) - e_{GA}(k) A_{GA}(k) - \frac{0.52}{0.48} e_{GA}(k-1) A_{GA}(k-1)$$
$$+ U_F(k) Q_{Mlt}(k) + \frac{0.52}{0.48} U_F(k-1) Q_{Mlt}(k-1) + \varepsilon_4(k),$$

where the unit conversion factor U_F is indexed by the appropriate time period, and $\varepsilon_4(k)$ is a white normal random process representing the error of this approximation. Based on the discussion of *Panattoni et al., 1978,* this error is assumed to have mean zero and variance 10.93^2 $(mcm/d)^2$.

The surface area and elevation of Gebel El Aulia is a rather complex function of reservoir storage *as well as* river stage at Melut and is given in the appendix. The appendix also includes the available data on the reservoir evaporation rates, water demands, target elevations, and storage and release constraints.

Existing and Planned Reservoirs along the Blue Nile in Ethiopia:

The water balance equations for the Ethiopian reservoirs are given by:

$$S_{TA}(k+1) = S_{TA}(k) + W_{TA}(k) - R_{TA}(k) - e_{TA} A_{TA}[S_{TA}(k)] - D_{TA}(k)$$

$$S_{KA}(k+1) = S_{KA}(k) + W_{KA}(k) + \beta_{TKA} R_{TA}(k) - R_{KA}(k) - e_{KA} A_{KA}[S_{KA}(k)] - D_{KA}(k)$$

$$S_{MA}(k+1) = S_{MA}(k) + W_{MA}(k) + \beta_{KAMA} R_{KA}(k) - R_{MA}(k) - e_{MA} A_{MA}[S_{MA}(k)] - D_{MA}(k)$$

$$S_{ME}(k+1) = S_{ME}(k) + W_{ME}(k) + \beta_{MAME} R_{MA}(k) - R_{ME}(k) - e_{ME} A_{ME}[S_{ME}(k)] - D_{ME}(k)$$

$$S_{BO}(k+1) = S_{BO}(k) + W_{BO}(k) + \beta_{MEBO} R_{ME}(k) - R_{BO}(k) - e_{BO} A_{BO}[S_{BO}(k)] - D_{BO}(k)$$

$$k = 1,2,3,\ldots,N$$

where the subscripts TA, KA, MA, ME, and BO respectively pertain to quantities of Lake Tana, Karadobi, Mabil, Mendaia, and Border; S (k) is the storage at the beginning of period k, R (k) is the release during period k; W (k) is the net basin supply during period k; D(k) is a water demand

during period k; and β is the water transmission loss coefficient from the upstream to the downstream reservoir.

Blue Nile Reservoirs in Sudan:

The water balance equations for reservoirs Roseires and Sennar are given by:

$$S_{RO}(k+1) = S_{RO}(k) + W_{RO}(k) + \beta_{BORO} R_{BO}(k) - R_{RO}(k) - e_{RO} A_{RO}[S_{RO}(k)] - D_{RO}(k)$$

$$S_{SE}(k+1) = S_{SE}(k) + W_{SE}(k) + \beta_{ROSE} R_{RO}(k) - R_{SE}(k) - e_{SE} A_{SE}[S_{SE}(k)] - D_{SE}(k)$$

where subscripts RO and SE respectively pertain to quantities of Roseires and Sennar; S(k) is the storage at the beginning of period k, R(k) is the release during period k; W(k) is the net basin supply during period k; D(k) is a water demand during period k; β is the water transmission loss coefficient from the upstream reservoir to downstream reservoir.

Flow at Khartoum on Blue Nile:

There were no historical records available for the Blue Nile to develop routing models. A simple water transmission loss in terms of the percentage of the total flow is used. The loss coefficient is specified for each river reach.

Flow downstream of Dinder:

$$Q_{DD}(k) = W_{DD}(k) + \beta_{SEDD} R_{SE}(k) - D_{SEDD}(k)$$

where Q_{DD} is the flow downstream of Dinder junction; $R_{SE}(k)$ is the release from Sennar; $D_{SEDD}(k)$ is the withdrawal in the river segment from Sennar to Dinder; β is the water transmission loss coefficient.

Flow downstream of Rahad:

$$Q_{RA}(k) = W_{RA}(k) + \beta_{DDRA} Q_{DD}(k) - D_{DDRA}(k)$$

where Q_{RA} is the flow downstream of Rahad junction; $W_{RA}(k)$ is the inflow from Rahad; $D_{DDRA}(k)$ is the withdrawal in the river segment from Dinder to Rahad; β is the water transmission loss coefficient.

Flow at Khartoum on Blue Nile:

$$Q_{KT}(k) = \beta_{RAKT} Q_{RA}(k) - D_{RAKT}(k)$$

where Q_{KT} is the flow at Khartoum on Blue Nile, which represents the flow enters into the main Nile; $D_{RAKT}(k)$ is the withdrawal in the river segment from Rahad to Khartoum; β is the water transmission loss coefficient.

Khashm el Girba Reservoir on Atbara River:

The water balance for Kirshm Girba is given by:

$$S_{KG}(k+1) = S_{KG}(k) + W_{KG}(k) - R_{KG}(k) - e_{KG} A_{KG}[S_{KG}(k)] - D_{KG}(k)$$

where S (k) is the storage at the beginning of period k, R (k) is the release during period k; W (k) is the inflow during period k; D(k) is a water demand during period k.

Flow at Atbara:

The release from reservoir Khashm el Girba enters into the Main Nile after some transmission loss. This flow is computed as below:

$$Q_{AT}(k) = \beta_{KGAT} R_{KG}(k) - D_{KGAT}(k)$$

where Q_{AT} is the flow entering the Main Nile from Atbara River; β is the water transmission loss coefficient.

Gebel El Aulia Exit (Mogren) to HAD Entrance (Dongola):

The response of this routing reach has been modeled in the previous chapter and includes

the inputs from the flow at Khartoum on the Blue Nile and Atbara Rivers. The associated equation is as follows:

$$Q_{HAD}(k) = \frac{d_1}{U_F(k)} R_{GA}(k) + \frac{d_2}{U_F(k-1)} R_{GA}(k-1) + \frac{d_3}{U_F(k-2)} R_{GA}(k-2)$$

$$+ d_4 Q_{KT}(k) + d_5 Q_{KT}(k-1) + d_6 Q_{KT}(k-2)$$

$$+ d_7 Q_{AT}(k) + d_8 Q_{AT}(k-1)$$

$$+ d_9 Q_{HAD}(k-1) + d_{10} Q_{HAD}(k-2) + d_{11} + \varepsilon_5(k) \quad ,$$

where $Q_{HAD}(k)$, $Q_{KT}(k)$, and $Q_{AT}(k)$ respectively represent the daily average flows at the HAD entrance, the Blue Nile at Khartoum, and the Atbara river, $R_{GA}(k)$ is the release of the Gebel El Aulia during period k, $\varepsilon_5(k)$ is a white normal random process with mean zero and variance 24.15^2 $(mcm/d)^2$, and $d_1 = 1.997358E\text{-}1$, $d_2 = 3.787839E\text{-}1$, $d_3 = -6.165313E\text{-}2$, $d_4 = 2.891700E\text{-}1$, $d_5 = 6.042574E\text{-}1$, $d_6 = -3.850977E\text{-}1$, $d_7 = 4.438153E\text{-}1$, $d_8 = 8.737212E\text{-}2$, $d_9 = 4.635983E\text{-}1$, $d_{10} = 3.330314E\text{-}2$, and $d_{11} = -5.757032$.

High Aswan Dam:

As in *Georgakakos et al., 1995a*, the High Aswan Dam response is modeled by the following water balance equation:

$$S_{HAD}(k+1) = S_{HAD}(k) - R_{HAD}(k) + U_F Q_{HAD}(k)$$
$$- e_{HAD}(k) A_{HAD}(S_{HAD}(k)) - S_{Tshk}(k) + v_{HAD}(k) \quad ,$$

where $S_{HAD}(k)$ represents HAD storage, $R_{HAD}(k)$ represents release, $Q_{HAD}(k)$ represents inflow, $e_{HAD}(k)$ represents evaporation rate, $A_{HAD}(k)$ represents surface area, $s_{Tshk}(k)$ represents spillage to Toshka (if any), and $v_{HAD}(k)$ represents a normal white random sequence with mean –0.004013 (bcm/10-day period) and variance 0.257634^2 (bcm/10-day period)^2 which is used to model seepage and bank storage losses.

The storage and release variables for all reservoirs are constrained to be within certain feasible ranges as follows:

$$S^{min}(k) \le S(k) \le S^{max}(k) \quad k = 1,2,...N,$$

$$R^{min}(k) \le R(k) \le R^{max}(k) \quad k = 1,2,..., N.$$

The upper and lower storage limits correspond to the reservoir conservation storage zones reported in the previous chapter. (Flood storage is not included in the conservation storage zone because the time resolution of the planning model is one 10-day. Namely, this storage is always assumed available to accommodate high frequency hydrologic events.) The lower release limits are constrained by environmental and water supply requirements both of which can change seasonally. The upper release bounds are determined based on hydro plant capacity and spillway capacity.

The above equations describe the dynamics of the White, Blue, and Main Nile reservoirs and river reaches, in response to natural inputs such as net basin supplies and tributary inflows as well as controllable inputs such as reservoir releases. The objective of the control model is to determine reservoir release sequences that bring about a desirable system response. In this sense, a system response is the response of certain key variables, called state variables, the knowledge of which fully describe the condition of the system. For a typical reservoir system, these variables usually include only reservoir storages, but in the case of the Nile basin, they also encompass other quantities related to the response of the river reaches.

5.2 State Augmentation

The purpose of this section is to compile all system dynamics relationships into one vector equation of the following form:

$$S(k+1) = f(S(k), u(k), \xi(k), k),$$

where **S**(k) is the state vector, **u**(k) is the vector of controllable quantities, **ξ**(k) is the vector of uncertain inputs, and **f**[ ] is the state transition (vector) function relating the previous quantities. This represents the *system state equation* and is a standard form necessary for the application of dynamic optimization (decision) methods.

An important feature of the above equation is that the quantities of its right side pertain only to time period k. Namely, there are no time-lagged quantities involved. This equation is called state transition equation in control theory terminology.

The state and control vectors are defined as:

$$S(k)=\begin{bmatrix} S_1(k) \\ S_2(k) \\ S_3(k) \\ S_4(k) \\ S_5(k) \\ S_6(k) \\ S_7(k) \\ S_8(k) \\ S_9(k) \\ S_{10}(k) \\ S_{11}(k) \\ S_{12}(k) \\ S_{13}(k) \\ S_{14}(k) \\ S_{15}(k) \\ S_{16}(k) \\ S_{17}(k) \\ S_{18}(k) \\ S_{19}(k) \\ S_{20}(k) \\ S_{21}(k) \\ S_{22}(k) \\ S_{23}(k) \\ S_{24}(k) \\ S_{25}(k) \end{bmatrix} = \begin{bmatrix} S_V(k) \\ S_K(k) \\ S_A(k) \\ Q_{mngl}(k-1) \\ Q_{ls}(k-1) \\ Q_{mlkl}(k-1) \\ Q_{mlt}(k-1) \\ S_{GA}(k-1) \\ S_{GA}(k) \\ u_{GA}(k-1) \\ u_{GA}(k-2) \\ S_{TA}(k) \\ S_{KA}(k) \\ S_{MA}(k) \\ S_{ME}(k) \\ S_{BO}(k) \\ S_{RO}(k) \\ S_{SE}(k) \\ Q_{KT}(k-1) \\ Q_{KT}(k-2) \\ S_{KG}(k) \\ Q_{AT}(k-1) \\ Q_{HAD}(k-1) \\ Q_{HAD}(k-2) \\ S_{HAD}(k) \end{bmatrix}, \quad u(k)=\begin{bmatrix} u_1(k) \\ u_2(k) \\ u_3(k) \\ u_4(k) \\ u_5(k) \\ u_6(k) \\ u_7(k) \\ u_8(k) \\ u_9(k) \\ u_{10}(k) \\ u_{11}(k) \\ u_{12}(k) \\ u_{13}(k) \end{bmatrix} == \begin{bmatrix} R_V(k) \\ R_K(k) \\ R_A(k) \\ R_{GA}(k) \\ R_{TA}(k) \\ R_{KA}(k) \\ R_{MA}(k) \\ R_{ME}(k) \\ R_{BO}(k) \\ R_{RO}(k) \\ R_{SE}(k) \\ R_{KG}(k) \\ R_{HAD}(k) \end{bmatrix},$$

Then, the state transition functions for the entire system can be defined as shown below:

$$
f(k)=\begin{bmatrix} f_1(k)\\ f_2(k)\\ f_3(k)\\ f_4(k)\\ f_5(k)\\ f_6(k)\\ f_7(k)\\ f_8(k)\\ f_9(k)\\ f_{10}(k)\\ f_{11}(k)\\ f_{12}(k)\\ f_{13}(k)\\ f_{14}(k)\\ f_{15}(k)\\ f_{16}(k)\\ f_{17}(k)\\ f_{18}(k)\\ f_{19}(k)\\ f_{20}(k)\\ f_{21}(k)\\ f_{22}(k)\\ f_{23}(k)\\ f_{24}(k)\\ f_{25}(k) \end{bmatrix} =
\begin{bmatrix}
f_1(k)=S_1(k)+W_V(k)-u_1(k)-D_V\\
f_2(k)=S_2(k)+W_K(k)+u_1-u_2(k)-D_K\\
f_3(k)=S_3(k)+W_A(k)+u_2-u_3(k)-D_A\\
f_4(k)=\dfrac{a_1}{U_F(k)}u_3+a_2Q_{trnt}(k)+a_3Q_{trnt}(k-1)+a_4S_4(k)+a_5+\varepsilon_1(k)\\
f_5(k)=b_1f_4(k)+b_2S_4(k)+b_3(k)S_5+b_4+\varepsilon_2(k)\\
f_6(k)=f_4(k)+Q_{sbt}(k)-f_5(k)\\
f_7(k)=c_1f_6(k)+c_2S_6(k)+c_3(k)S_7+c_4+\varepsilon_3(k)\\
f_8(k)=S_9(k)\\
f_9(k)=-\dfrac{0.04}{0.48}S_9(k)+\dfrac{0.52}{0.48}S_8(k)-\dfrac{1}{0.48}u_4(k)-D_{GA}(k)-\dfrac{052}{0.48}D_{GA}(k-1)\\
-e_{GA}(k)A_{GA}(k)-\dfrac{0.52}{0.48}e_{GA}(k-1)A_{GA}(k-1)+\\
U_F(k)f_7(k)+\dfrac{0.52}{0.48}U_F(k-1)S_7(k)+\varepsilon_4(k)\\
f_{10}(k)=u_4(k)\\
f_{11}(k)=S_{10}(k)\\
f_{12}(k)=S_{12}(k)+W_{TA}(k)-u_5(k)-e_{TA}A_{TA}(k)-D_{TA}\\
f_{13}(k)=S_{13}(k)+W_{KA}(k)+\beta_{TAKA}u_5-u_6(k)-e_{KA}A_{KA}(k)-D_{KA}\\
f_{14}(k)=S_{14}(k)+W_{MA}(k)+\beta_{KAMA}u_6-u_7(k)-e_{MA}A_{MA}(k)-D_{MA}\\
f_{15}(k)=S_{15}(k)+W_{ME}(k)+\beta_{MAME}u_7-u_8(k)-e_{ME}A_{ME}(k)-D_{ME}\\
f_{16}(k)=S_{16}(k)+W_{BO}(k)+\beta_{MEBO}u_8-u_9(k)-e_{BO}A_{BO}(k)-D_{BO}\\
f_{17}(k)=S_{17}(k)+W_{RO}(k)+\beta_{BORO}u_9-u_{10}(k)-e_{RO}A_{RO}(k)-D_{RO}\\
f_{18}(k)=S_{18}(k)+W_{SE}(k)+\beta_{ROSE}u_{10}-u_{11}(k)-e_{SE}A_{SE}(k)-D_{SE}\\
f_{19}(k)=\beta_{RAKT}(W_{RA}(k)+\beta_{DDRA}(W_{DD}(k)+\beta_{SEDD}u_{11}(k)-D_{SEDD}(k))\\
-D_{DDRA}(k))-D_{RAKT}(k)\\
f_{20}(k)=S_{19}(k)\\
f_{21}(k)=S_{21}(k)+W_{KG}(k)-u_{12}(k)-e_{KG}A_{KG}(k)-D_{KG}(k)\\
f_{22}(k)=\beta_{KGAT}u_{12}(k)-D_{KGAT}(k)\\
f_{23}=\dfrac{d_1}{U_F(k)}u_4(k)+\dfrac{d_2}{U_F(k-1)}S_{10}(k)+\dfrac{d_3}{U_F(k-2)}S_{11}(k)\\
+d_4f_{19}(k)+d_5S_{19}(k)+d_5S_{20}(k)+d_7(k)f_{22}(k)\\
+d_8S_{22}(k)+d_9S_{23}(k)+d_{10}S_{25}(k)+d_{11}+\varepsilon_5(k)\\
f_{24}(k)=S_{25}(k)\\
f_{25}(k)=S_{25}(k)+u_{13}(k)+U_F(k)f_{23}(k)\\
-e_{HAD}(k)A_{HAD}(k)-SPL_{HAD}(k)+\nu_{HAD}(k)
\end{bmatrix}, \qquad (5-B)
$$

Based on the previous relationships, the uncertain inputs associated with each transition equation are as follows:

$$\xi(k) = \begin{bmatrix} f_1(k):\{W_V(k)\} \\ f_2(k):\{W_K(k)\} \\ f_3(k):\{W_A(k)\} \\ f_4(k):\{Q_{trnt}(k),\varepsilon_1(k)\} \\ f_5(k):\{Q_{trnt}(k),\varepsilon_1(k),\varepsilon_2(k)\} \\ f_6(k):\{Q_{trnt}(k),Q_{sbt}(k),\varepsilon_1(k),\varepsilon_2(k)\} \\ f_7(k):\{Q_{trnt}(k),Q_{sbt}(k),\varepsilon_1(k),\varepsilon_2(k),\varepsilon_3(k)\} \\ f_8(k):\{\text{none}\} \\ f_9(k):\{Q_{trnt}(k),Q_{sbt}(k),\varepsilon_1(k),\varepsilon_2(k),\varepsilon_3(k),\varepsilon_4(k)\} \\ f_{10}(k):\{\text{none}\} \\ f_{11}(k):\{\text{none}\} \\ f_{12}(k):\{W_{TA}(k)\} \\ f_{13}(k):\{W_{KA}(k)\} \\ f_{14}(k):\{W_{MA}(k)\} \\ f_{15}(k):\{W_{ME}(k)\} \\ f_{16}(k):\{W_{BO}(k)\} \\ f_{17}(k):\{W_{RO}(k)\} \\ f_{18}(k):\{W_{SE}(k)\} \\ f_{19}(k):\{\beta_{RAKT},W_{RA}(k),\beta_{DDRA},W_{DD}(k),\beta_{SEDD}\} \\ f_{20}(k):\{\text{none}\} \\ f_{21}(k):\{W_{KG}(k)\} \\ f_{22}(k):\{\text{none}\} \\ f_{23}:\{\beta_{RAKT},W_{RA}(k),\beta_{DDRA},W_{DD}(k),\beta_{SEDD},\varepsilon_5(k)\} \\ f_{24}(k):\{\text{none}\} \\ f_{25}(k):\{\beta_{RAKT},W_{RA}(k),\beta_{DDRA},W_{DD}(k),\beta_{SEDD},\varepsilon_5(k),\nu_{HAD}(k)\} \end{bmatrix},$$

In each case, the combined effect of these inputs represents the influence of the uncertain input vector $\xi(k)$. In particular, the net basin supply and tributary inflow terms include both a deterministic and a random component as explained in Chapter 2. Though, the deterministic part could be incorporated in the state dynamics, for parsimony reasons, it is treated as part of the

time varying transition functions $f_i(k)$.

The previous equations summarize the system simulation model. In decision systems terminology, S is the state variable; u is the control variable; and W and D are system inputs. The significance of the system dynamics is that the value of the state variable for the next time period S(k+1) can be computed if the decision vector u is given. Of course, for a stochastic system, one can only determine the uncertainty characteristics.

In view of the uncertain system nature, the reservoir storage constraints are more properly expressed in a probabilistic form:

$$\text{Prob}[\, S_i^{min}(k) \le S_i(k) \,] \ge \pi_i^{min}(k)$$

$$\text{Prob}[\, S_i(k) \le S_i^{max}(k) \,] \ge \pi_i^{max}(k)$$

$$i \in \text{reservoirs}, \quad k = 0, 1, \ldots, N,$$

where π^{min} and π^{max} are reliability levels. These levels as well as the upper and lower storage and release thresholds are denoted here as time-varying but are usually time-invariant.

The goal of the river basin management algorithm is to identify the release sequences for all reservoirs $\{u_i^*(k)$, i=1, 2, ..., 13; k=0,1, ..., N-1$\}$ such that system objectives and constraints are met successfully. The element of the formulation that brings this to bear and also measures the success of the various operational alternatives is the performance index discussed next.

5.3. Performance Index

The goal of the control procedure is to maximize the benefit gained from the whole reservoir system, while meeting its environmental and water supply demands. To achieve this objective, we minimize the following performance index:

$$J = E\ \{\ \sum_{k=0}^{N-1} [\ P_h(S(k)) \quad + \quad P_{eng}(u(k),S(k)) \quad + \quad P_{htrg}(S(k)) \quad + \quad P_{utrg}(u(k))$$

$$+ \quad P_{spl}(u(k),S(k)) \quad + \quad P_{hp}(S(k))] \quad + \quad P_h(S(N)) \quad + \quad P_{hp}(S(N))\}, \qquad (5-D)$$

where

$$P_h(S(k)) = \sum_{i \in reservoirs} \alpha_{1i} \left[\frac{[\ H_i^{max} - H_i(S_i(k))\ ]^2}{1 + e^{\frac{H_i^{max} - H_i(S_i(k))}{T_H}}} + \frac{[\ H_i(S_i(k)) - H_i^{min}\ ]^2}{1 + e^{\frac{H_i(S_i(k)) - H_i^{min}}{T_H}}} \right]$$

$$P_{eng}(u(k),S(k)) = - \sum_{i \in powerplants} \alpha_{2i} E_i(u_i(k),S_i(k)),$$

$$P_{htrg}(S(k)) = \sum_{i \in reservoirs} \alpha_{3i} \left[\frac{H_i(S_i(k)) - H_i^{trg}(k)}{H_i^{max} - H_i^{min}} \right]^2$$

$$P_{utrg}(S(k)) = \sum_{i \in Reservoirs} \alpha_{4i} \left[\frac{[U_i(k) - U_i^{trg}(k)]^2}{[U_i^{max}(k) - U_i^{min}(k)]^2} \right]$$

$$P_{spl}(u(k),S(k)) = \sum_{i=\in Reservoirs} \alpha_{5i} SPL_i(u_i(k),S_i(k))$$

$$P_{hp}(S(k)) = \sum_{i,j \in reservoirs} \alpha_{6i} \left[\frac{H_i(S_i(k)) - H_i^{min}(k)}{H_i^{max} - H_i^{min}} - \frac{H_j(S_j(k)) - H_j^{min}(k)}{H_j^{max} - H_j^{min}} \right]^2$$

In the above, E{ } denotes expectation of the quantity in the brackets with respect to the joint probability distribution of the reservoir inflows.

There are six terms in the performance index. They are the penalty terms to be minimized through the optimization algorithm. The first term $P_h(\mathbf{S}(k))$ uses the barrier functions (one for each reservoir) to enforce the elevation (or equivalently) storage constraints. In this term, $H_i^{min}(k)$ and $H_i^{max}(k)$ are the lower and upper elevation limits for the ith reservoir, $H_i(S_i(k))$ are the elevation versus storage functions, and T_H is a barrier function parameter. Their most important feature is that they are everywhere analytical (with continuous first and second derivatives) and yet delimit with desirable accuracy the feasible elevation regions. Namely, inside the $[\ H_i^{min}(k)\ ,\ H_i^{max}(k)\ ]$ range, they vanish, while outside of it, they impose a quadratic penalty the severity of which is controlled by the weighing coefficient α_{1i}. The value of α_{1i} should be high enough to ensure that these constraints have priority over other performance index terms. The parameter T_H controls the smoothness of the transition over $H_i^{min}(k)$ and $H_i^{max}(k)$ and requires some experimentation. (A value of $T_H = 0.002$ usually works well.)

The second term $P_{eng}(\mathbf{u}(k), \mathbf{S}(k))$ represents the penalty for the energy generated from all hydro power facilities in the system. The energy generation for each reservoir is a function of elevation and release. The negative sign implements a minimum objective.

The third term $P_{htrg}(\mathbf{S}(k))$ represents the penalty for the target elevation. The purpose of this penalty is to force the reservoir elevation to follow a certain target value. In this case, the maximum elevation is assigned as the target value to operate the turbines at high efficiency. This term also improves the convergence speed of the adopted optimization algorithm as discussed later.

Similar to the third term, the fourth term $P_{utrg}(\mathbf{u}(k))$ is the penalty for the target release. The purpose of this penalty is to force the reservoir release to follow a certain target value (or pattern). This term is useful if the release target pattern or value is provided. A sample case is provided in the later case studies. Placing the control variable in this quadratic term also improves the convergence speed of the optimization algorithm.

The fifth term, $P_{spl}(\mathbf{u}(k),\mathbf{S}(k))$, represents the penalty for the spillage. The spillage is defined as the portion of the release larger than the turbine capacity. Since the release in the dynamics represents the total of the turbine release and the spillage, the spillage occurs only if the release exceeds the turbine capacity. Minimizing spillage is consistent with the long-term goal of maximizing energy generation.

The last term $P_{hp}(\mathbf{S}(k))$ represents the penalty for the uniform reservoir fluctuation. The rationale of this term is to minimize the differences in relative levels among the reservoirs.

Penalty parameters α_{ij} are used to introduce priorities in the performance index terms. These parameters should be determined such that the first term of the performance index is dominant. The rest of the terms are adjusted based on the priority of the operating objective. The logic is to determine feasible sequences guaranteed to minimize the other terms.

5.4. Control Method

The control problem formulated in the previous section is solved using the Extended Linear Quadratic Gaussian (ELQG) control method which was originally introduced by *Georgakakos and Marks, 1987,* and further developed by *Georgakakos 1989, 1991, 1993, Georgakakos et al., 1995a, and Georgakakos and Yao, 1995,* and *Georgakakos et al., 1997a,b,c*. ELQG is an iterative optimization procedure starting from an initial control sequence $\{\mathbf{u}(k); k = 0, 1, 2, .., N-1\}$ and subsequently generating increasingly better sequences until convergence. Convergence is achieved when the value of the performance index cannot be reduced any further. ELQG is reliable, computationally efficient, and especially suited for uncertain, multi- reservoir systems. A more detailed account of the ELQG optimization algorithm and features are included in Appendix D and in the cited references.

5.5. Heuristic Reservoir Regulation Rules

The optimal reservoir control approach presented in the previous chapter is a system wide optimization management tool. It utilizes the forecasted inflows and finds releases that maximize the system benefit as defined by the performance index. However, for a large system like the Nile Basin where the state dimensions are high, decision models may take some time to converge, and long term assessments may be computationally slow. Furthermore, decision systems are advanced mathematical methods and may be too advanced for some users.

For these reasons, the Nile RSM includes simpler and more practically intuitive reservoir regulation rules. Most such rules apply to individual reservoirs, in which the reservoir release depends on reservoir storage. Those rules are simple to implement. A typical example is the current operation rule of Lake Victoria. The current release of the Lake Victoria is given by the Agreed Curve, which specifies a relationship between lake level and release. Obviously, these rules do not offer any system wide (multi-reservoir) coordination. One such possibility includes rules that maintain uniform reservoir levels across a number of reservoirs. The Nile RSM includes four single reservoir regulation rules and two regional coordination rules. The following section describes those rules.

5.5.1 Reservoir Release-Elevation Rule

This is a single reservoir regulation rule. The release of a reservoir at any particular time is determined by its elevation:

$$u_i(k) = g(h_i(k))$$

where u is the discharge in cubic meters per second , h is the reservoir elevation in meters, and g is a function provided by the user.

Currently, this type of rule is used by the Equatorial Lakes. Figures 5.1 through 5.3 show these curves.

Figure 5.1: Natural Outflow Curve for Lake Victoria

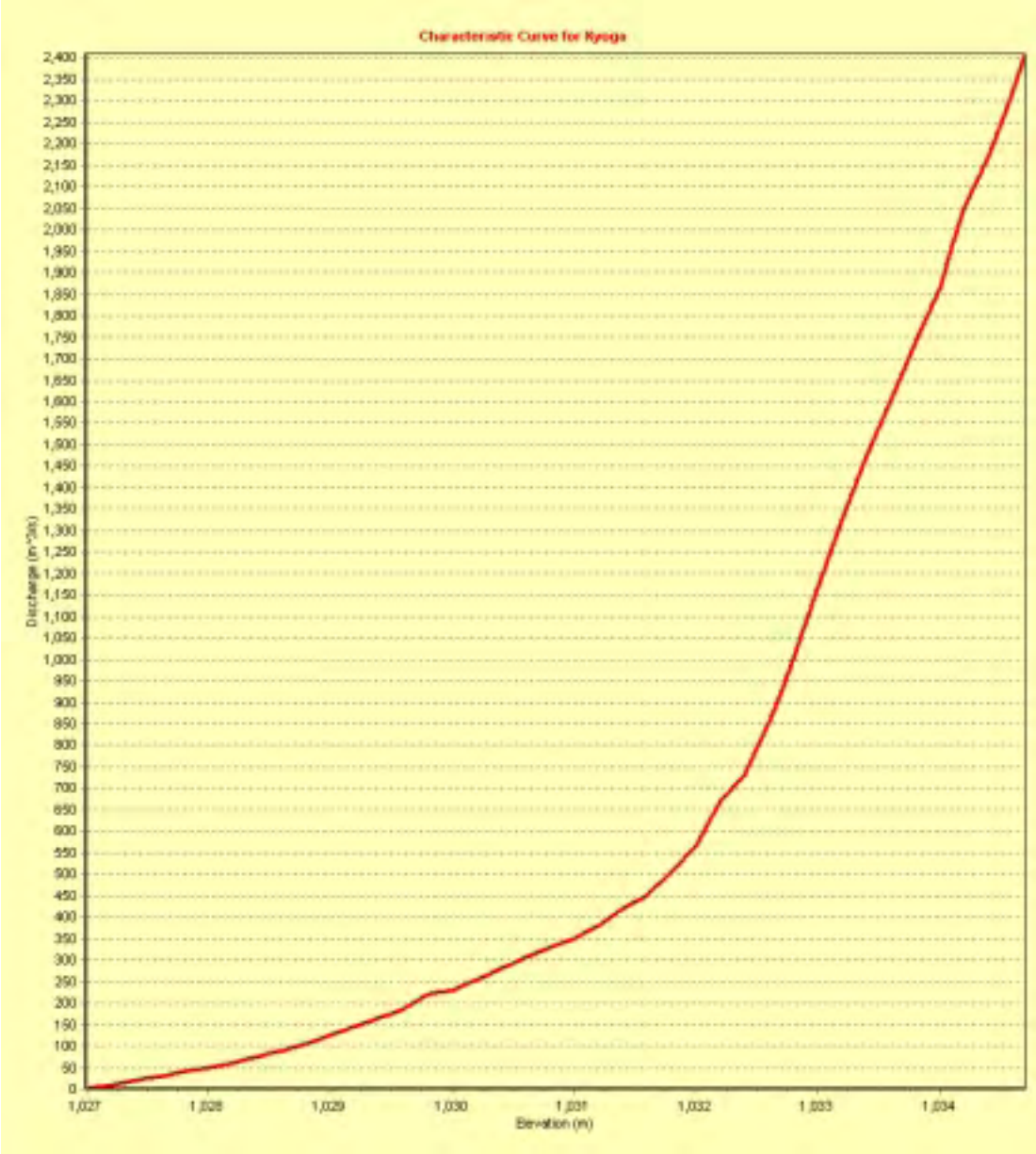

Figure 5.2: Natural Outflow Curve for Lake Kyoga

Figure 5.3: Natural Outflow Curve for Lake Albert

5.5.2 Reservoir Release-Elevation Rule (simplified version)

This is another single reservoir regulation rule. The release of a reservoir at any particular time is determined by its elevation. However, this function is not a smooth curve. Figure 5.4 depicts this rule. The rule divides the reservoir elevation into three zones: zone 1, zone 2, and zone 3. If the elevation is in zone 2, the release equals a constant Q_0; if the elevation is in zone 1, the release linearly slides to a minimum value; and if the elevation is in zone 3, the release linearly increases to a maximum value. The boundaries of the zones, the constant value Q_0, and the minimum and the maximum values are all user specifiable. The release is given by:

$$u_i(k) = \begin{cases} Q_{min} + \dfrac{h_i - h_{i\,min}}{h_1 - h_{i\,min}}(Q_0 - Q_{min}) & h_i \le h_{i1} \\ Q_0 & h_{i1} \le h_i \le h_{i2} \\ Q_0 + \dfrac{h_i - h_{i2}}{h_{i\,max} - h_{i2}}(Q_{max} - Q_0) & h_i \ge h_{i2} \end{cases}$$

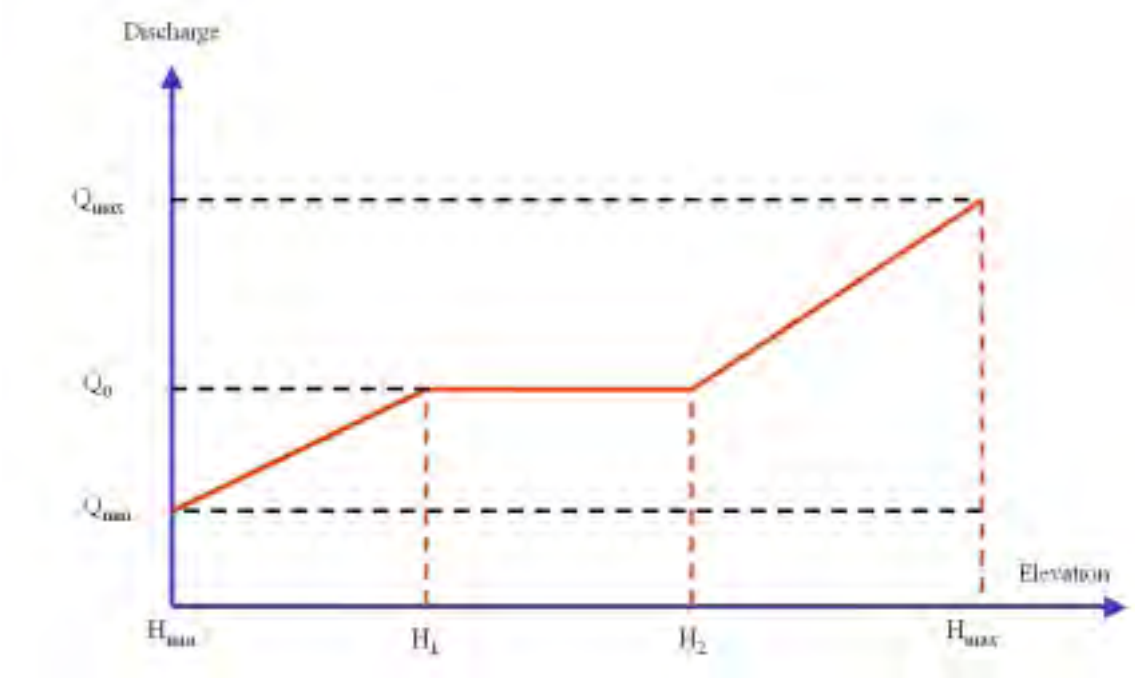

Figure 5.4: Simplified Release-Elevation Rule Curve

5.5.3 Target Reservoir Elevation Rule

This rule also applies to single reservoirs. The rule tries to follow target reservoir elevation sequence over time. The release for each period is determined by:

$$u_i(k) = S_i(k) + W_i(k) - e_i A_i(k) - D_i(k) - S_i(H_{tgt}(k+1))$$

where S is the storage, $H_{tgt}(k+1)$ is the target elevation at the end of the period, W is the inflow, D is the withdrawal, and eA is the evaporation loss (as a product of net evaporation rate, e, times surface area, A). Since inflow W is unknown at the beginning of the period, a forecasted value is used in the calculation.

A typical 10-day target elevation sequence for Gebel El Aulia is shown in Figure 5.5.

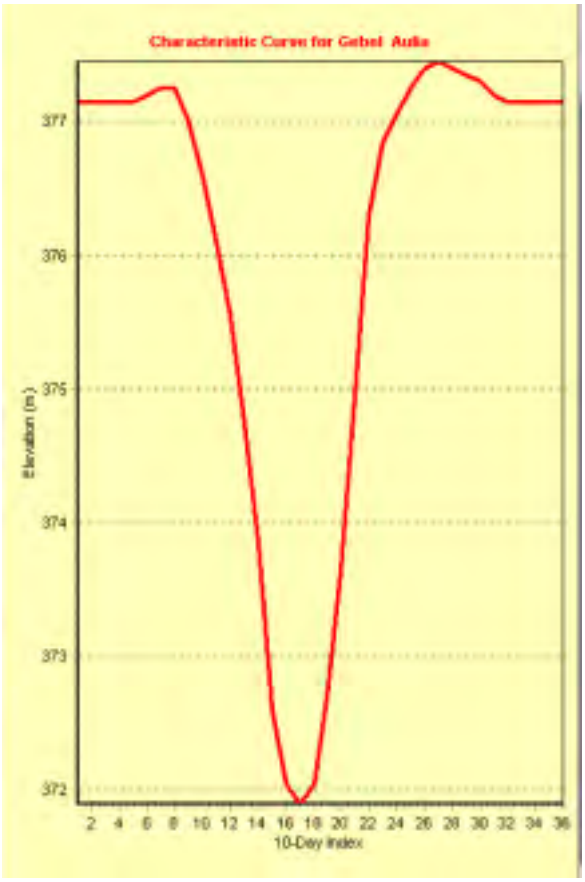

Figure 5.5: Gebel El Aulia Target Elevation

5.5.4 Target Release Rule

This single reservoir regulation rule operates the reservoir to follow a target release sequence. The release is simply equal to its target value:

$$u_i(k) = R_{itgt}(k)$$

where $R_{itgt}(k)$ is the target release for period k. The normal operation of the High Aswan Dam follows this type of rule, the target values being the 10-day downstream irrigation demands. A sample target release sequence is shown in Figure 5.6.

Figure 5.6: Sample HAD 10-day Irrigation Demands

5.5.5 Regional Coordination Rule

The Nile RSM additionally provides two coordination release rule options. The fist of these rules aims at keeping reservoir elevations fluctuating uniformly. This is accomplished as described below.

This coordination rule is built upon the single release rule. Figure 5.7 illustrates this rule.

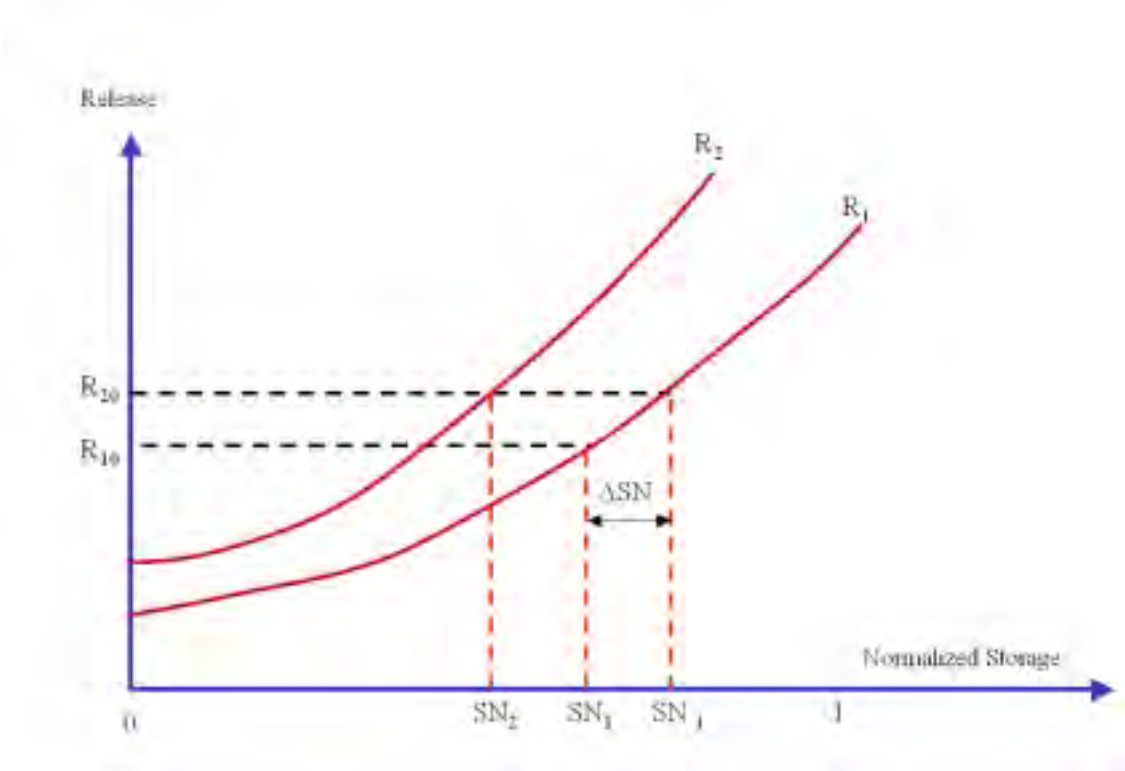

Figure 5.7: Reservoir Release Coordination Rule

As shown in the figure, R_1 and R_2 are the two single release rule curves for reservoir 1 and 2. The x-axis is the normalized storage value defined by:

$$SN_i(k) = \frac{S_i(k) - S_{i\,min}(k)}{S_{i\,max}(k) - S_{i\,min}(k)} \qquad i = 1,2,$$

where SN ranges from 0 to 1. To keep uniform reservoir levels implies that the SN values of both reservoirs are nearly equal at any period k. If the SN values are the same, the releases follow the individual rules. Otherwise, an adjustment is made according to the coordination rule.

The adjustment consists of changing the release from the upstream reservoir. Assume Reservoir 1 is the upstream reservoir, and the SN values are different. Then, a release adjustment is made according to

$$R_1(k) = R_{10} + \alpha \Delta SN$$
$$\Delta SN = SN_1^{'} - SN_1,$$

where R_{10} is the release determined based on the single release rule curve; SN_1 is the normalized storage value; SN_1' is the normalized storage value of the Reservoir 1 corresponding to release value R_2. α is a user definable coefficient to change the strength of the coordination. If α is zero, no coordination is used. It is noted that the two reservoirs do not necessarily have to be in a cascade formation. Furthermore, the rule can be applied to multiple reservoirs.

5.5.6 Customized Regulation Rules

The last type of rule that can be implemented by the Nile RSM is a customized rule that may include relationships among various variables of one or more reservoirs. Such a rule is included in Appendix E for Roseires, Sennar, and Girba.

Chapter 6

Scenario Assessment

The decision model developed in Chapter 5 provides a tool for managing the system over several months at 10-day time steps. However, to evaluate the long term system performance, or to compare different scenarios, a retrospective assessment model is needed.

The long term assessment model quantifies the performance of the system assuming that operations proceed according to the decision made by the decision model. At the beginning of each 10-day period in the historical record, the assessment model uses past historical data and generates forecasts of tributary inflows and lake net basin supplies. Next, it identifies the release policy for each system reservoir and implements only the releases of the first 10-day period. The release policies can be provided by the decision model or by the regulation rules. Lastly, it records the actual inflow and net basin supply values, simulates the system response, and repeats this cycle at the next 10-day period. At the end, this process generates sequences of every important system variable (including reservoir levels and releases, evaporation losses, and energy generation) and can provide a reliable assessment of system performance. The assessment framework is shown on Figure 6.1.

The Nile RSM assessment model can be used in various assessments. Typical applications are listed below:

- Value of various regulation, hydro-power, and irrigation projects along the White, Blue, and Main Nile branches; Such assessments could quantify the incremental benefits from individual development projects as well as the combined benefits from various project configurations;
- Implications of reservoir regulation rules for local, upstream, and downstream riparians;
- Marginal value (gain or loss) of irrigation with respect to hydropower at various basin locations;
- Irrigation versus hydropower tradeoffs for each nation, region, and the entire basin.

The Nile RSM utilizes several assessment criteria of possible interest to the Nile Basin nations. These criteria include

(i) severity and frequency of shortages with respect to user-specified water supply targets;

(ii) water withdrawals and losses over user-selected regions and times of the year;

(iii) reservoir and lake level drawdown and spillage statistics;

(iv) in-stream flow availability at user-selected river nodes and reaches;

(v) flood and drought severity and frequency;

(vi) wetland extent and variability; and

(vii) annual and firm energy generation statistics.

Clearly, the number of scenarios that can be defined is very large, adding to the versatility and value of the Nile RSM. At the completion of each assessment process, the results are analyzed to provide quantitative measures of system response and to compare different scenarios. In what follows, several assessment applications are presented and discussed.

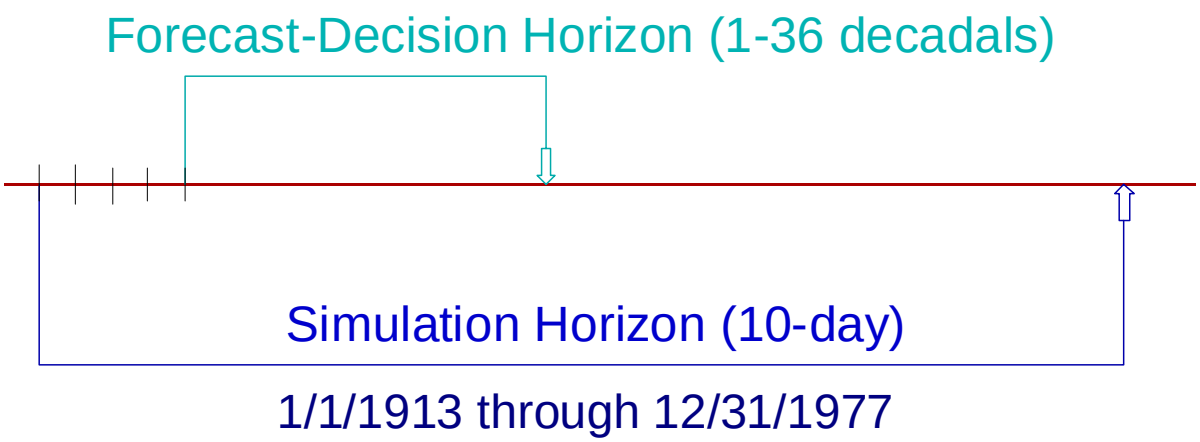

Figure 6.1: Scenario Assessment Framework

6.1. Scenario Assessment Examples

In this section, the scenario assessment process is applied to four case studies. These are defined next:

1. Baseline (Present basin conditions);
2. Southern Nile case study;
3. Eastern Nile case study;
4. Basin wide case study.

The first scenario represents the existing conditions of the Nile basin, and will serve as the baseline for all other scenarios. The Southern Nile scenario assessment attempts to quantify the effects of a change in the regulation of Lake Victoria aiming to maximize firm energy generation at the Owen Falls hydro electric facilities. A possible increase in the firm energy generation would certainly benefit the power sector. However, the question is whether the impacts to the downstream and upstream users would be appreciable. The Eastern Nile scenario aims to quantify the energy generation potential of the Ethiopian reservoirs and their possible impacts on the downstream users. The last scenario involves both Nile regions considering irrigation demand increases in both areas, full development in Ethiopia, and the construction of the Jonglei Canal.

In all scenarios, the historical monthly inflow records from 1/ 1913 to 12/1977 are used. This is the period when concurrent records exist for all locations. The reservoir initial elevations, annual withdrawals, and the transmission loss coefficients from the river reaches on Blue Nile are summarized in Table 6.1. The 10-day distributions of the annual withdrawals were discussed in Chapter 2.

Each assessment run generates voluminous output data. The results are saved into database for further study and analysis. Specifically, for reservoirs, the simulated sequences include elevation, release, inflow, energy, spillage, water deficit, and evaporation loss. For river nodes, the simulated sequences include inflow, water deficit, minimum deficit, and river flow. The simulated results can be viewed by different time resolution (10-day, monthly, or yearly), by

different plot type (time sequence chart or frequency chart), by different locations (reservoirs or river nodes), or by different parameters.

Table 6.1: Baseline Conditions

Reservoir/River Node	Initial Level (m)	Withdrawal (bcm/yr)	Loss Coef.
Victoria	1134	0	
Kyoga	1032	0	
Albert	622	0	
Gebel Aulia	377.15	1.5	
Tana	1786.5	0	
Karadobi	1140	0	
Mabil	900	0	
Mendaia	735	0	
Border	570	0	
Roseires	475	1.38	0.98
Sennar	420	15.62	0.99
Girba	465	1.5	0.97
HAD	175	0	
Diem		0	0.99
Dinder		0	0.99
Rahad		0	0.99

Baseline Scenario Assessment

The reservoir release rules used for this scenario are as follows:

- Lake Victoria, Kyoga, and Albert follow the natural outflow policy, as discussed in Chapter 5;
- Roseries, Sennar, and Girba follow the customized operating rules which are currently used in practice. Those rules are described in Appendix E;
- The High Aswan Dam releases according to the downstream demand target levels shown in Figure 5.6;
- The Gebel el Aulia reservoir operates according to its target elevation rule defined in

Chapter 5.

Figures 6.3 to 6.6 show the simulated 10-day sequences of levels, releases, energy, and river flows for selected reservoirs and river nodes. The elevation sequence indicates that the Equatorial lakes experienced a very significant rise during 1962 to 1964. Further downstream, the loss in the Sudd is also significant. Annual Mongala flow is 34.54 bcm, while the outflow upstream of Malakal is 16.59 bcm. The Sobat river contributes about 13.51 bcm a year. The annual flow at Diem on the Blue Nile is 50.33 bcm. After the Sudanese withdrawals, 34.31 bcm per year enters the Main Nile. Finally, about 68.67 bcm a year arrives Dongola, the entrance of Lake Nasser (High Aswan Dam). Of 68.67 bcm, 13 bcm lost to evaporation, and Egypt uses 55.5 bcm per year for irrigation and domestic water supply. In the baseline scenario, water withdrawals from the Equatorial Lake region and from the Blue Nile river basins in Ethiopia are negligible. Total Sudanese withdrawals (from both the White and the Blue Nile reaches) amount to 18.5 bcm. The simulation results show that the entire system has enough water to sustain the current needs. All reservoir elevations are relatively high. No water deficits occur in Sudan and Egypt.

Southern Nile Scenario Assessment

The reservoir release rules used for this scenario are as follows:

- Lakes Kyoga and Albert follow the natural outflow policy, as discussed in Chapter 5;
- Lake Victoria release rule is modified as shown in Figure 6.2; In addition, a minimum release bound is enforced at 60 mcm/day; The objective of this rule is to maintain high minimum flow;
- The rest of the reservoirs are regulated as in the baseline;
- Irrigation withdrawals as in the baseline.

Figure 6.7 compares the Owen Falls annual energy generation frequency curves for this and the base case. The comparison shows that under re-regulation the annual generation at Owen Falls is higher than the baseline for approximately 40% of the time (26 years). Annual firm energy is increased from 2400 to 3500 MWh/day, nearly a 50% increase. This increase is only due to the change of the existing release rule of Lake Victoria. The impact of the modified regulation rule on lake elevation and other quantities is shown in Figures 6.8 to 6.10. Figure 6.8 shows the Lake

Victoria elevation, release, and energy sequences. The elevation is slightly higher under this scenario than under the baseline. Lake release is constant during dry periods even though lake levels are low. The energy sequence follows the same pattern as the release. The simulated reservoir elevation sequences for Victoria, Kyoga, Albert, and HAD are shown in Figure 6.9. The elevation of Kyoga and Albert are smoother than the baseline for low flow periods since the Lake Victoria releases are more uniform. The impacts to the HAD are negligible. Figure 6.10 shows the flows at selected river nodes. The impacts to the flows at Pakwatch and Mongala are noticeable showing lesser variations than in the baseline case. The flow impacts downstream of Malakal are insignificant. This is also indicated by the frequency curves shown in Figure 6.11. The annual average flows at all locations are nearly the same as in the baseline case.

Eastern Nile Scenario Assessment

The reservoir release rules used for this scenario are as follows:

- The Ethiopian reservoirs (Tana, Karadobi, Mabil, Mendaia, and Border) follow a regional coordination rule with coordination coefficient $\alpha = 0.1$ and the individual reservoir release curves included in Appendix E;
- The rest of the reservoirs are regulated as in the baseline;
- Irrigation withdrawals as in the baseline.

Figure 6.12 plots the annual energy comparison by country between this case and the baseline. With all planned power facilities online, the Ethiopian annual energy generation reaches an average of 31,000 GWh, nearly three times the total hydro generation in Egypt, Sudan, and Uganda. The energy generation in Egypt and Uganda are the same as in the baseline case. However, the energy generation in Sudan is increased due to regulated outflow from the Ethiopian reservoirs. Figures 6.13 to 6.15 show the simulated sequences of elevation, release, and energy for the Ethiopian reservoirs. Reservoir levels are maintained high within their active range. Figure 6.16 shows the river flow sequences at Diem, Khartoum, and Dongola. The flows at all locations exhibit a smaller variation range than in the baseline case. The frequency curves (Figure 6.17) indicate that the maximum flow at Khartoum is reduced from 800 mcm/day to 520 mcm/day, a significant and desirable impact from a flood protection standpoint. Benefits also accrue from a drought management standpoint. Under this scenario, the time the river is dry is

only 2% comparing to more than 40% in the baseline case. Thus, in addition to energy generation, the planned reservoirs in Ethiopia can provide flood protection in Sudan and sustain the river flow during dry periods. The impact to HAD is mainly on the reservoir elevation. As shown in Figure 6.18, the HAD elevation fluctuation within a year is much less than the baseline case because of the regulated Blue Nile flows. No irrigation deficits are recorded.

Basin wide Scenario Assessment

The reservoir release rules used for this scenario are as follows:

- The Ethiopian reservoirs (Tana, Karadobi, Mabil, Mendaia, and Border) follow the regional coordination rule described in the Eastern Nile case study;
- The rest of the reservoirs are regulated as in the baseline;
- Irrigation withdrawals increase by 2 billion cubic meters per year in the Equatorial Lake region and by 8 bcm/year in Ethiopia; Irrigation withdrawals in Sudan and Egypt remain as in the baseline case;
- The Jonglei Canal is operational with a conveyance capacity of 43 mcm/day.

Figure 6.19 shows the flow sequence at Malakal and Melut. Clearly, the Jonglei Canal augments the flows by reducing Sudd evaporation from 17.8 to 6.73 bcm per year. The flow frequency curves for the same locations are shown in Figure 6.20. Figure 6.21 shows the flow sequences at Dongola. The flow fluctuations are much smaller due to the regulated flows from the Blue Nile reservoirs. The annual average flow is 70.5 bcm compared to 68.5 bcm of the baseline case. Namely, all irrigation requirements (new and old) are met fully. Figure 6.22 shows the corresponding elevation, release, and energy sequences for HAD. The release and Energy generation sequences are the same as in the baseline case, while higher HAD elevation sequence is due to the additional water generated at the Sudd. The previous assessment does not quantify the effects of the Jonglei Canal on the Sudd. At present, however, this capability does not exist within the Nile RSM. Under this scenario, Lake Victoria energy generation decreases by approximately 6% due to upstream withdrawals. Similarly, Ethiopian energy generation decreases by 24% as a result of Ethiopian irrigation withdrawals and lower reservoir levels. The annual statistics for all scenarios are summarized in Tables 6.2 and 6.3. The units are GWh for energy generation and bcm for all other quantities.

Table 6.2: Reservoir Annual Statistics

ID	Name	Parameters	Scenarios			
			Baseline	E. Nile	S. Nile	Basinwide
1	Victoria	Energy	1535.88	1535.88	1515.06	1423.80
1	Victoria	Local Inflow	27.26	27.26	27.26	27.26
1	Victoria	Outflow	26.18	26.18	25.58	24.32
1	Victoria	Req Withdrawal	0.00	0.00	0.00	2.00
1	Victoria	Withdrawal Deficit	0.00	0.00	0.00	0.00
2	Kyoga	Energy	0.00	0.00	0.00	0.00
2	Kyoga	Local Inflow	-0.51	-0.51	-0.51	-0.51
2	Kyoga	Outflow	25.60	25.60	25.00	23.75
2	Kyoga	Req Withdrawal	0.00	0.00	0.00	0.00
2	Kyoga	Withdrawal Deficit	0.00	0.00	0.00	0.00
3	Albert	Energy	0.00	0.00	0.00	0.00
3	Albert	Local Inflow	3.70	3.70	3.70	3.70
3	Albert	Outflow	29.32	29.32	28.72	27.47
3	Albert	Req Withdrawal	0.00	0.00	0.00	0.00
3	Albert	Withdrawal Deficit	0.00	0.00	0.00	0.00
4	Gebel Aulia	Energy	0.00	0.00	0.00	0.00
4	Gebel Aulia	Local Inflow	0.00	0.00	0.00	0.00
4	Gebel Aulia	Outflow	25.43	25.49	25.33	35.15
4	Gebel Aulia	Req Withdrawal	1.50	1.50	1.50	1.50
4	Gebel Aulia	Withdrawal Deficit	0.00	0.00	0.00	0.00
5	Tana	Energy	0.00	1752.91	0.00	1586.81
5	Tana	Local Inflow	4.16	4.16	4.16	4.16
5	Tana	Outflow	4.16	4.15	4.16	3.21
5	Tana	Req Withdrawal	0.00	0.00	0.00	1.00
5	Tana	Withdrawal Deficit	0.00	0.00	0.00	0.00
6	Karadobi	Energy	0.00	7749.22	0.00	4002.71
6	Karadobi	Local Inflow	15.48	15.48	15.48	15.48
6	Karadobi	Outflow	19.65	19.42	19.65	13.71
6	Karadobi	Req Withdrawal	0.00	0.00	0.00	4.99
6	Karadobi	Withdrawal Deficit	0.00	0.00	0.00	0.00
7	Mabil	Energy	0.00	5872.14	0.00	3685.96
7	Mabil	Local Inflow	8.79	8.79	8.79	8.79
7	Mabil	Outflow	28.43	28.12	28.43	22.44
7	Mabil	Req Withdrawal	0.00	0.00	0.00	0.00
7	Mabil	Withdrawal Deficit	0.00	0.00	0.00	0.00
8	Mendaia	Energy	0.00	9494.48	0.00	8251.60
8	Mendaia	Local Inflow	13.37	13.37	13.37	13.37
8	Mendaia	Outflow	41.80	41.32	41.80	33.65
8	Mendaia	Req Withdrawal	0.00	0.00	0.00	2.00
8	Mendaia	Withdrawal Deficit	0.00	0.00	0.00	0.00
9	Border	Energy	0.00	6441.22	0.00	6174.04
9	Border	Local Inflow	8.52	8.52	8.52	8.52
9	Border	Outflow	50.33	49.66	50.33	41.95
9	Border	Req Withdrawal	0.00	0.00	0.00	0.00
9	Border	Withdrawal Deficit	0.00	0.00	0.00	0.00
10	Roseires	Energy	1384.64	2010.97	1384.64	1925.52
10	Roseires	Local Inflow	0.00	0.00	0.00	0.00
10	Roseires	Outflow	47.94	47.16	47.94	39.53
10	Roseires	Req Withdrawal	1.38	1.38	1.38	1.38
10	Roseires	Withdrawal Deficit	0.00	0.00	0.00	0.00
11	Sennar	Energy	63.56	126.93	63.56	122.99
11	Sennar	Local Inflow	0.00	0.00	0.00	0.00
11	Sennar	Outflow	31.29	30.32	31.29	22.85
11	Sennar	Req Withdrawal	15.61	15.61	15.61	15.61
11	Sennar	Withdrawal Deficit	0.16	0.00	0.16	0.00
12	Girba	Energy	822.24	822.24	822.24	822.24
12	Girba	Local Inflow	11.79	11.79	11.79	11.79
12	Girba	Outflow	11.65	11.65	11.65	11.65
12	Girba	Req Withdrawal	0.00	0.00	0.00	0.00
12	Girba	Withdrawal Deficit	0.00	0.00	0.00	0.00
13	HAD	Energy	11726.58	11675.94	11715.18	12157.65
13	HAD	Local Inflow	0.00	0.00	0.00	0.00
13	HAD	Outflow	55.50	55.50	55.50	55.50
13	HAD	Req Withdrawal	0.00	0.00	0.00	0.00
13	HAD	Withdrawal Deficit	0.00	0.00	0.00	0.00

Table 6.3: River Node Annual Statistics

NodeID	NodeName	Parameters	Scenarios			
			Baseline	E. Nile	S. Nile	Basinwide
40	Pakwatch	Local Inflow	0.00	0.00	0.00	0.00
40	Pakwatch	Outflow	29.32	29.32	28.72	27.47
40	Pakwatch	Required WithDrawal	0.00	0.00	0.00	0.00
40	Pakwatch	Withdrawal Deficit	0.00	0.00	0.00	0.00
50	Torrents	Local Inflow	4.81	4.81	4.81	4.81
50	Torrents	Outflow	34.13	34.13	33.53	32.29
50	Torrents	Required WithDrawal	0.00	0.00	0.00	0.00
50	Torrents	Withdrawal Deficit	0.00	0.00	0.00	0.00
60	Mongala	Local Inflow	0.00	0.00	0.00	0.00
60	Mongala	Outflow	34.49	34.54	34.11	33.39
60	Mongala	Required WithDrawal	0.00	0.00	0.00	0.00
60	Mongala	Withdrawal Deficit	0.00	0.00	0.00	0.00
70	Sudd	Local Inflow	0.00	0.00	0.00	0.00
70	Sudd	Outflow	16.58	16.59	16.47	26.66
70	Sudd	Required WithDrawal	0.00	0.00	0.00	0.00
70	Sudd	Withdrawal Deficit	0.00	0.00	0.00	0.00
80	Sobat	Local Inflow	13.51	13.51	13.51	13.51
80	Sobat	Outflow	13.51	13.51	13.51	13.51
80	Sobat	Required WithDrawal	0.00	0.00	0.00	0.00
80	Sobat	Withdrawal Deficit	0.00	0.00	0.00	0.00
90	Malakal	Local Inflow	0.00	0.00	0.00	0.00
90	Malakal	Outflow	30.09	30.11	29.99	40.18
90	Malakal	Required WithDrawal	0.00	0.00	0.00	0.00
90	Malakal	Withdrawal Deficit	0.00	0.00	0.00	0.00
100	Melut	Local Inflow	0.00	0.00	0.00	0.00
100	Melut	Outflow	30.02	30.06	29.91	40.50
100	Melut	Required WithDrawal	0.00	0.00	0.00	0.00
100	Melut	Withdrawal Deficit	0.00	0.00	0.00	0.00
170	Diem	Local Inflow	0.00	0.00	0.00	0.00
170	Diem	Outflow	50.33	49.66	50.33	41.95
170	Diem	Required WithDrawal	0.00	0.00	0.00	0.00
170	Diem	Withdrawal Deficit	0.00	0.00	0.00	0.00
200	Dinder	Local Inflow	2.94	2.94	2.94	2.94
200	Dinder	Outflow	33.91	32.95	33.91	25.56
200	Dinder	Required WithDrawal	0.00	0.00	0.00	0.00
200	Dinder	Withdrawal Deficit	0.00	0.00	0.00	0.00
210	Rahad	Local Inflow	1.09	1.09	1.09	1.09
210	Rahad	Outflow	34.66	33.71	34.66	26.39
210	Rahad	Required WithDrawal	0.00	0.00	0.00	0.00
210	Rahad	Withdrawal Deficit	0.00	0.00	0.00	0.00
220	Khartoum	Local Inflow	0.00	0.00	0.00	0.00
220	Khartoum	Outflow	34.31	33.38	34.31	26.12
220	Khartoum	Required WithDrawal	0.00	0.00	0.00	0.00
220	Khartoum	Withdrawal Deficit	0.00	0.00	0.00	0.00
230	BNJunction	Local Inflow	0.00	0.00	0.00	0.00
230	BNJunction	Outflow	11.30	11.30	11.30	11.30
230	BNJunction	Required WithDrawal	0.00	0.00	0.00	0.00
230	BNJunction	Withdrawal Deficit	0.00	0.00	0.00	0.00
260	Atbara	Local Inflow	0.00	0.00	0.00	0.00
260	Atbara	Outflow	71.40	70.51	71.29	72.92
260	Atbara	Required WithDrawal	0.00	0.00	0.00	0.00
260	Atbara	Withdrawal Deficit	0.00	0.00	0.00	0.00
280	Dongola	Local Inflow	0.00	0.00	0.00	0.00
280	Dongola	Outflow	68.62	67.86	68.51	70.50
280	Dongola	Required WithDrawal	0.00	0.00	0.00	0.00
280	Dongola	Withdrawal Deficit	0.00	0.00	0.00	0.00
300	DS HAD	Local Inflow	0.00	0.00	0.00	0.00
300	DS HAD	Outflow	0.00	0.00	0.00	0.00
300	DS HAD	Required WithDrawal	55.50	55.50	55.50	55.50
300	DS HAD	Withdrawal Deficit	0.00	0.00	0.00	0.00

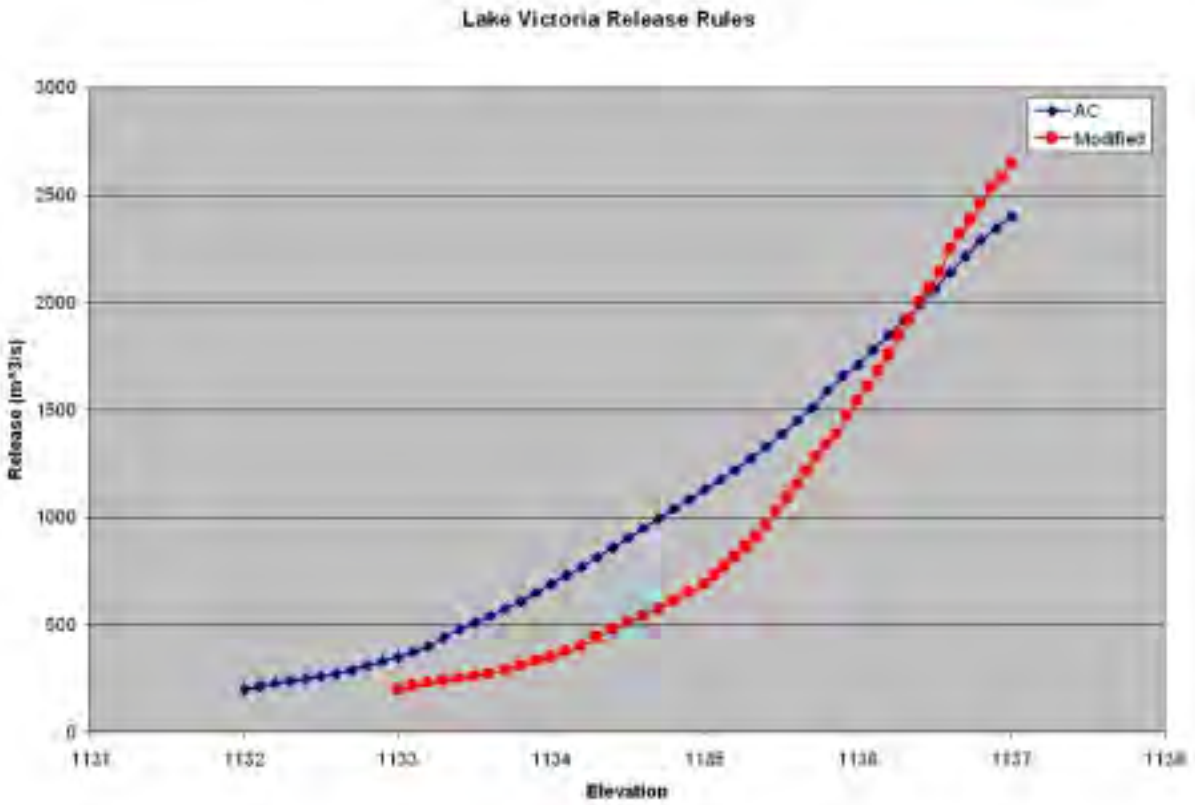

Figure 6.2: Modified Release Rule for Lake Victoria

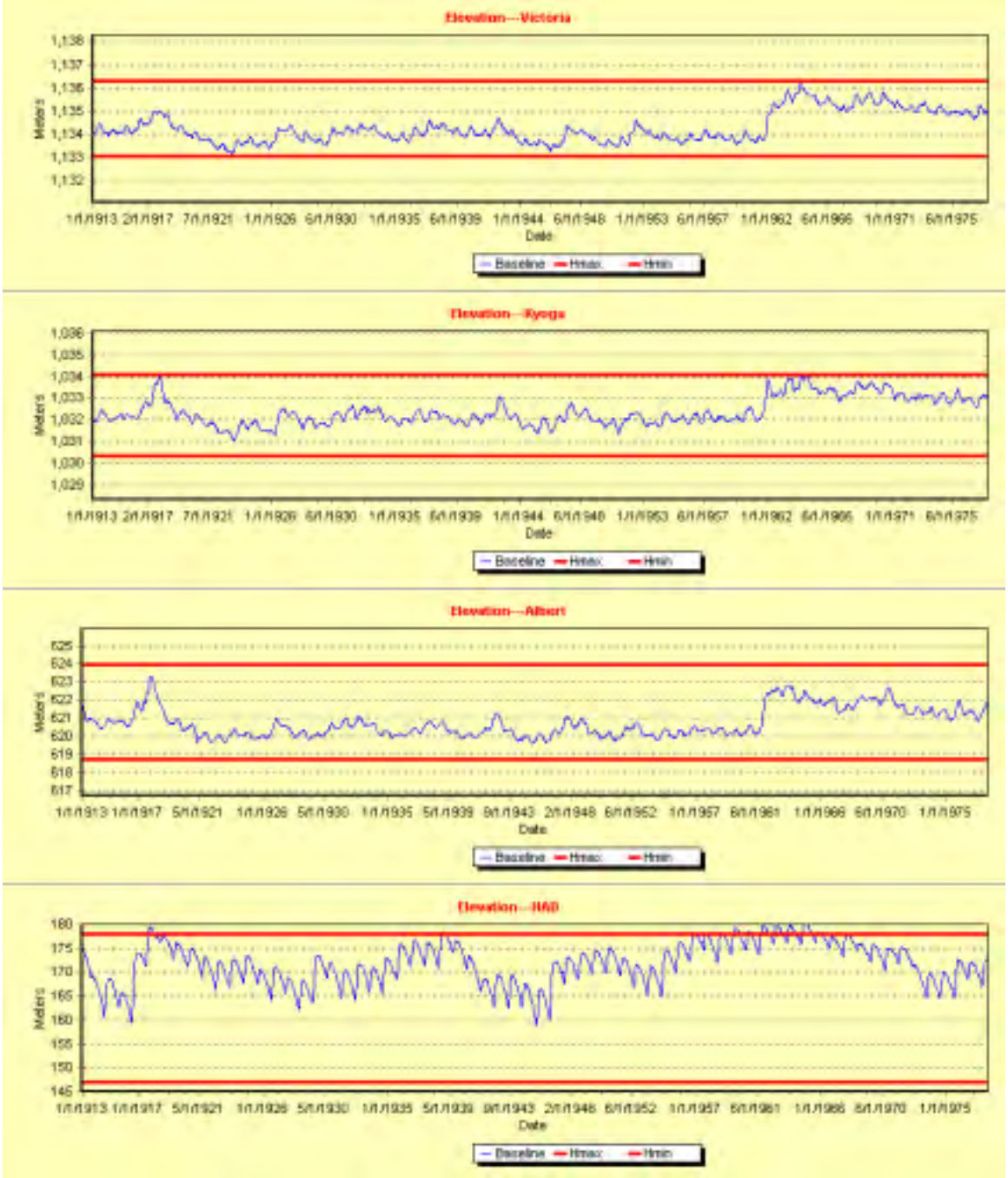

Figure 6.3: Simulated Elevation Sequences for Selected Reservoirs; Baseline Case

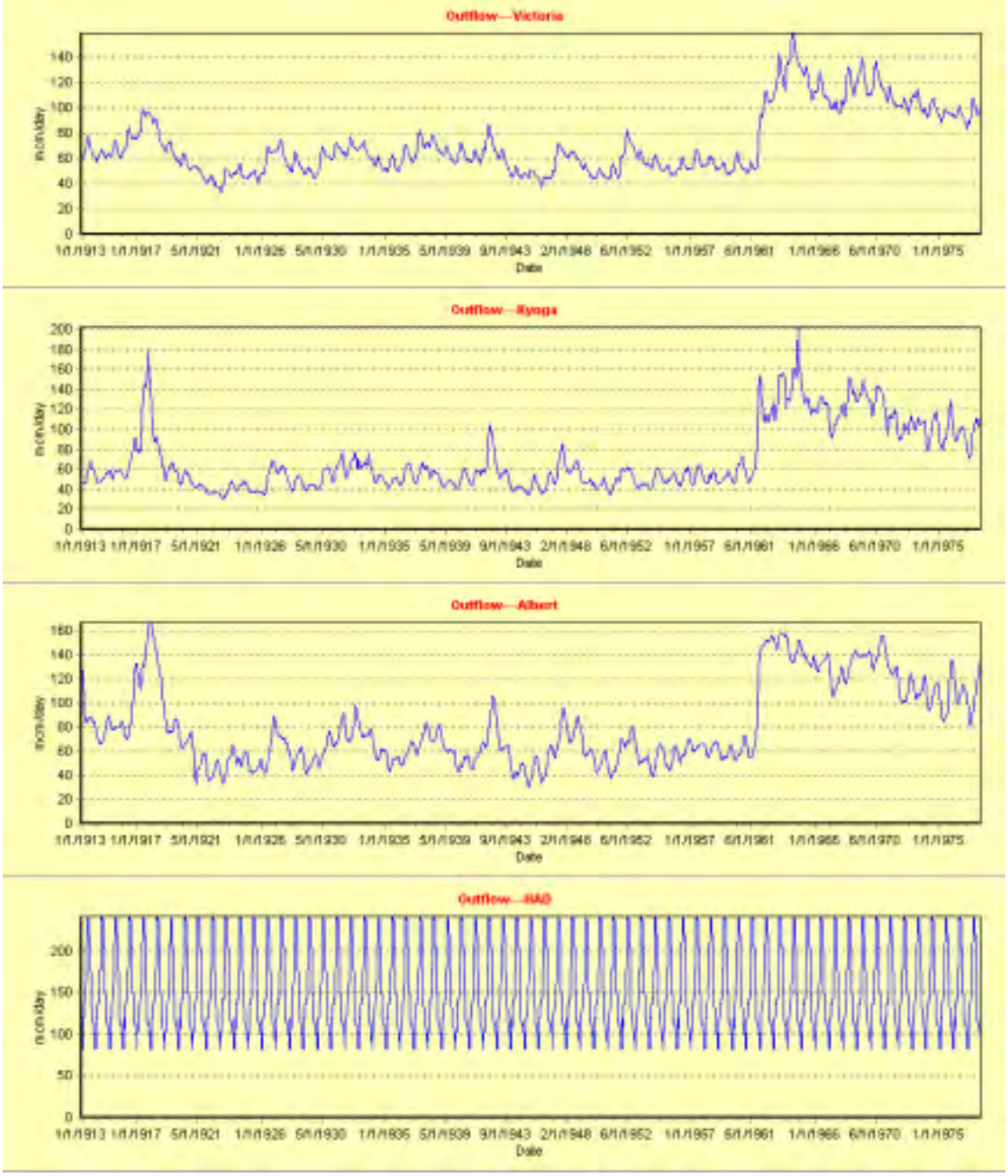

Figure 6.2: Simulated Release Sequences for Selected Reservoirs; Baseline Case

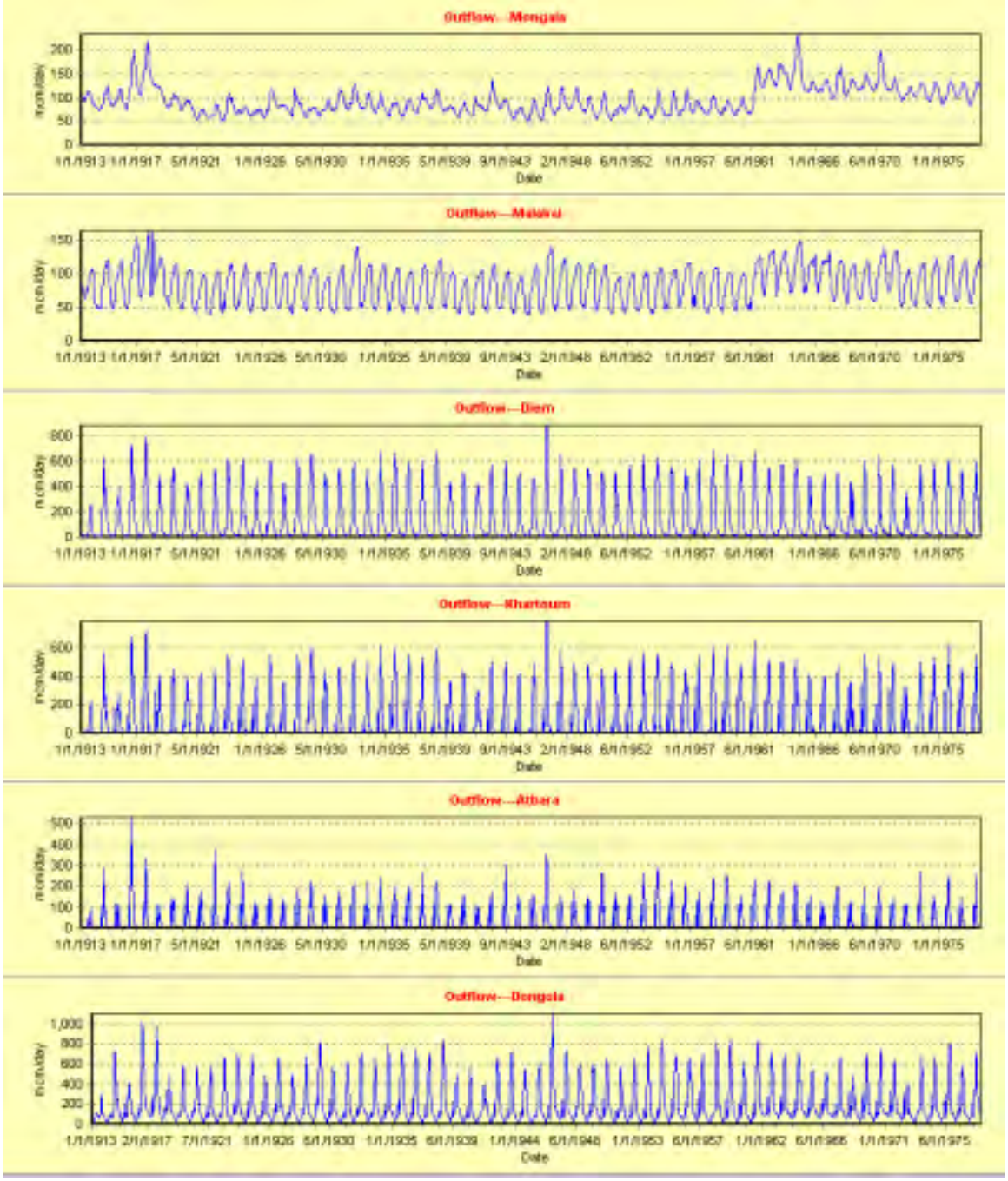

Figure 6.5: Simulated Flow Sequences for Selected River Nodes; Baseline Case

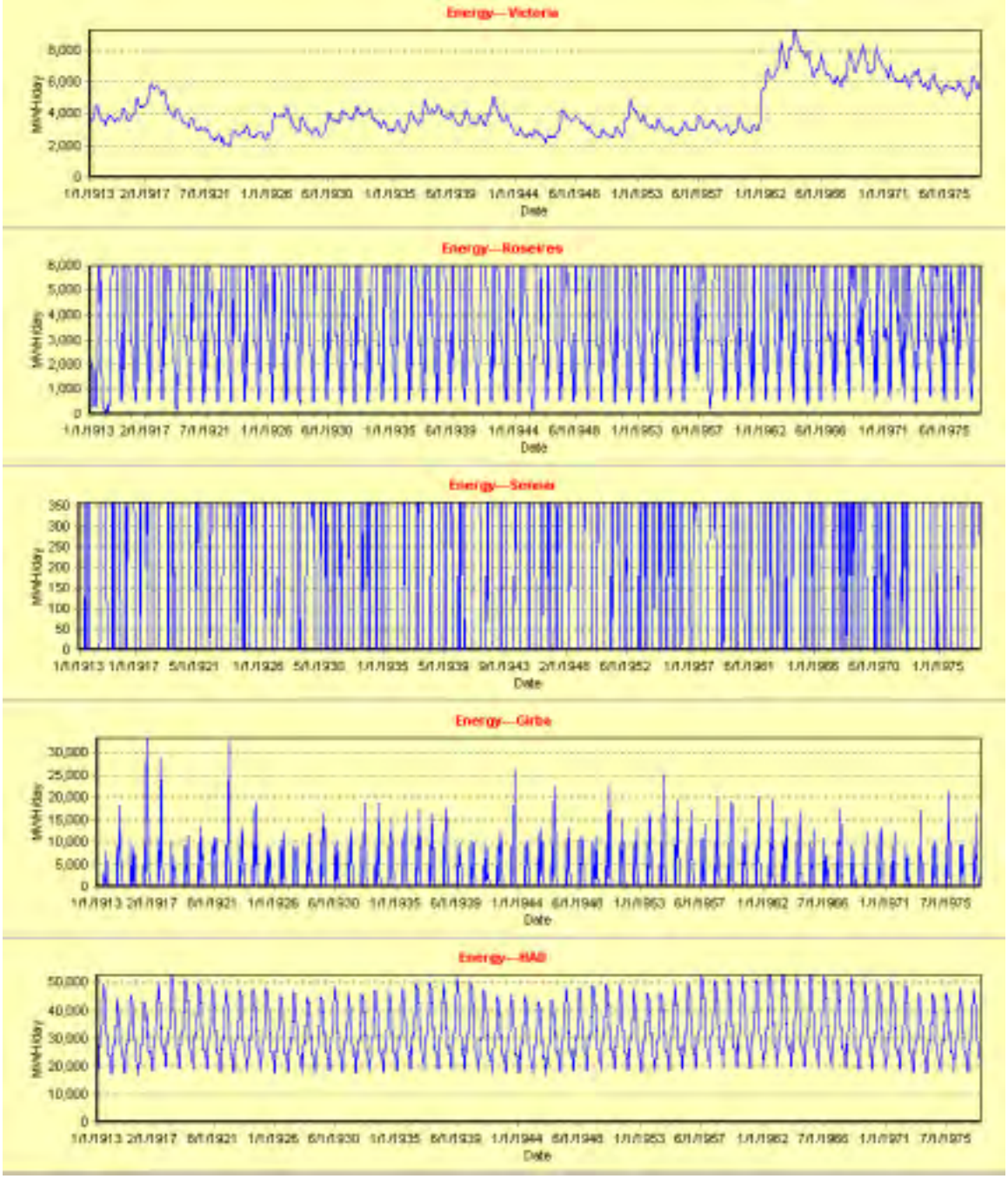

Figure 6.6: Simulated Energy Sequences for Selected Reservoirs; Baseline Case

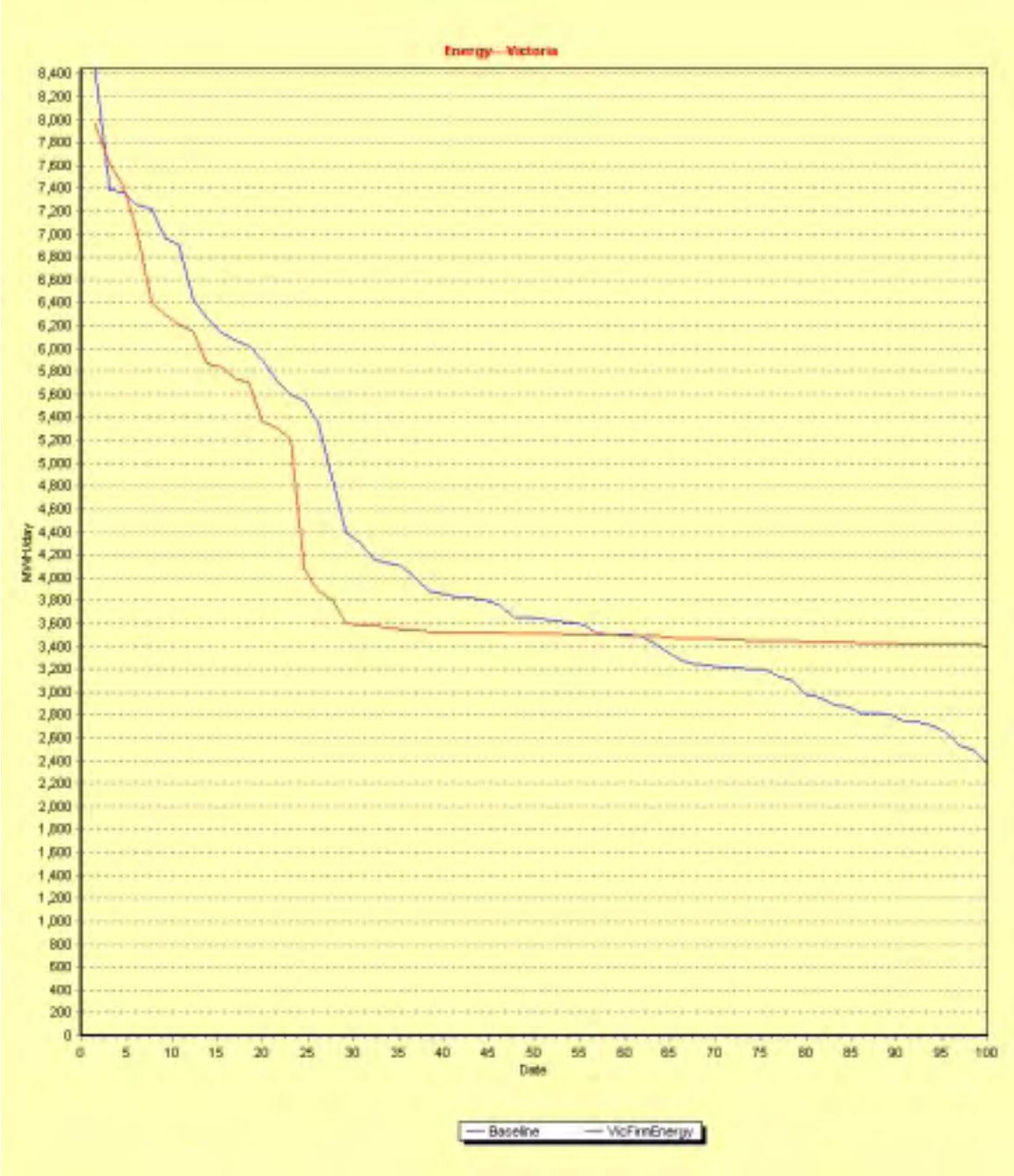

Figure 6.7: Simulated Annual Energy Frequency Curve Comparison

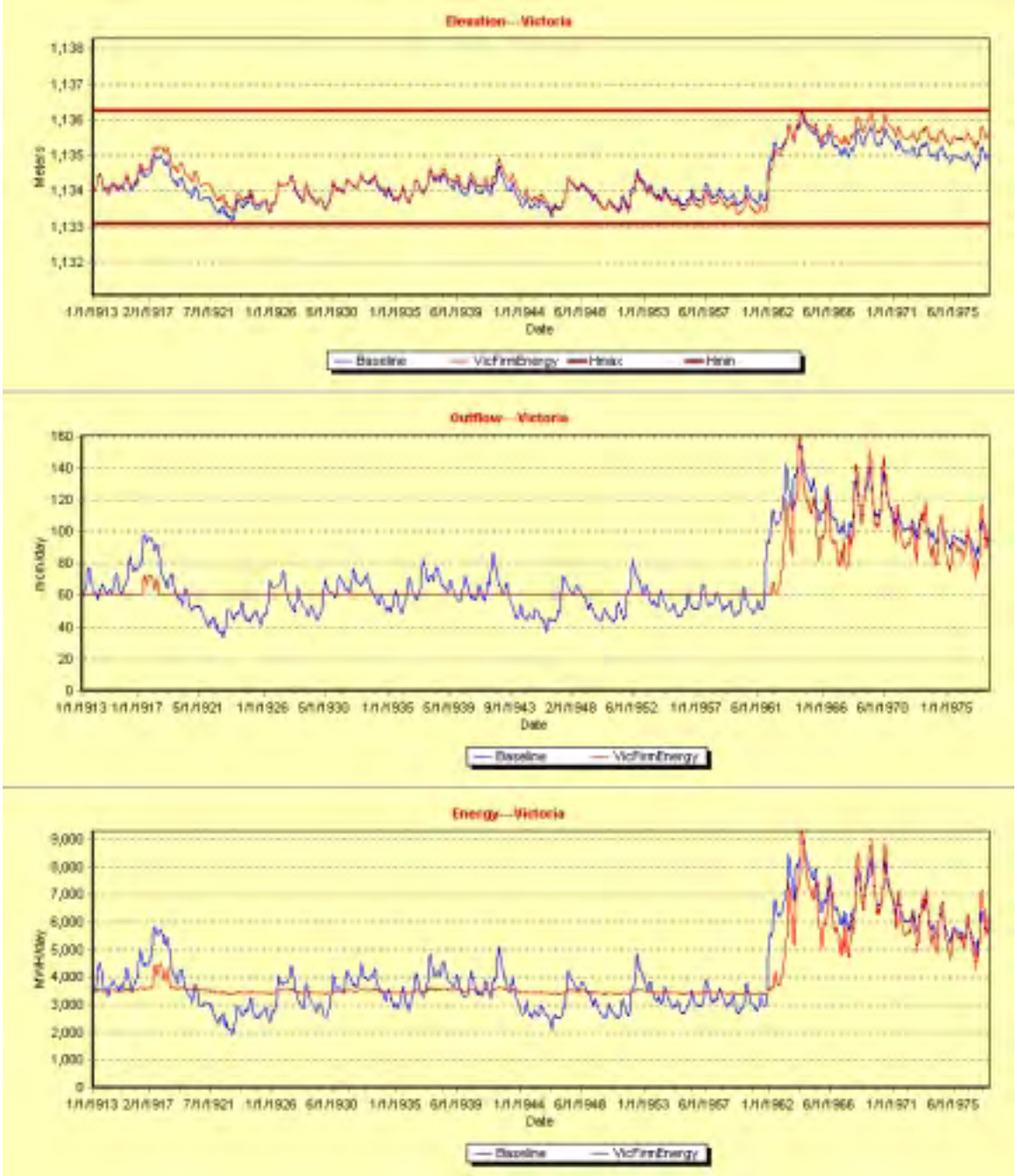

Figure 6.8: Simulated Sequences for Lake Victoria; Southern Nile Scenario

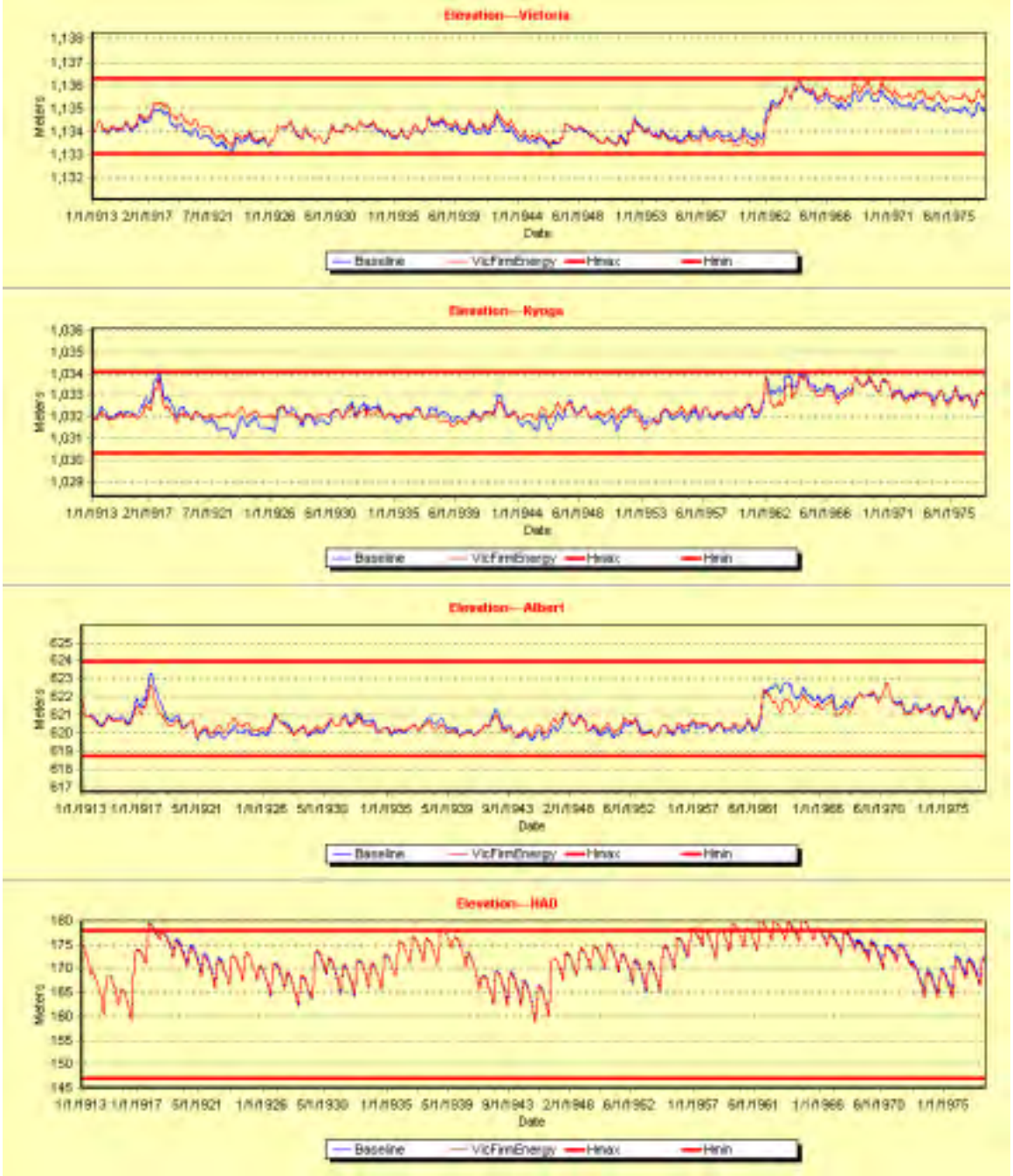

Figure 6.9: Simulated Elevation Sequences for Selected Reservoirs; Southern Nile Scenario

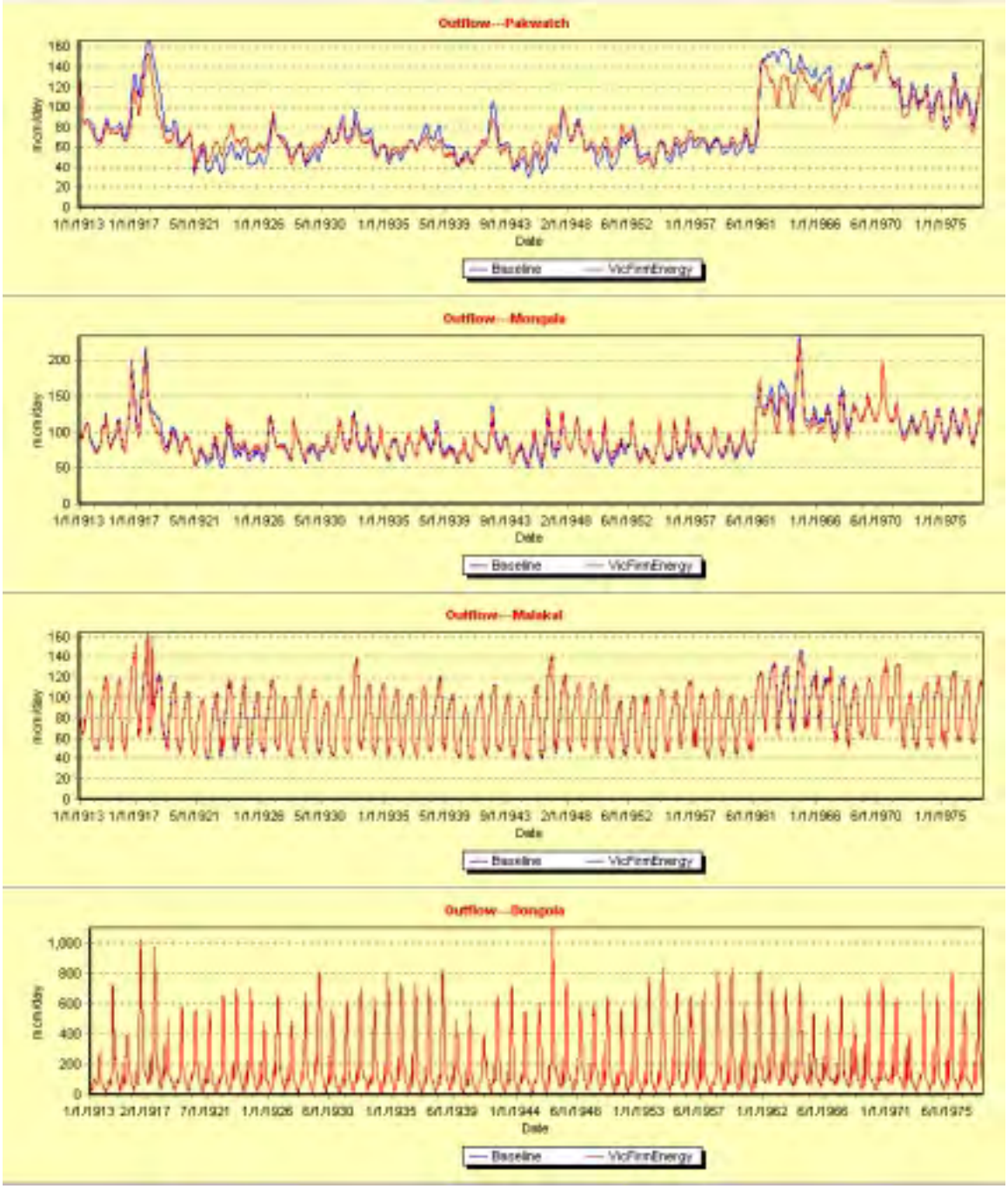

Figure 6.10: Simulated River Flow Sequences at Selected River Nodes; Southern Nile Scenario

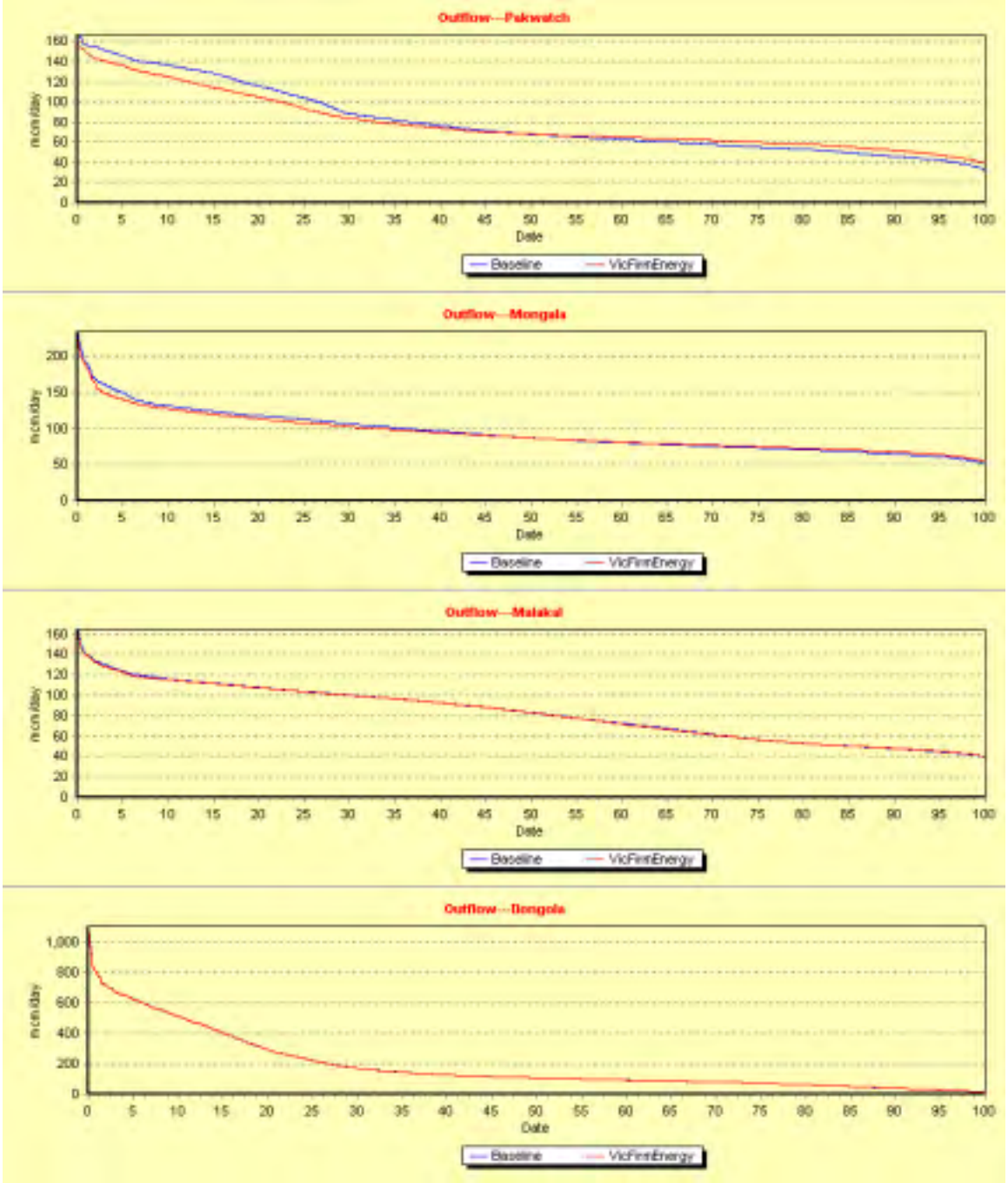

Figure 6.11: Simulated River Flow Frequency Curves at Selected River Nodes; Southern Nile Scenario

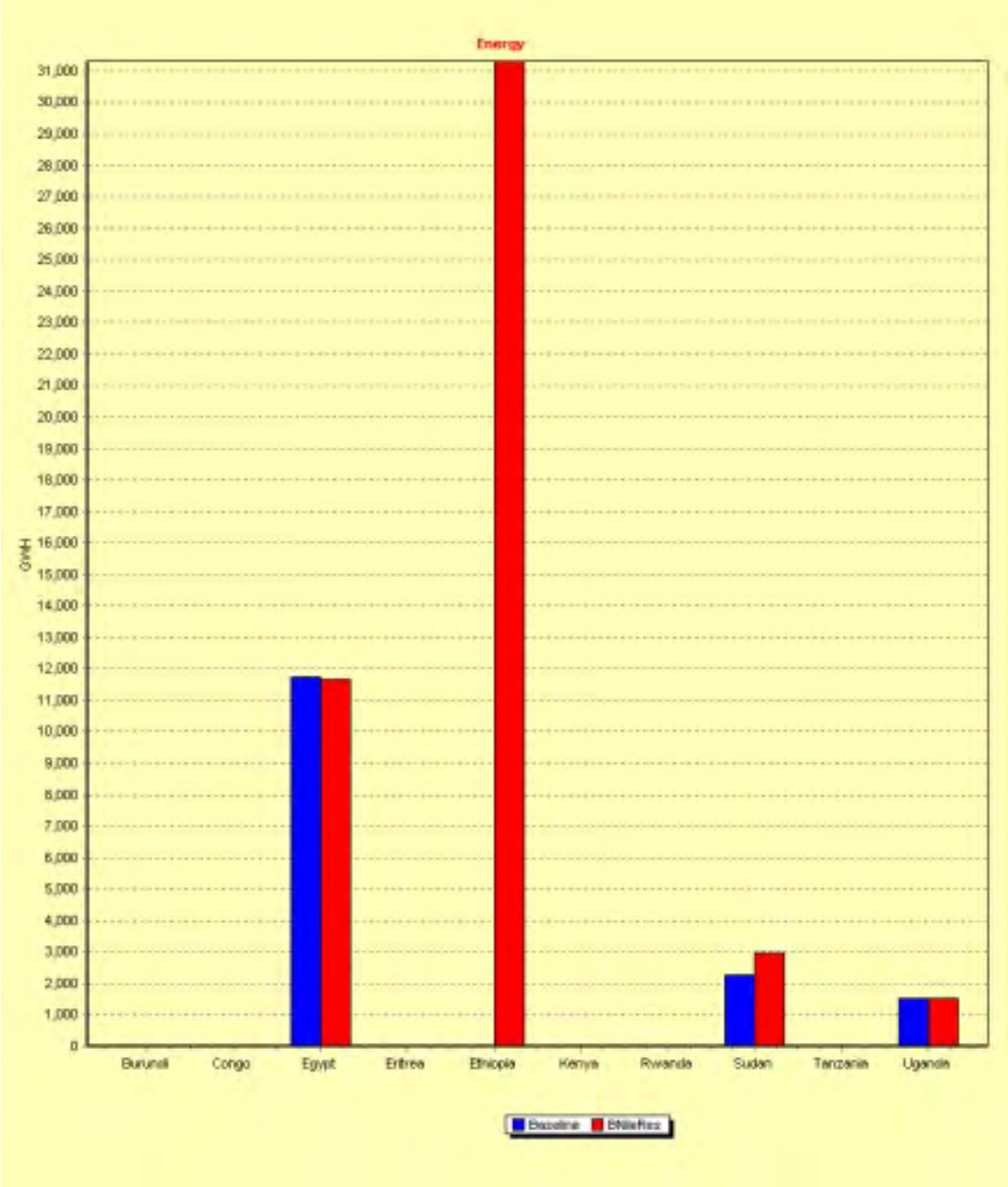

Figure 6.12: Energy Generation by Country; Eastern Nile Scenario

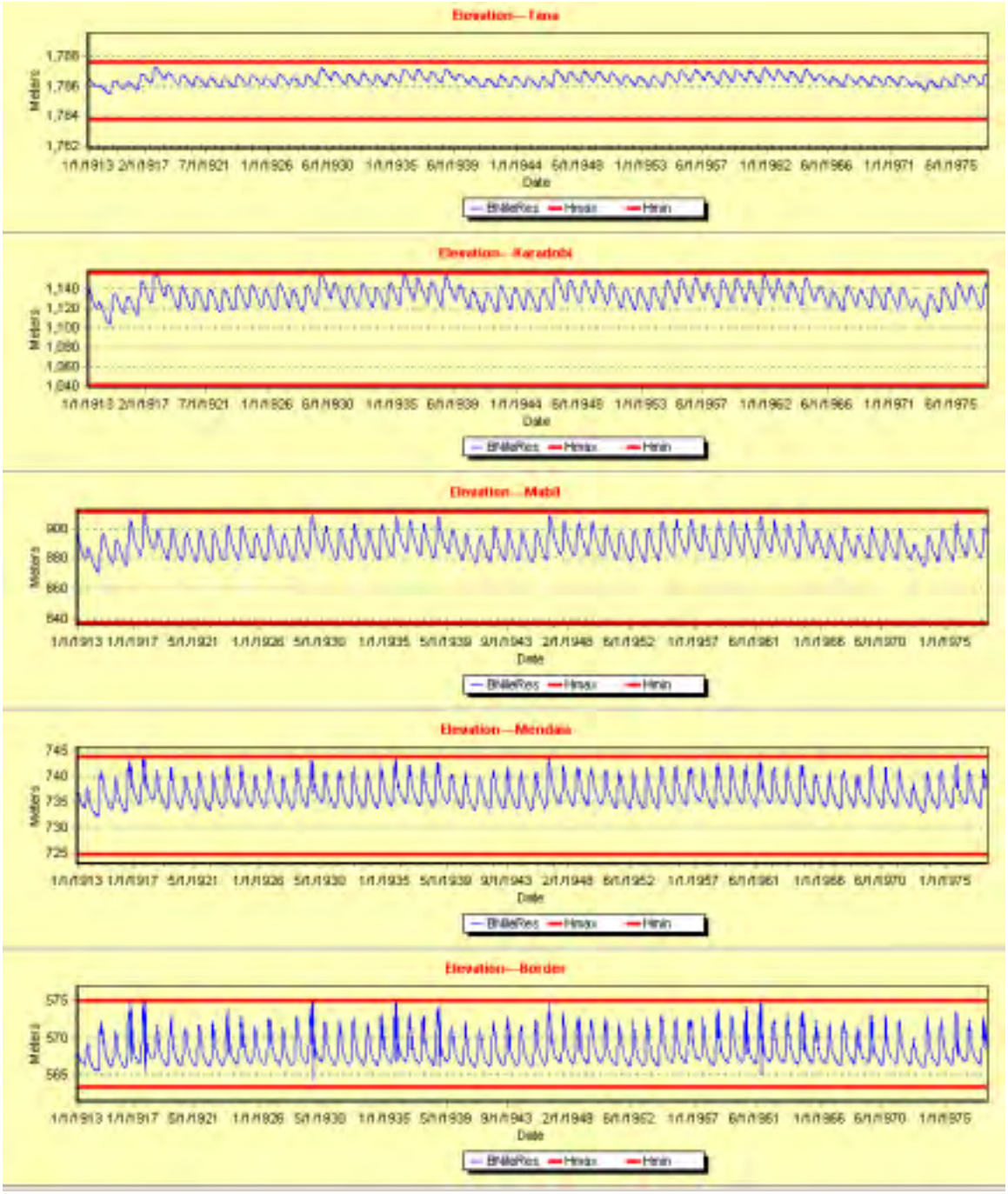

Figure 6.13: Simulated Reservoir Elevation for Blue Nile Reservoirs; Eastern Nile Scenario

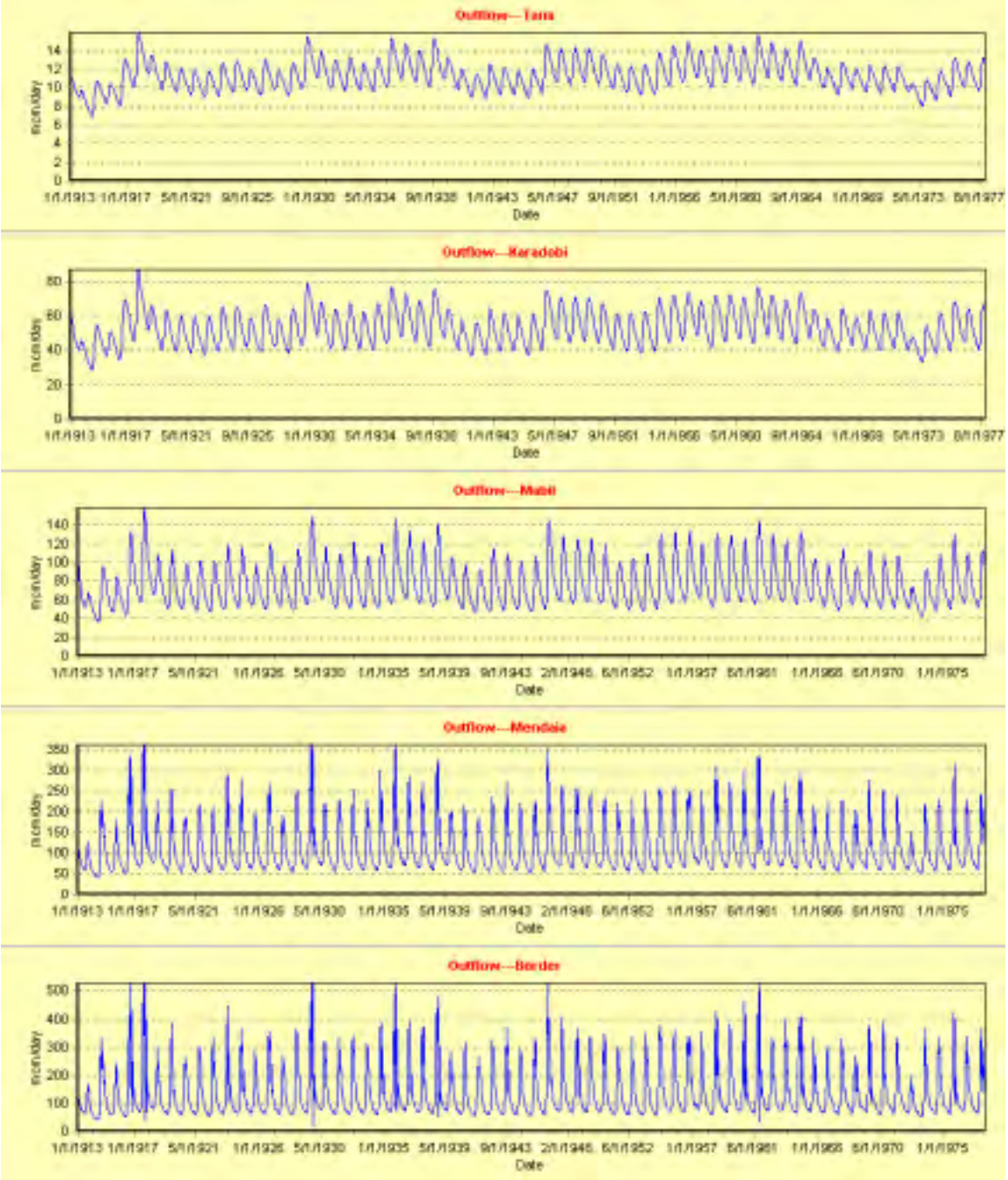

Figure 6.14: Simulated Reservoir Release for Blue Nile Reservoirs; Eastern Nile Scenario

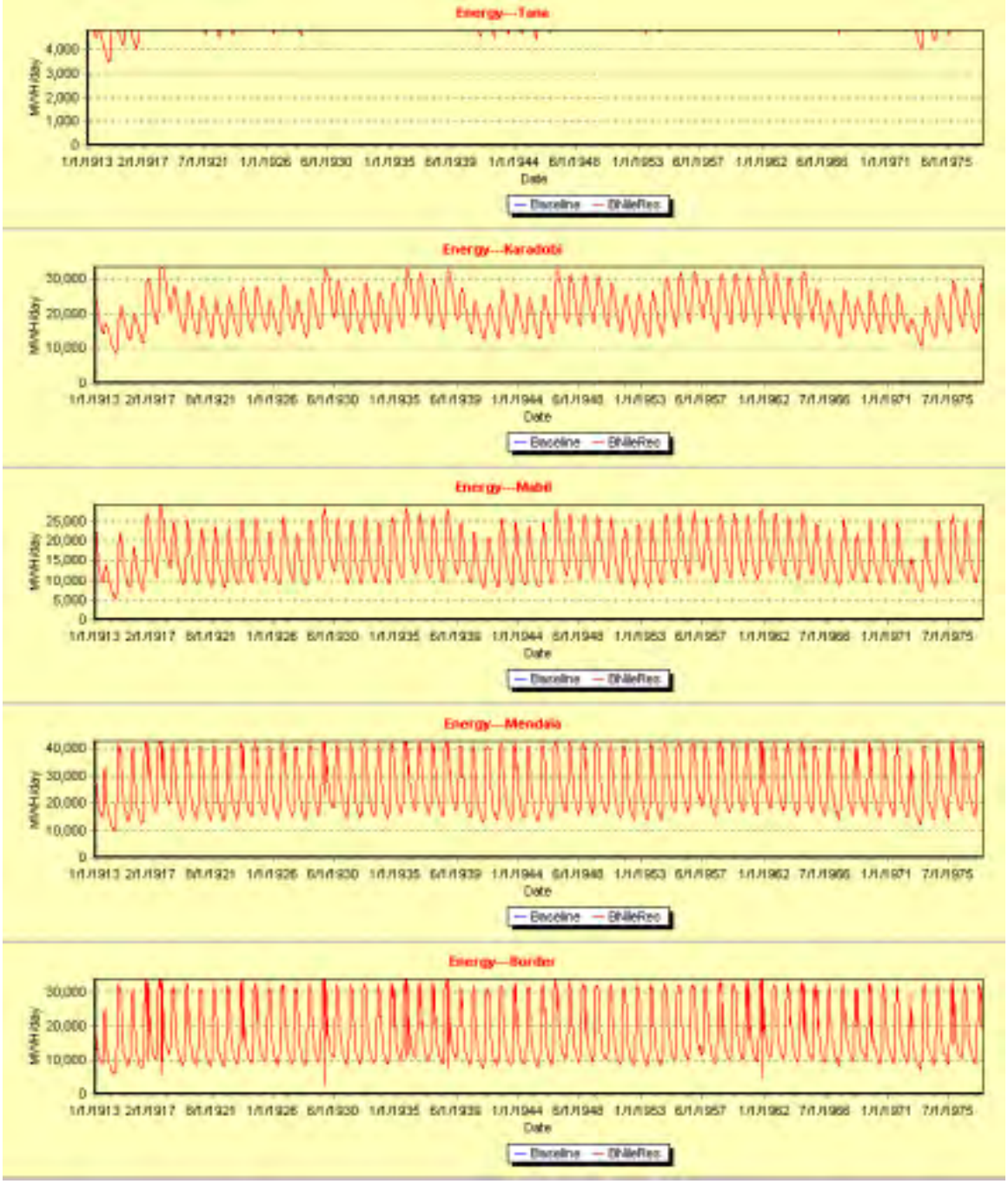

Figure 6.15: Simulated Reservoir Energy for Blue Nile Reservoirs; Eastern Nile Scenario

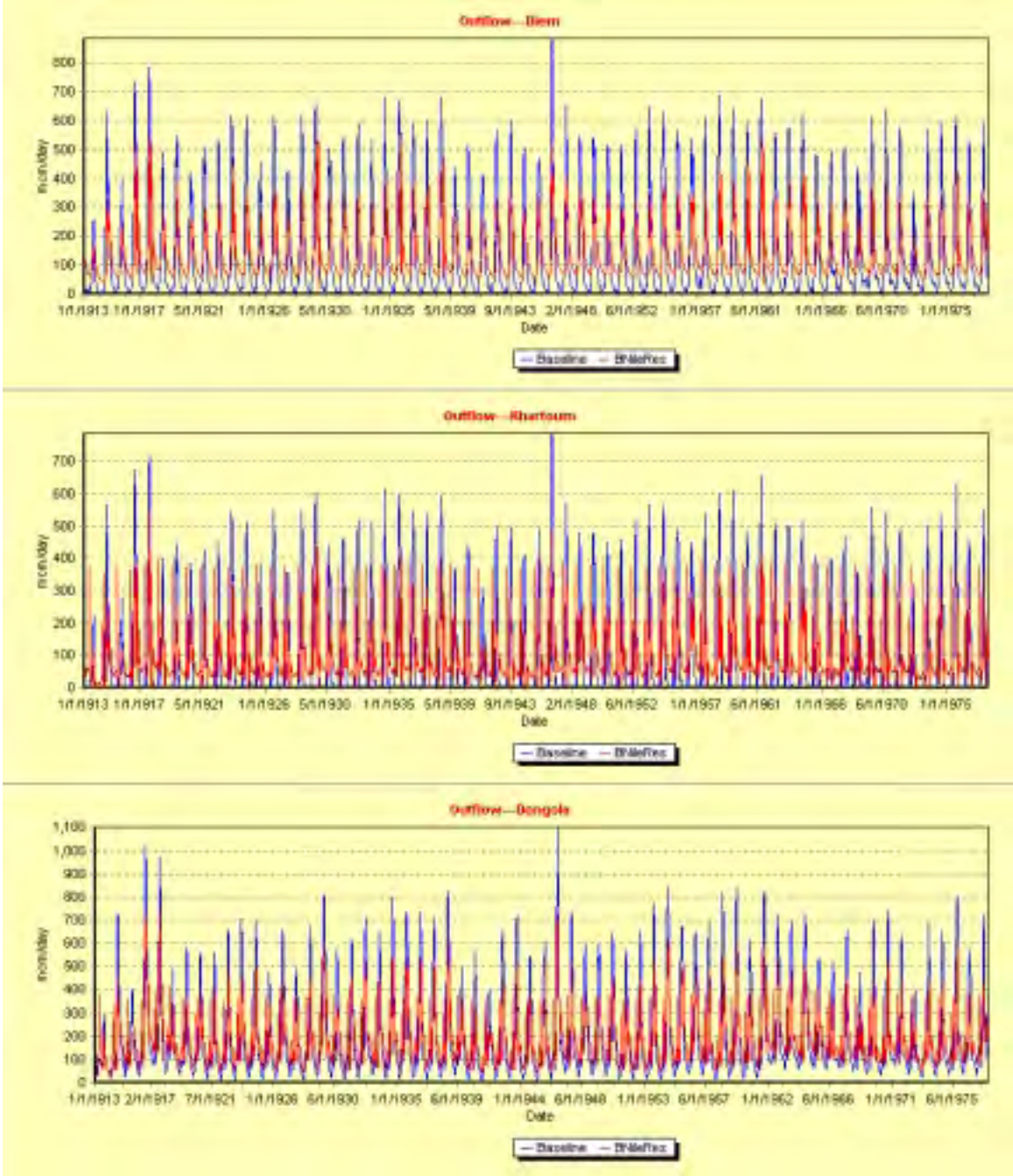

Figure 6.16: Simulated River Flow Sequences at Selected Rived Nodes; Eastern Nile Scenario

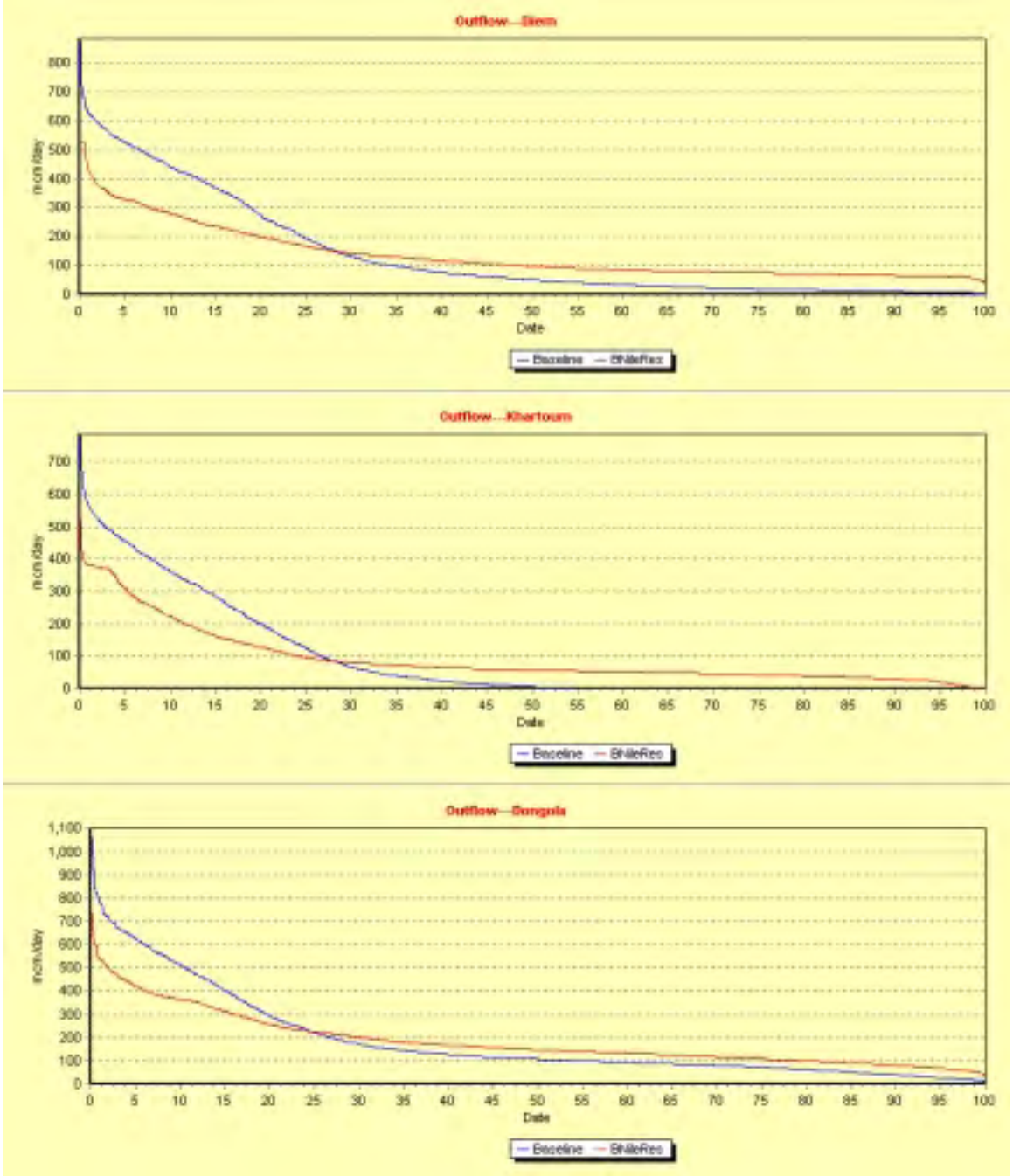

Figure 6.17: Simulated River Flow Frequency Curves at Selected Rived Nodes; Eastern Nile Scenario

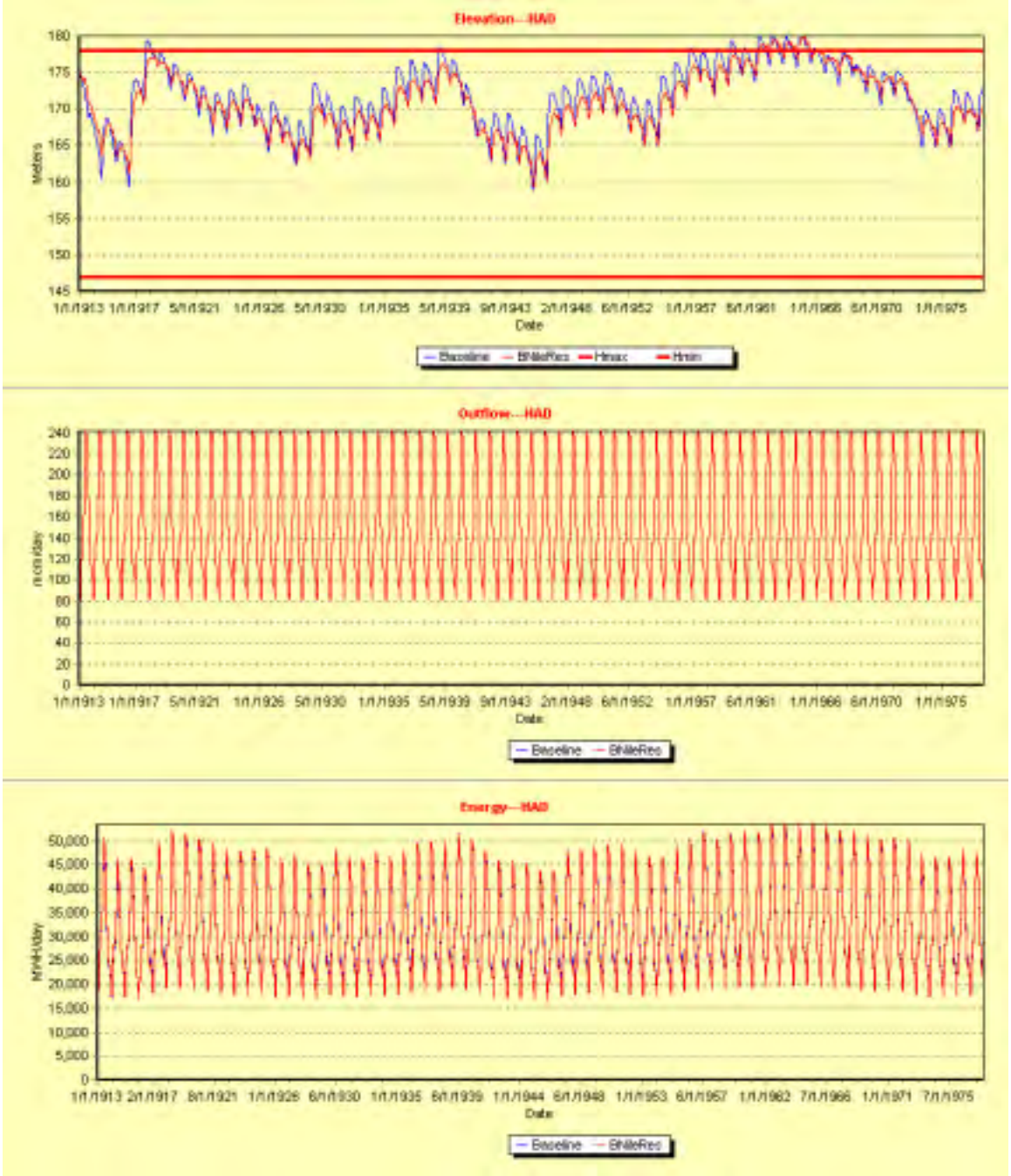

Figure 6.18: Simulated HAD Sequences; Eastern Nile Scenario

Figure 6.19: Simulated River Flow Sequences at Selected River Nodes; Basin Wide Scenario

Figure 6.20: Simulated River Flow Frequency Curves at Selected River Nodes; Basin Wide Scenario

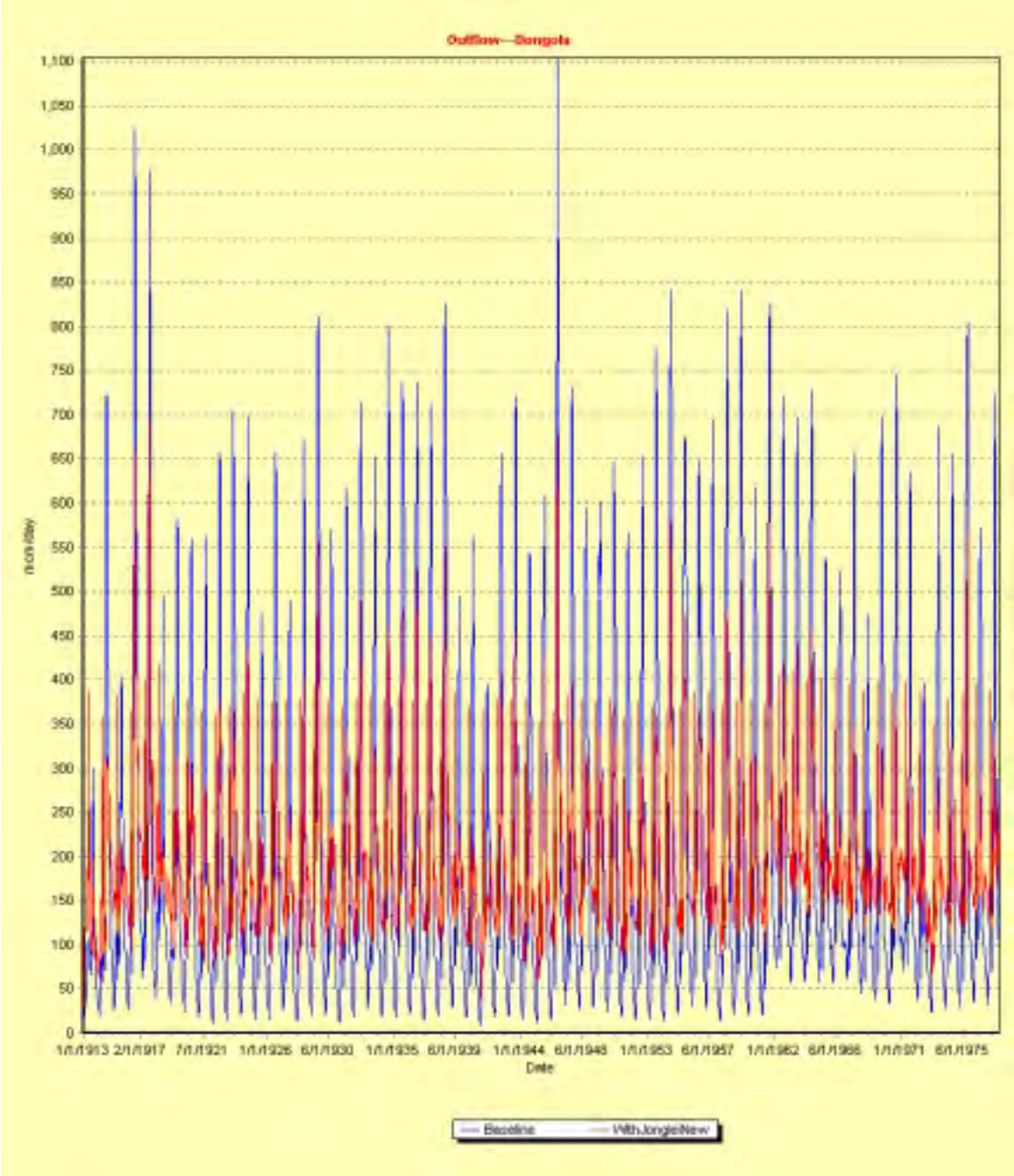

Figure 6.21: Simulated River Flow Sequence at Dongola; Basin Wide Scenario

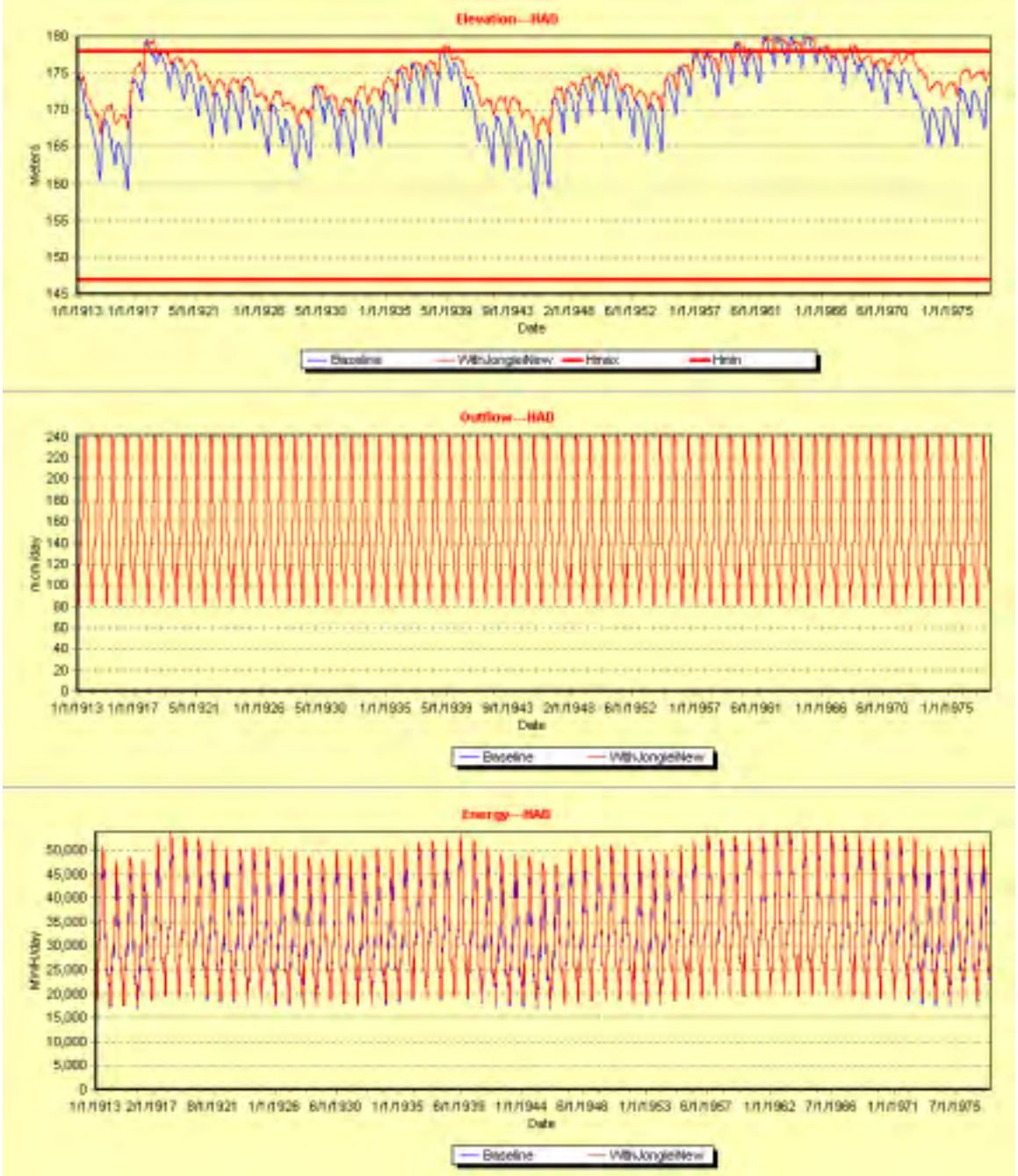

Figure 6.22: Simulated Sequences for High Aswan Dam; Basin Wide Scenario

Chapter 7

Conclusion and Further Work

This report describes the Nile river simulation and management model of the Nile DST. This model performs river and reservoir simulation, reservoir management, and scenario assessment. It was shown through typical applications that the model can be used to support basin wide and regional water sharing policy debates.

However, the model can be improved further by incorporating data still missing and models for all Nile River reaches. A listing of outstanding data and information is included below:

Southern and White Nile

- Planned hydro-projects in the Lake Victoria basin;
- Reach of River Semliki upstream of the entrance to Lake Albert;
- Relationship of wetland extent and river flow at the Sudd;
- The Sobat River and its major tributaries (Baro, Akobo, Pibor) including their potential storage facilities; (The reaches on the Sobat River can be better defined when more detailed information becomes available regarding the location of the proposed reservoirs;)

Blue Nile

- Lake Tana and its basin up to the Lake Tana outlet;
- Reach between Lake Tana outlet and Karadobi entrance;
- Karadobi Reservoir;
- Reach between Karadobi outlet and Mabil entrance;
- Mabil Reservoir;
- Reach between Mabil outlet and Mendaia entrance;
- Mendaia Reservoir;
- Reach between Mendaia outlet and Border entrance;
- Border Reservoir;

- Additional reaches can be added if hydro projects are planned on the Blue Nile tributaries from Lake Tana to Border;
- Reach between Border outlet and Roseires entrance;
- Roseires Reservoir;
- Reach between Roseires outlet and Sennar entrance;
- Sennar Reservoir;
- Reach between Sennar outlet and Khartoum upstream of the Blue-White Nile confluence;
- Node at the confluence of the Blue and White Niles;

Atbara

- Reach of the Atbara River upstream of the Khasm el Girba reservoir entrance; (this reach could be further subdivided if it includes potential or existing reservoir sites;)

Main Nile

- Reach between the Blue-White Nile confluence and upstream Atbara-Blue Nile confluence;
- Reach between Old Aswan Dam and Isna Barrage entrance;
- Isna Barrage;
- Reach between Isna Barrage outlet and Nag Hamadi entrance;
- Nag Hamadi Barrage;
- Reach between Nag Hamadi outlet and Asyut entrance;
- Asyut Barrage;
- Reach between Asyut outlet and Delta Barrage entrance;
- Delta Barrage;
- Reach of Rosetta Branch (Idfina Barrage);
- Reach of Damietta Branch including any water transfers to the Sinai Peninsula (Zifta Barrage).

It is our hope that the Nile RSM will be useful to the Nile Basin countries in their search for sustainable water development and management options. It is clear that the opportunities that the Nile offers far outweigh the challenges. Perhaps the biggest challenge is to recognize that the total answer is not contained within just one country, but it is scattered in each and every one of them.

References

Chan, S-O. and P. S. Eagleson, “Water Balance Studies in the Bahr el Ghazal Swamp,” Dept. of Civ. Eng., MIT, Technical Report No. 261, 1980.

El-Hemry, I. I., and P. S. Eagleson, “Water Balance Estimates of the Machar Marshes,” Dept. of Civ. Eng., MIT, Technical Report No. 260, 1980.

Fahmy, A. and S. Fahmy, “Mathematical Model of the Upper Nile System,” *Proceedings of the 2nd International Conference of Water Resources Planning*, Cairo, Egypt, 1981.

Garstin, W., “Report upon the Basin of the Upper Nile,” *Parliamentary Accounts and Papers, U.K.*, 111, 315-735, 1904.

Georgakakos, A. P., and Marks, D. H., "A Stochastic Control Method for the Real-Time Operation of Reservoir Systems", *Water Resources Research*, Vol. 23, No. 7, pg. 1376 - 1390, July 1987.

Georgakakos, A. P., "Extended Linear Quadratic Gaussian (ELQG) Control: Further Extensions", *Water Resources Research*, Vol. 25, No. 2, pg. 191 - 201, 1989.

Georgakakos, A.P., “A Computer-Aided Management of the Southeastern U.S. Reservoir System”, in " *Decision Support Systems*," D.P. Loucks, ed., NATO ASI Series, Vol. G 26, pg. 407-428, 1991.

Georgakakos, A.P., "Operational Tradeoffs in Reservoir Control", *Water Resources Research*, 29(11), 3801-3819, 1993.

Georgakakos, A.P., H. Yao, and Y. Yu, “A Decision Support System for the High Aswan Dam”, Technical Report No. GIT/CEE-HYDRO-95-2, School of Civil and Environmental Engineering, Georgia Tech, Atlanta, 1995a, 307p.

Georgakakos, A.P., and H. Yao, “A Decision Support System for the Equatorial Lakes”, Technical Report No. GIT/CEE-HYDRO-95-7, School of Civil and Environmental Engineering, Georgia Tech, Atlanta, September 1995, 150p.

Georgakakos, A.P., Y. Yu, and H. Yao, “A Inflow Forecasting Models for the High Aswan Dam”, Technical Report No. GIT/CEE-HYDRO-95-3, School of Civil and Environmental Engineering, Georgia Tech, Atlanta, 1995b, 208p.

Georgakakos, A. P., C. Barrett, and B. Attia, "A Decision Support System for the High Aswan

Dam," *Proceedings* of the Fifth International Workshop on Water Resources Operations Management, sponsored by ASCE, Georgakakos, A.P., and Q.W. Martin Eds., pg. 34-66, Arlington, VA, March 4-6, 1996.

Georgakakos, A.P., and W. Klohn, "A Decision Support System for the Nile River," *Proceedings* of the 5th Nile 2002 Conference, Addis Ababa, Ethiopia, February 24-28, 1997a.

Georgakakos, A.P., Yao, H., and Y. Yu, "A Control Model for Dependable Hydropower Capacity Optimization," *Water Resources Research*, 33(10), 2349-2365, 1997b.

Georgakakos, A.P., H. Yao, and Y. Yu, "Control Models for Hydroelectric Energy Optimization," *Water Resources Research*, 33(10), 2367-2379, 1997c.

Georgakakos, A.P., H. Yao, and Y. Yu, "A Control Model for Hydroelectric Energy Value Optimization," *ASCE J. for Wat. Res. Plan. and Mgt*, 123(1), 30-38, 1997d.

Georgakakos, A.P., M. Andgelic, and K.P. Georgakakos, "A Decision Support System for Lake Victoria," *Proceedings* of the 6th Nile 2002 Conference, Kigali, Rwanda, 12p, February 23-27, 1998b.

Howell, P., M. Lock, and S. Cobb, "*The Jonglei Canal: Impact and Opportunity*," Cambridge University Press, 1988.

Hurst, H. E., and P. Philips, "*Nile Basin Vol. I: General Description of the Basin, Meteorology, Topography of the White Nile Basin*," Government Press, Cairo, 1931.

Hurst, H. E., and P. Philips, "*Nile Basin Vol. V: The Hydrology of the Lake Plateau and Bahr el Jebel*," Government Press, Cairo, 1938.

Hurst, H.E., R. P. Black, and Y. M. Simaika, "*Nile Basin Vol. VII: The Future Conservation of the Nile*," Government Press, Cairo, 1946.

Hurst, H.E., "*Nile Basin Vol. VIII: The Hydrology of the Sobat and White Nile and the Topography of the Blue Nile and Atbara*," Government Press, Cairo, 1950.

Hurst, H.E., R. P. Black, and Y. M. Simaika, "*Nile Basin Vol. X: The Major Nile Projects*," Government Press, Cairo, 1966.

Jonglei Investigation Team, "The Equatorial Nile Project and its Effects in the Aglo-Egyptian Sudan," *Technical Report of the Jonglei Investigation Team*, Government of Sudan, 1954.

Panattoni, L., E. Todini, and A. Fahmy, AMathematical Model of the Upper Nile System,@ UNDP Technical Report No. 15, Egyptian Ministry of Irrigation, 1978, 94p.

Sutcliffe, J.V., and Y. P. Parks, "*The Hydrology of the Nile*," IAHS Special Publication No. 5, 1999.

United Nations Development Program, "*Mathematical Model of the Upper Nile,*" Water Master Plan Technical Report No. 15, Ministry of Irrigation, Egypt, 1981.

U.S. Bureau of Reclamation, "*Land and Water Resources of the Blue Nile Basin, Ethiopia,*" Main Reconnaissance Report and Appendices, prepared for the U.S. Agency for International Development and the Ethiopian Government, 1964.

Yao, H, and A. Georgakakos (2001), "Assessment of Folsom Lake Response to Historical and Potential Future Climate Scenarios," *Journal of Hydrology*, 249, 176-196.

Appendix A

Reservoir Data

A.1. Elevation vs. Storage Relationships

Table A.1.1: Elevation vs. Storage Data for Equatorial Lakes

Victoria		Kyoga		Albert	
Storage(bcm)	**Elevation (m)**	**Storage(bcm)**	**Elevation (m)**	**Storage(bcm)**	**Elevation (m)**
2834.755	1132	0.576	1027	142.001	618
2841.293	1132.1	0.644	1027.1	142.495	618.1
2847.83	1132.2	0.711	1027.2	142.989	618.2
2854.384	1132.3	0.779	1027.3	143.487	618.3
2860.937	1132.4	0.847	1027.4	143.985	618.4
2867.505	1132.5	0.914	1027.5	144.489	618.5
2874.074	1132.6	0.982	1027.6	144.992	618.6
2880.658	1132.7	1.05	1027.7	145.501	618.7
2887.242	1132.8	1.118	1027.8	146.01	618.8
2893.842	1132.9	1.185	1027.9	146.525	618.9
2900.442	1133	1.253	1028	147.04	619
2907.057	1133.1	1.347	1028.1	147.561	619.1
2913.672	1133.2	1.442	1028.2	148.081	619.2
2920.302	1133.3	1.55	1028.3	148.608	619.3
2926.933	1133.4	1.657	1028.4	149.134	619.4
2933.579	1133.5	1.78	1028.5	149.666	619.5
2940.225	1133.6	1.903	1028.6	150.198	619.6
2946.886	1133.7	2.044	1028.7	150.736	619.7
2953.548	1133.8	2.185	1028.8	151.274	619.8
2960.225	1133.9	2.343	1028.9	151.818	619.9
2966.902	1134	2.502	1029	152.361	620
2973.594	1134.1	2.679	1029.1	152.911	620.1
2980.286	1134.2	2.856	1029.2	153.461	620.2
2986.994	1134.3	3.051	1029.3	154.017	620.3
2993.702	1134.4	3.246	1029.4	154.572	620.4
3000.425	1134.5	3.459	1029.5	155.133	620.5
3007.149	1134.6	3.671	1029.6	155.694	620.6
3013.888	1134.7	3.902	1029.7	156.261	620.7
3020.535	1134.8	4.133	1029.8	156.828	620.8
3027.381	1134.9	4.381	1029.9	157.401	620.9
3034.135	1135	4.63	1030	157.973	621
3040.905	1135.1	4.863	1030.1	158.549	621.1
3047.675	1135.2	5.162	1030.2	159.126	621.2
3054.46	1135.3	5.444	1030.3	159.707	621.3
3061.245	1135.4	5.727	1030.4	160.287	621.4
3068.047	1135.5	6.024	1030.5	160.871	621.5
3074.848	1135.6	6.321	1030.6	161.455	621.6
3081.665	1135.7	6.633	1030.7	162.042	621.7
3088.481	1135.8	6.944	1030.8	162.629	621.8
3095.313	1135.9	7.269	1030.9	163.219	621.9
3102.145	1136	7.595	1031	163.809	622
3108.99	1136.1	7.934	1031.1	164.401	622.1

3115.836	1136.2	8.273	1031.2	164.994	622.2
3122.691	1136.3	8.624	1031.3	165.589	622.3
3129.546	1136.4	8.976	1031.4	166.184	622.4
3136.412	1136.5	9.34	1031.5	166.782	622.5
3143.277	1136.6	9.703	1031.6	167.38	622.6
3150.153	1136.7	10.07	1031.7	167.98	622.7
3157.029	1136.8	10.45	1031.8	168.58	622.8
3163.915	1136.9	10.83	1031.9	169.182	622.9
3170.8	1137	11.22	1032	169.784	623
		11.61	1032.1	170.388	623.1
		12.01	1032.2	170.992	623.2
		12.41	1032.3	171.599	623.3
		12.81	1032.4	172.205	623.4
		13.23	1032.5	172.813	623.5
		13.64	1032.6	173.421	623.6
		14.06	1032.7	174.03	623.7
		14.48	1032.8	174.64	623.8
		14.91	1032.9	175.251	623.9
		15.34	1033	175.862	624
		15.77	1033.1	176.477	624.1
		16.21	1033.2	177.091	624.2
		16.65	1033.3	177.706	624.3
		17.1	1033.4	178.321	624.4
		17.55	1033.5	178.936	624.5
		18	1033.6	179.55	624.6
		18.45	1033.7	180.165	624.7
		18.91	1033.8	180.78	624.8
		19.38	1033.9	181.394	624.9
		19.84	1034	182.009	625
		20.32	1034.1	182.44	625.1
		20.79	1034.2	182.871	625.2
		21.27	1034.3	183.302	625.3
		21.75	1034.4	183.733	625.4
		22.23	1034.5	184.161	625.5
		22.72	1034.6	184.596	625.6
		23.21	1034.7	185.027	625.7
		23.71	1034.8	185.458	625.8
		24.21	1034.9	185.889	625.9
		24.71	1035		
		25.23	1035.1		
		25.75	1035.2		
		26.27	1035.3		
		26.7	1035.4		
		27.32	1035.5		
		27.84	1035.6		
		28.36	1035.7		
		28.88	1035.8		
		29.4	1035.9		
		29.92	1036		

Table A.1.2: Elevation vs. Storage Data for Ethiopia Reservoirs

Tana		Karadobi		Mabil	
Storage(bcm)	**Elevation (m)**	**Storage(bcm)**	**Elevation (m)**	**Storage(bcm)**	**Elevation (m)**
0	1783	1.4	1000	0.8	800
1.5	1783.5	2.4	1020	1	805
2.9	1784	3.8	1040	1.25	810
4.5	1784.5	6.5	1060	1.5	815
5.1	1784.75	10	1080	1.8	820
6	1785	15	1100	2.2	825
7.5	1785.5	20.5	1120	2.5	830
9	1786	27	1140	3	835
10.5	1786.5	36	1160	3.4	840
12	1787			4.3	850
13.6	1787.5			5.5	860
15.3	1788			6	863
16.9	1788.5			7	870
18.4	1789			8.5	880
				10.4	890
				12.1	900
				14	910
Mendaia		**Border**			
Storage(bcm)	**Elevation (m)**	**Storage(bcm)**	**Elevation (m)**		
1.2	660	1.4	540		
1.5	665	2	545		
2.1	670	2.9	550		
2.5	675	4	555		
3.1	680	5.2	560		
3.7	685	6.8	565		
4.3	690	8.6	570		
5	695	10.75	575		
5.9	700	13.1	580		
6.8	705				
7.8	710				
10	720				
11	723				
12.5	730				
15.6	740				

Table A.1.3: Elevation vs. Storage Data for Sudanese Reservoirs

Roseires		Sennar		Kirshm Girba	
Storage(bcm)	**Elevation (m)**	**Storage(bcm)**	**Elevation (m)**	**Storage(bcm)**	**Elevation (m)**
0.01	460	0.001	407	0.0074	440
0.015	461	0.005	408	0.0094	441

0.02	462	0.013	409	0.012	442
0.03	463	0.025	410	0.015	443
0.045	464	0.042	411	0.0188	444
0.067	465	0.064	412	0.0232	445
0.101	466	0.092	413	0.029	446
0.152	467	0.127	414	0.0357	447
0.226	468	0.177	415	0.0429	448
0.321	469	0.236	416	0.0513	449
0.441	470	0.312	417	0.0613	450
0.582	471	0.411	418	0.0729	451
0.735	472	0.537	419	0.0862	452
0.9	473	0.678	420	0.1019	453
1.079	474	0.825	421	0.12	454
1.271	475			0.1409	455
1.477	476			0.1649	456
1.699	477			0.1921	457
1.937	478			0.2228	458
2.194	479			0.2574	459
2.474	480			0.296	460
				0.3389	461
				0.386	462
				0.4377	463
				0.4962	464
				0.5618	465
				0.635	466
				0.7156	467
				0.803	468
				0.896	469

Table A.1.4: Elevation vs. Storage Data for High Aswan Dam

High Aswan Dam	
Storage(bcm)	**Elevation (m)**
31.6	147
33.4	148
35.3	149
37.2	150
39.2	151
41.3	152
43.5	153
45.8	154
48.1	155
50.5	156
53.1	157
55.7	158
58.5	159
61.5	160
64.5	161

67.6	162
70.9	163
74.3	164
77.9	165
85.3	167
89.2	168
93.3	169
97.6	170
101.9	171
106.4	172
111.1	173
116.1	174
121.3	175
126.5	176
131.9	177
137.5	178
143.4	179
149.5	180
155.8	181
162.3	182
168.9	183
175.7	184
182.7	185

Table A.1.5: Elevation vs. Storage Data for Gebel El Aulia Reservoir

The reservoir storage and area function for Gebel El Aulia reservoir is a complicated function due the backwater effect. It is approximated by different functions for different season and different Melut gauge height. All functions have the following formulation:

$$H_{GA} = \alpha_1 S_{GA} + \alpha_2 H_{Mlt} + \alpha_3 \text{Log}(S_{GA}+1) + \alpha_4 \text{Log}(H_{Mlt}) + \alpha_5 S_{GA} H_{Mlt} + \alpha_6 ,$$

where,

H_{GA}: Gebel El Aulia reservoir elevation (meters),

S_{GA}: Gebel El Aulia reservoir storage (mcm),

H_{Mlt}: Melut elevation (meters),

and the α_i coefficients are given in the following table:

	Rising Stage (May - Nov.)		Falling Stage	
	H_{GA}<374 m	H_{GA}>374 m	H_{GA}<374 m	H_{GA}>374 m
α_1	0.001635223654	0.001166139290	0.005838955735	0.001128831629
α_2	-1.02282308943	0.541089246667	-0.56670904427	0.326810837396
α_3	0.255638405453	-1.74493921292	0.349284861713	0.870033776445
α_4	18.30143826458	0.968863305264	13.74242904986	0.591156060677
α_5	0.000188204985	-0.00007197817	-0.00027095310	-0.00006114188
α_6	338.1150087991	366.2362322065	343.8557647195	363.5801211040
Error Mean (m)	0.0	0.0	0.0	0.0
Err. St.D., (m)	0.175	0.093	0.16	0.085

Surface area function of Gebel El Aulia has the following formulation:

$$A_{GA} = \beta_1 H_{GA} + \beta_2 H_{Mlt} + \beta_3 \text{Log}(H_{GA}) + \beta_4 \text{Log}(H_{Mlt}) + \beta_5 H_{GA} H_{Mlt} + \beta_6 ,$$

where

A_{GA}: Gebel El Aulia surface area (km^2),

H_{GA}: Gebel El Aulia elevation (m),

H_{mlt}: Melut elevation (m),

and the β_i coefficients are given in the following table:

	Rising Stage (May - Nov.)		Falling Stage	
	HGA<374 m	HGA>374 m	HGA<374 m	HGA>374 m
β_1	6294.216171413	42487.9565666	16555.49948087	32744.02106616
β_2	9830.8432152	5941.7357949	7890.516382952	5092.940948632
β_3	-2208371.5748	-15761497.03	-6060794.96751	-12110518.1664
β_4	-1861.415138	-780.548454687	-2590.21283436	-1565.36269005
β_5	-26.05039047	-15.8818704581	-20.6746726837	-13.4508231692
β_6	10732622.07	77486682.73	29718597.29	59502784.79
Err. Mean (km^2)	-0.07	0.17	-0.062	0.18
Err. St.D. (km^2)	5.502	23.9	6.79	31.11

Table A.1.2: Elevation vs. Storage Relationship for Messochora

Regression Coefficients for Elevation-Storage Curve

Elevation (Y): Meters
Storage (X): million cubic meters
Function: **Y=AX+BX^2+CX^.5+DLn(X)+E/X+F**

Name	A	B	C	D	E	F
Albert	-5.0943356	0.0052029	91.0951614	0.0000000	0.0000000	150.9648743
Border	-2.4602580	0.0359042	25.6690331	0.0000000	0.0000000	513.1635132
Girba	-11.0860281	2.5056865	26.0743027	3.0086262	0.0000000	452.5910339
HAD	-0.1423096	0.0001016	5.5905533	6.8900223	0.0000000	96.1497574
Karadobi	8.6053181	-0.0497777	-58.3667870	64.1840973	0.0000000	1035.1009521
Kyoga	0.2788267	-0.0009940	-0.9449904	1.5809729	0.0000000	1028.3416748
Mabil	-10.8853798	0.1895075	87.8486023	-11.8162966	0.0000000	727.6727905
Mendaia	-9.8298178	0.1124876	87.4783020	-21.7053642	0.0000000	580.1969604
Roseires	9.8021908	-0.8282065	-11.8781633	3.3418984	0.0000000	476.4587097
Sennar	-17.0294247	4.5744052	29.0515003	-0.0885237	0.0000000	405.5109253
Tana	0.3456704	-0.0010213	-0.0072078	0.0000000	0.0000000	1782.9998779
Victoria	-0.0000029	0.0000000	1.6352686	0.0000000	0.0000000	1045.0073242

Name	Err. Mean	Err. Std.	Corr.Coef	Max. X	Min. X	Max. Y	Min. Y
Albert	-0.0000136	0.0312861	0.9999094	185.8890076	142.0010071	625.9000244	618.0000000
Border	0.0000000	0.1587473	0.9999328	13.1000004	1.4000000	580.0000000	540.0000000
Girba	0.0000000	0.0389076	0.9999902	0.8960000	0.0074000	469.0000000	440.0000000
HAD	-0.0000001	0.0170781	0.9999989	182.6999969	31.6000004	185.0000000	147.0000000
Karadobi	0.0000000	0.7175693	0.9999142	36.0000000	1.4000000	1160.0000000	1000.0000000
Kyoga	0.0000000	0.0157393	0.9999822	29.9200001	0.5760000	1036.0000000	1027.0000000
Mabil	0.0000000	0.4527893	0.9999125	14.0000000	0.8000000	910.0000000	800.0000000
Mendaia	0.0000000	0.4742991	0.9998141	15.6000004	1.2000000	740.0000000	660.0000000
Roseires	0.0000000	0.0360964	0.9999831	2.4740000	0.0100000	480.0000000	460.0000000
Sennar	0.0000000	0.0277879	0.9999807	0.8250000	0.0010000	421.0000000	407.0000000
Tana	0.0000000	0.0182037	0.9999541	18.3999996	0.0000000	1789.0000000	1783.0000000
Victoria	-0.0000050	0.0003204	1.0000000	3170.8000488	2834.7548828	1137.0000000	1132.0000000

A.2 Rating Curves at Various Locations

Location	Rating Curve
Khartoum Blue Nile	$D = 1236.-253.6\ Q + 13.13Q^2$

Dongala		$D = 597. - 171.8\ Q + 12.32Q^2$
Malakal		$D = 453.2 - 92.59\ Q + 5.182Q^2$
Melut	Rising Stage (May-Nov)	$D = 0.083316\ Q - 1.179\ \text{Log}\ (Q) - 0.000205\ Q^2 + 11.121$
	Falling Stage (Dec - Apr)	$D = (0.03513 + \text{Log}\ (Q)\ ) / 0.3779$

where

D: River stage elevation (m), and

Q: Flow (mcm/day).

Appendix B

Hydro Turbine Characteristic Curves and Hydro Power Data

B.1. Hydro Turbine Curves

The hydro turbine curves are used in estimate the hydro energy generation. The data are available for stations at Owen Falls and Aswan Dam. For these without no data, generic approximation functions are used.

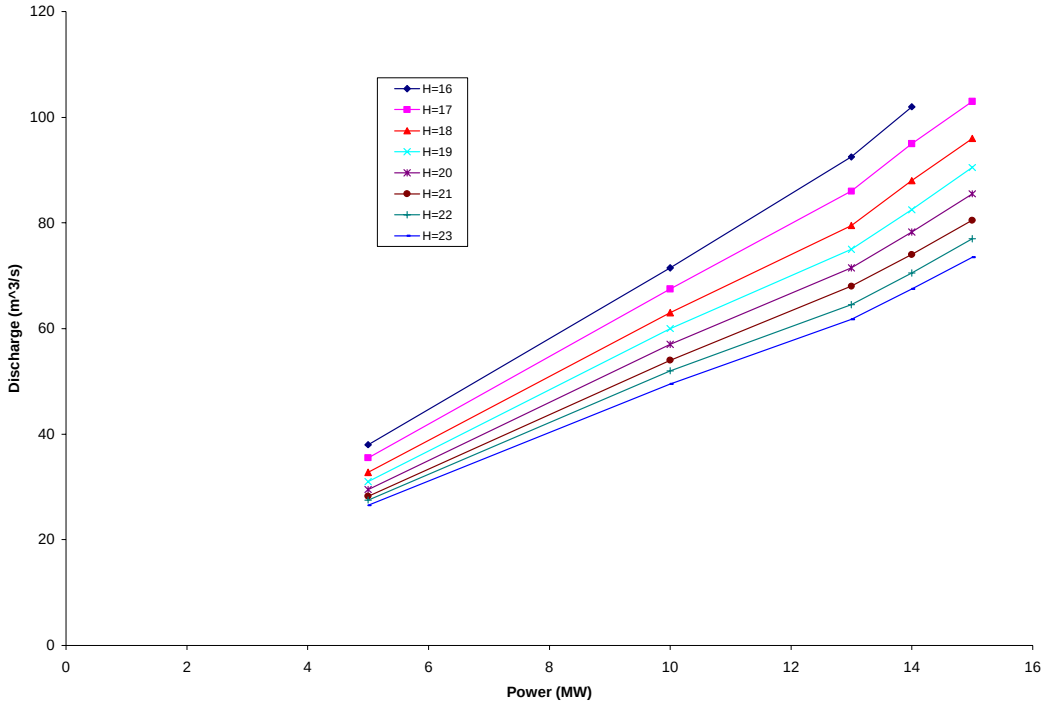

Figure B.1: Owen Falls Turbine Characteristics (Existing Plant)

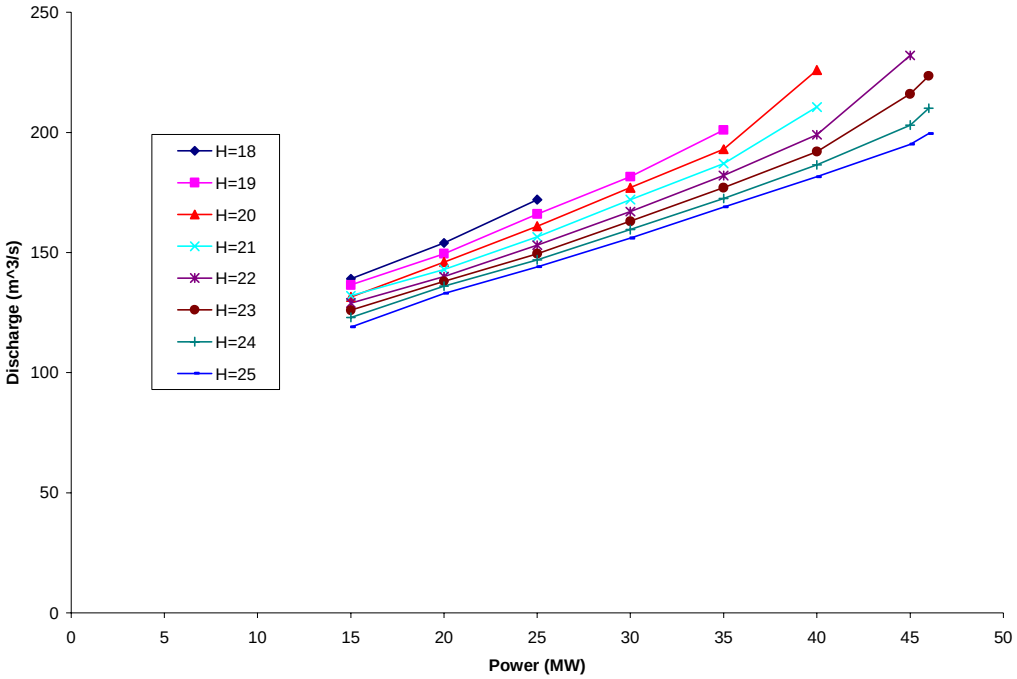

Figure B.2: Owen Falls Turbine Characteristics (Extension Plant)

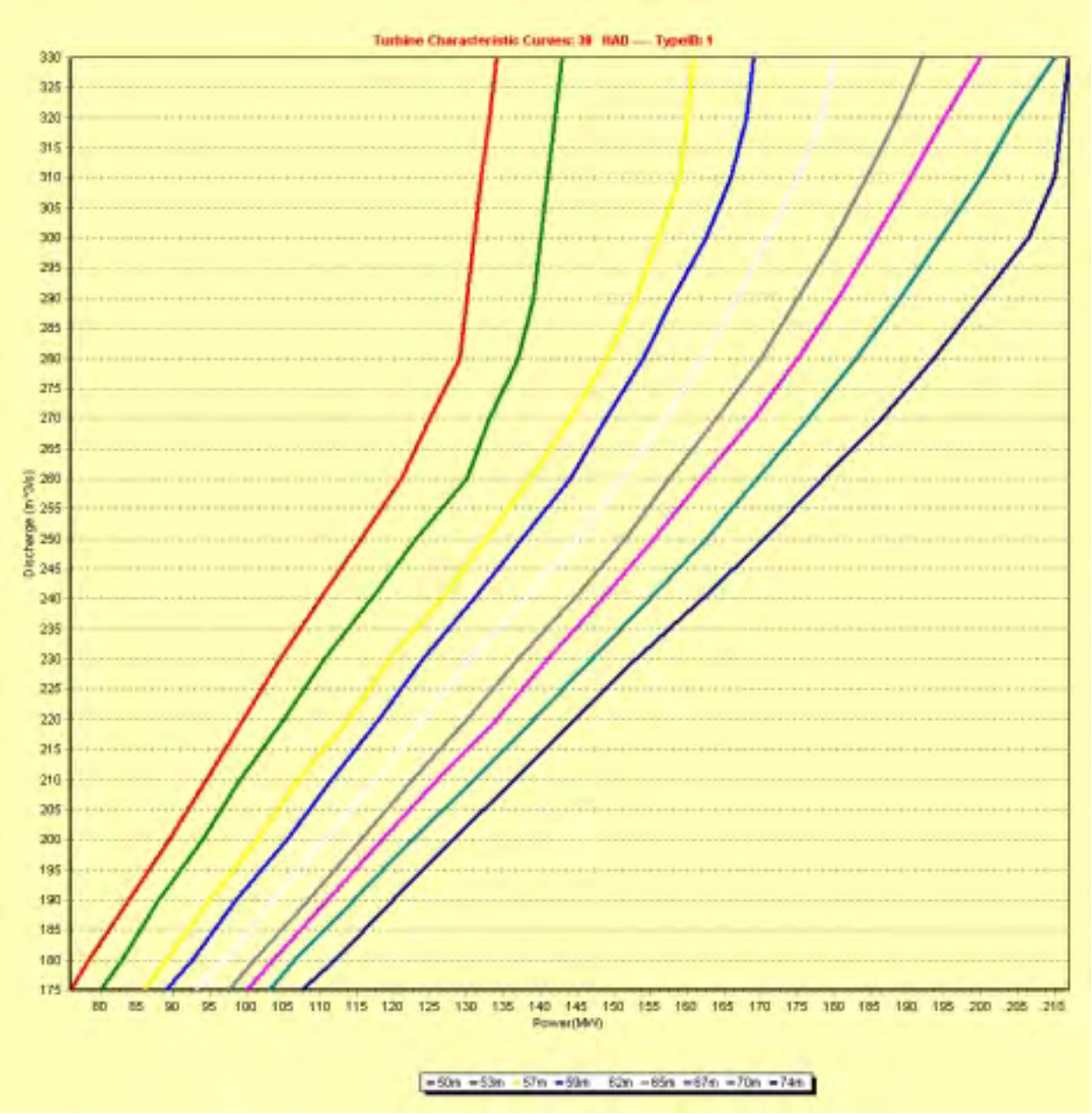

Figure B.3: HAD Turbine Characteristics

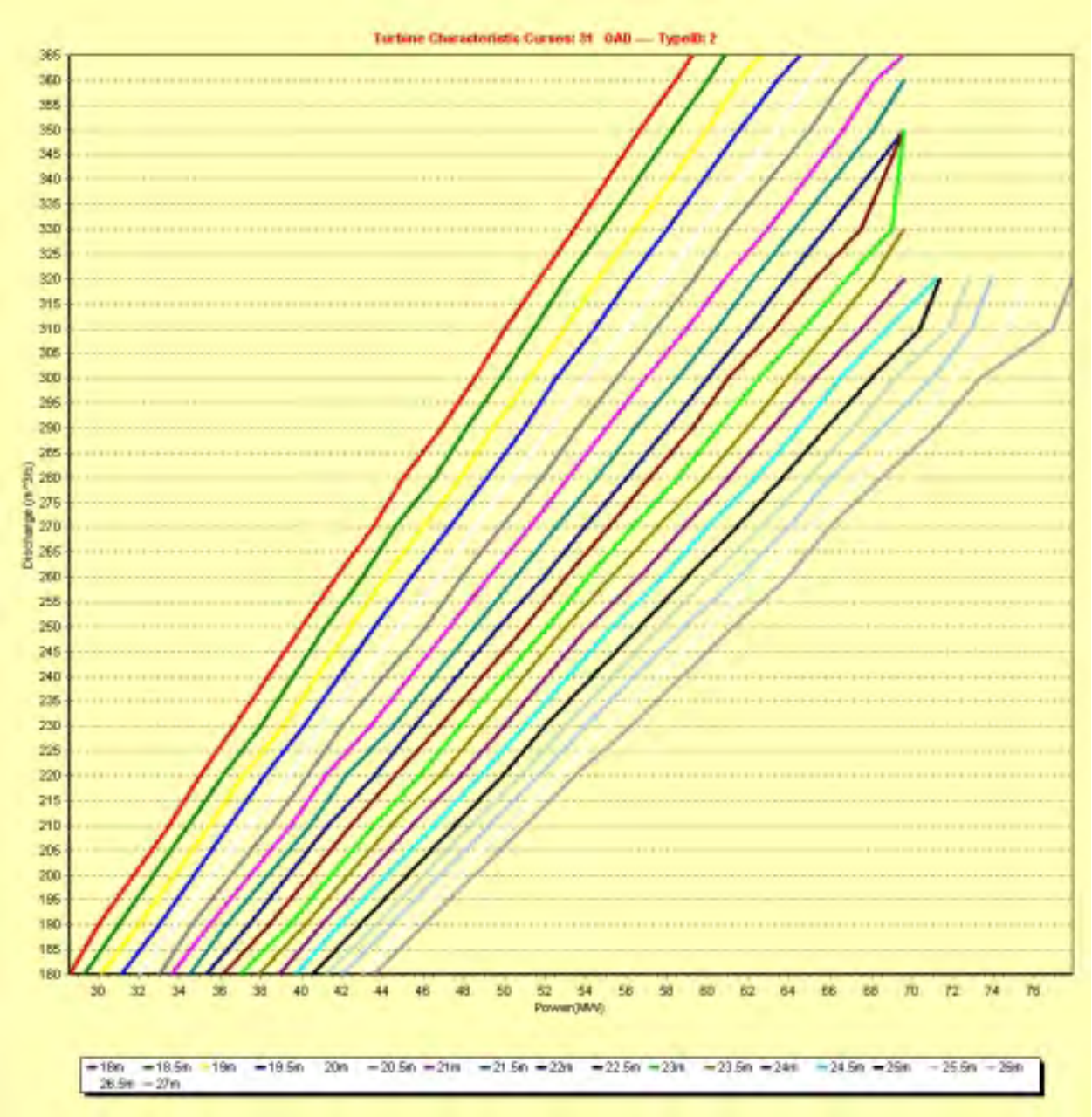

Figure B.4: Old Aswan Dam Turbine Characteristics

B.2. Hydro Power Data

B.2.1. Lake Tana

Turbine number N (Francis): 4
Designed Power Capacity P_{max} (MW): 50
Designed Discharge Q_{max} (m^3/s): 27.5
Designed Hydraulic Head H_{net0} (m): 239

For a given release volume V over a time period T, the total energy generation function is derived from the similarity theory and is given by:

$$E = NP_r P_{\max} T$$

where,
N: the number of turbines,
E: the total energy in MWH,
$P_{max:}$: the designed single turbine power capacity in MW,
P_r : the power output percentage,
and T: the total power generation hours.
Both P_r and T are computed based on the following procedure:

$ Compute the net head H_{net}:

$$H_{net} = H - H_T$$

$ Compute the head percentage H_r:

$$H_r = H_{net} / H_{net0}$$

$ Compute the power output percentage $P_{r:}$

$$P_r = -0.6477 + 1.6538 H_r$$

$ Compute the discharge percentage Q_r (m^3/s):

$$Q_r = 0.3666 + 0.6400 H_r$$

$ Compute the maximum turbine release V_i (bcm)

$$V_i = 3600 Q_r Q_{\max} N T_{\max} / 10^9$$

$ Compute the power generation hours T:

$$T = \frac{V}{V_i}$$

B.2.2. Karadobi

Turbine number N (Francis): 12
Designed Power Capacity P_{max} (MW): 113
Designed Discharge Q_{max} (m^3/s): 69.3
Designed Head H_{net0} (m): 181.4
Tailwater (m): 971.6

The energy generation follows the same procedure as for Lake Tana.

B.2.3. Mabil

Turbine number N (Francis): 12
Designed Power Capacity P_{max} (MW): 100
Designed Discharge Q_{max} (m^3/s): 106
Designed Head H_{net0} (m): 117.4
Tailwater (m): 792.4

The energy generation follows the same procedure as for Lake Tana

B.2.4. Mendaia

Turbine number N (Francis): 12
Designed Power Capacity P_{max} (MW): 135
Designed Discharge Q_{max} (m^3/s): 146
Designed Head H_{net0} (m): 113.6
Tailwater (m): 623.6

The energy generation follows the same procedure as for Lake Tana.

B.2.5. Border

Turbine number N (Francis): 14
Designed Power Capacity P_{max} (MW): 100
Designed Discharge Q_{max} (m^3/s): 170.
Designed Head H_{net0} (m): 75
Tailwater (m): 500

The energy generation follows the same procedure as for Lake Tana.

B.2.6. Roseires

Turbine number N: 7
Designed Power Capacity P_{max} (MW): 3 X 30 + 4 X 40 = 250
Operating Head Range (m): 17-35
Tailwater H_t (m):

$$H_t = (\frac{Q}{33.04})^{\frac{1}{1.353}} - 443$$

where Q is the daily averaged discharge in mcm and given by:

$$Q = \frac{1000U}{N_d},$$

where U is the release in bcm over a period, N_d is the number of days in the period.

Finally, the energy generation (GWH) is given by:

$$E = 2.73\eta U H_{net}$$

where η is the efficient coefficient, a value of 0.88 are assigned for both Roseires and Sennar; H_{net} is the net head in meters, the difference between the reservoir elevation and tailwater level.

B.2.7. Sennar

Turbine number N: 2
Designed Power Capacity P_{max} (MW): 2 X 7.5
Operating Head Range (m): 6-16
Tailwater H_t (m):

$$H_t = (\frac{Q}{34.85})^{\frac{1}{1.927}} - 403.7$$

The energy generation is given by:

$$E = 2.73\eta U H_{net}$$

All symbols are defined as in Roseires.

B.2.8. Kirshm Girba

Turbine number N: 5
Designed Power Capacity P_{max} (MW): 2 X 3.5 + 3 X 2 = 13
Operating Head Range (m): 17-40
Tailwater H_t (m): 433

The energy generation is given by:

$$E = 2.73\eta U H_{net}$$

All symbols are defined as in Roreires.

Appendix C

Statistics of Net Basin Supply and Tributary Inflows

C.1. Historical Record Periods and Annual Average Values

Nodes	Start Date	End Date	AVG (bcm)
Victoria	1/1/1912	12/21/1977	27.272
Kyoga	1/1/1912	12/21/1977	-.573
Albert	1/1/1912	12/21/1977	3.719
Torrents	1/1/1912	12/21/1977	4.794
Sobat	1/1/1912	12/21/1977	13.440
Tana	1/1/1912	12/21/1977	4.117
Karadobi	1/1/1912	12/21/1977	15.307
Mabil	1/1/1912	12/21/1977	8.685
Mendaia	1/1/1912	12/21/1977	13.215
Border	1/1/1912	12/21/1977	8.425
Dinder	1/1/1912	12/21/1977	2.908
Rahad	1/1/1912	12/21/1977	1.081
Girba	1/1/1912	12/21/1977	11.660

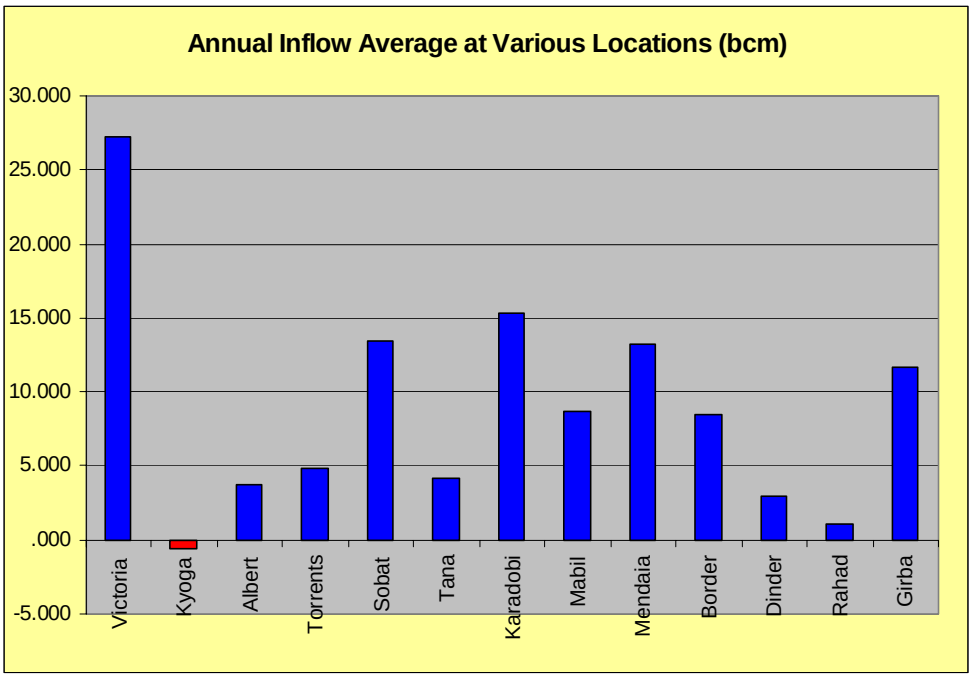

C.2. 10-day Historical Inflow Sequences

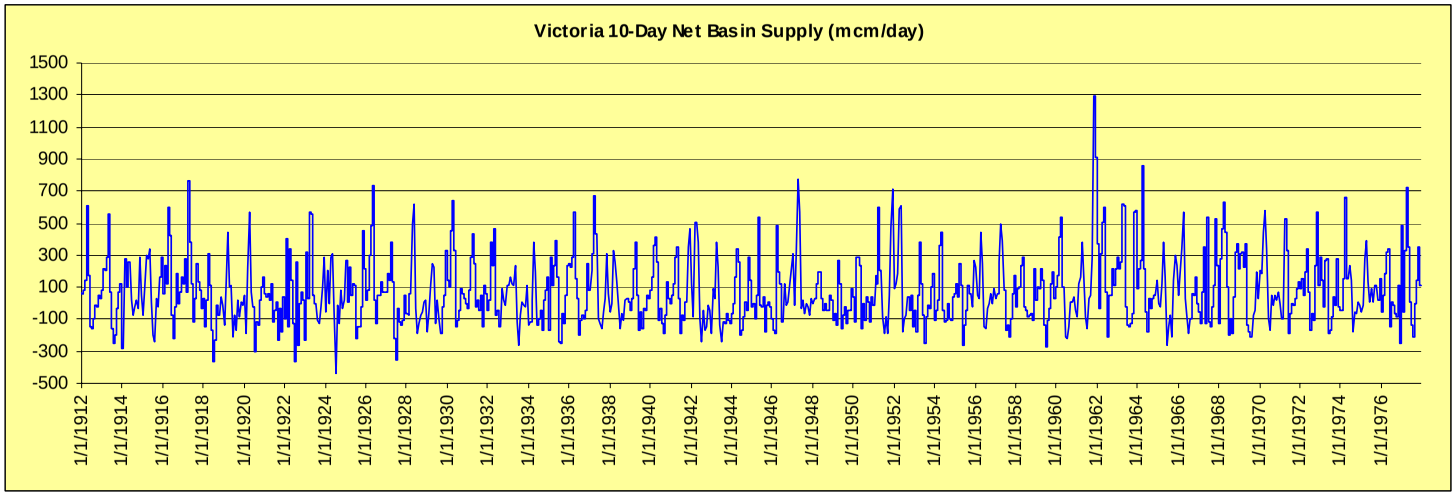

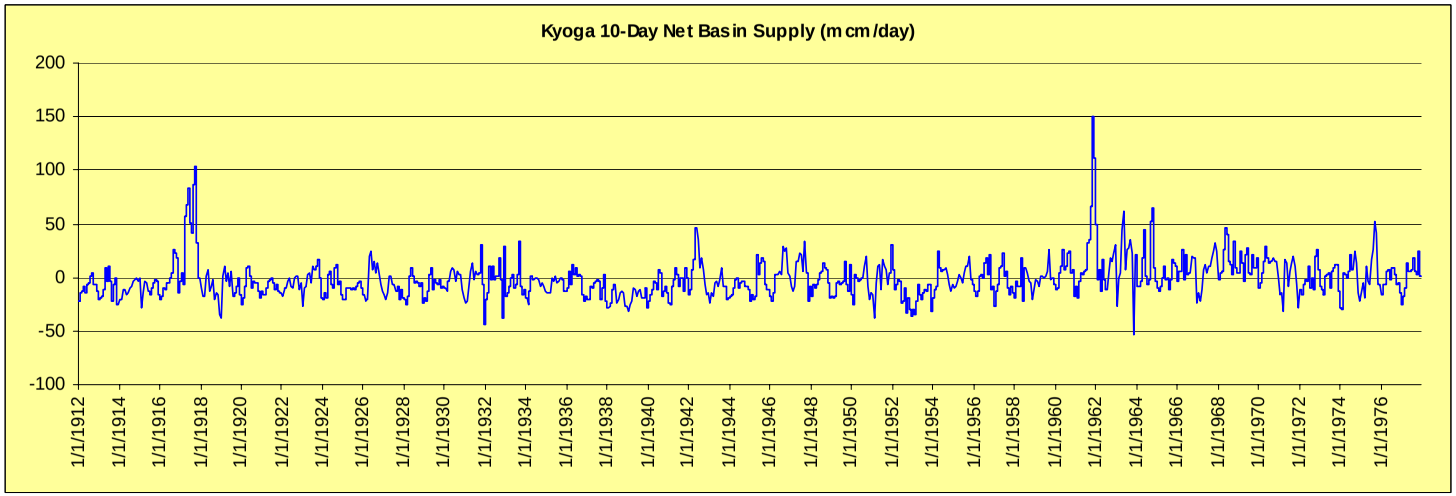

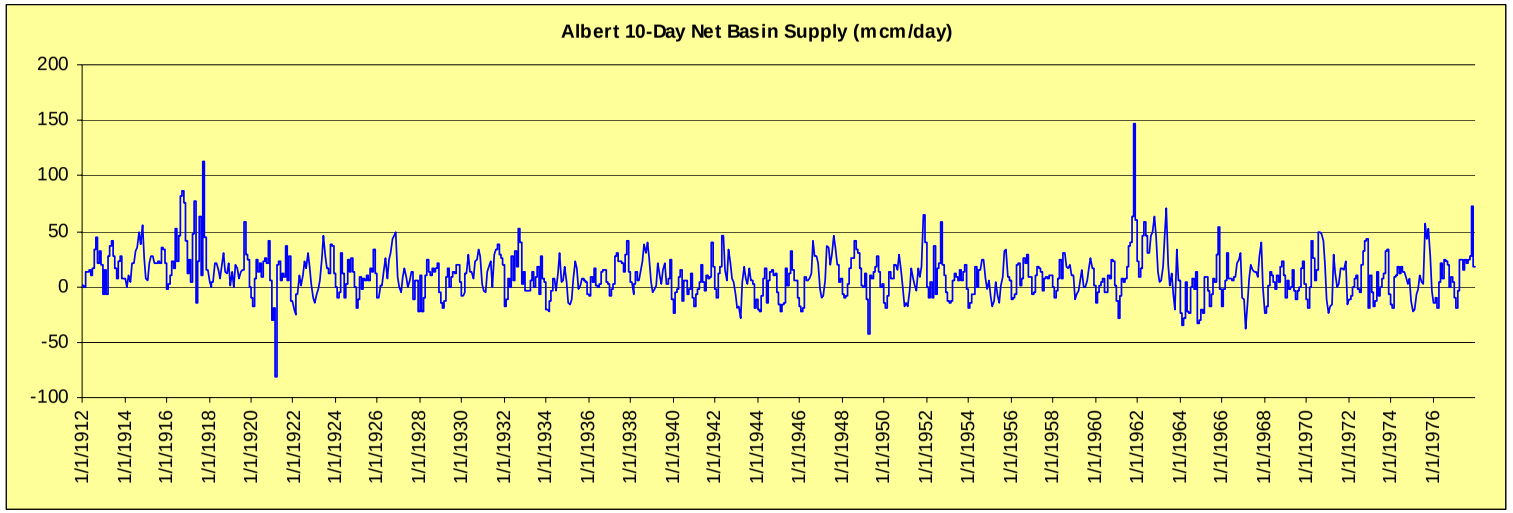
Albert 10-Day Net Basin Supply (mcm/day)
200
150
100
50
0
-50
-100
1/1/1912
1/1/1914
1/1/1916
1/1/1918
1/1/1920
1/1/1922
1/1/1924
1/1/1926
1/1/1928
1/1/1930
1/1/1932
1/1/1934
1/1/1936
1/1/1938
1/1/1940
1/1/1942
1/1/1944
1/1/1946
1/1/1948
1/1/1950
1/1/1952
1/1/1954
1/1/1956
1/1/1958
1/1/1960
1/1/1962
1/1/1964
1/1/1966
1/1/1968
1/1/1970
1/1/1972
1/1/1974
1/1/1976

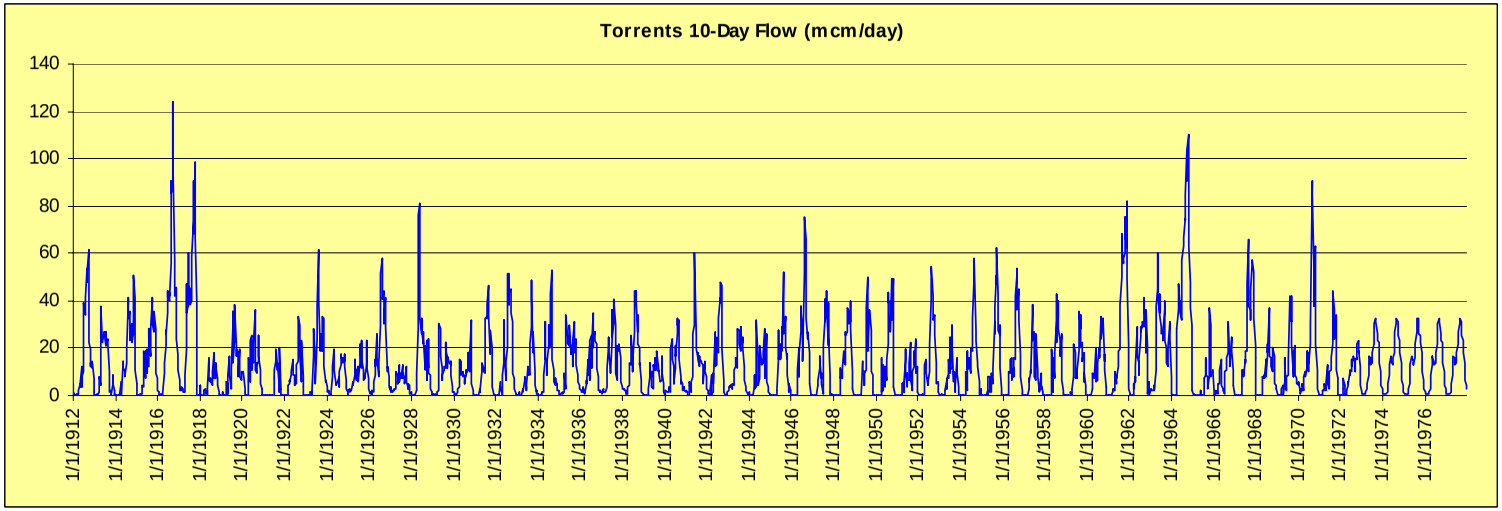
Torrents 10-Day Flow (mcm/day)
140
120
100
80
60
40
20
0
1/1/1912
1/1/1914
1/1/1916
1/1/1918
1/1/1920
1/1/1922
1/1/1924
1/1/1926
1/1/1928
1/1/1930
1/1/1932
1/1/1934
1/1/1936
1/1/1938
1/1/1940
1/1/1942
1/1/1944
1/1/1946
1/1/1948
1/1/1950
1/1/1952
1/1/1954
1/1/1956
1/1/1958
1/1/1960
1/1/1962
1/1/1964
1/1/1966
1/1/1968
1/1/1970
1/1/1972
1/1/1974
1/1/1976

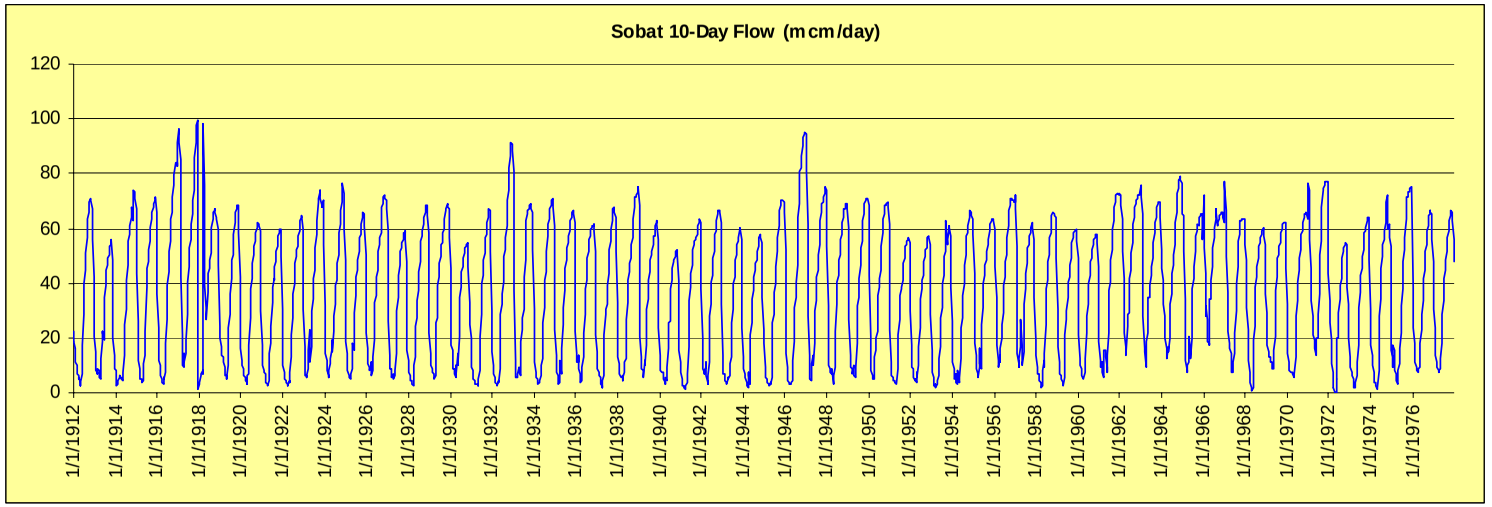
Sobat 10-Day Flow (mcm/day)
120
100
80
60
40
20
0
1/1/1912
1/1/1914
1/1/1916
1/1/1918
1/1/1920
1/1/1922
1/1/1924
1/1/1926
1/1/1928
1/1/1930
1/1/1932
1/1/1934
1/1/1936
1/1/1938
1/1/1940
1/1/1942
1/1/1944
1/1/1946
1/1/1948
1/1/1950
1/1/1952
1/1/1954
1/1/1956
1/1/1958
1/1/1960
1/1/1962
1/1/1964
1/1/1966
1/1/1968
1/1/1970
1/1/1972
1/1/1974
1/1/1976

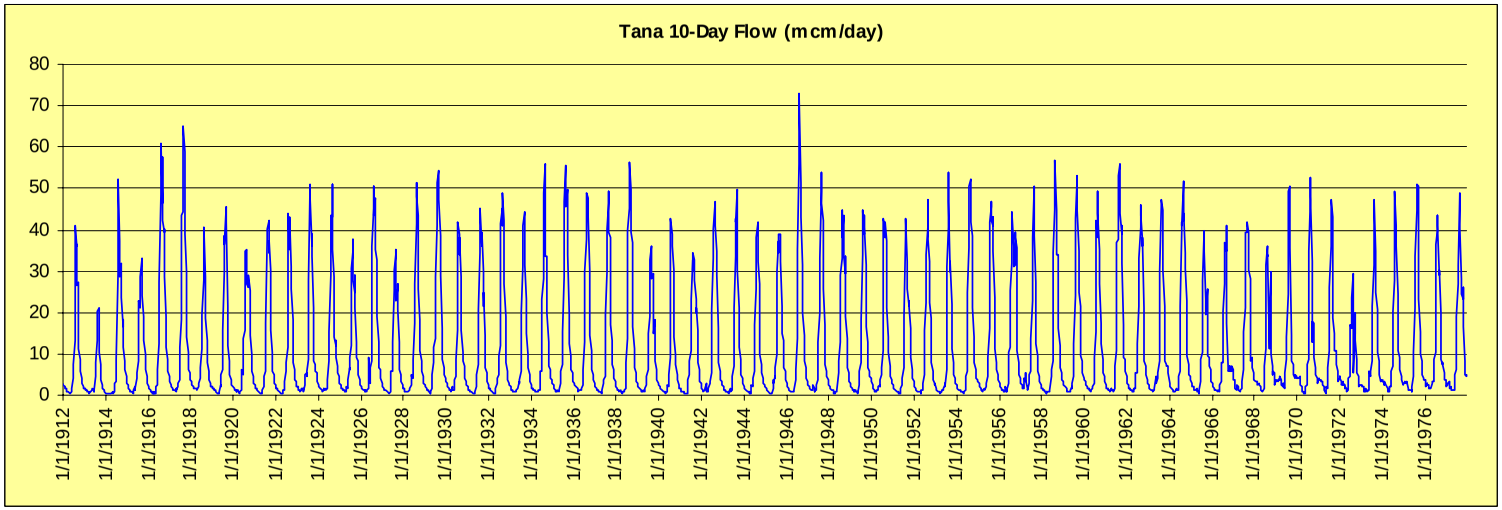
Tana 10-Day Flow (mcm/day)
80
70
60
50
40
30
20
10
0
1/1/1912
1/1/1914
1/1/1916
1/1/1918
1/1/1920
1/1/1922
1/1/1924
1/1/1926
1/1/1928
1/1/1930
1/1/1932
1/1/1934
1/1/1936
1/1/1938
1/1/1940
1/1/1942
1/1/1944
1/1/1946
1/1/1948
1/1/1950
1/1/1952
1/1/1954
1/1/1956
1/1/1958
1/1/1960
1/1/1962
1/1/1964
1/1/1966
1/1/1968
1/1/1970
1/1/1972
1/1/1974
1/1/1976

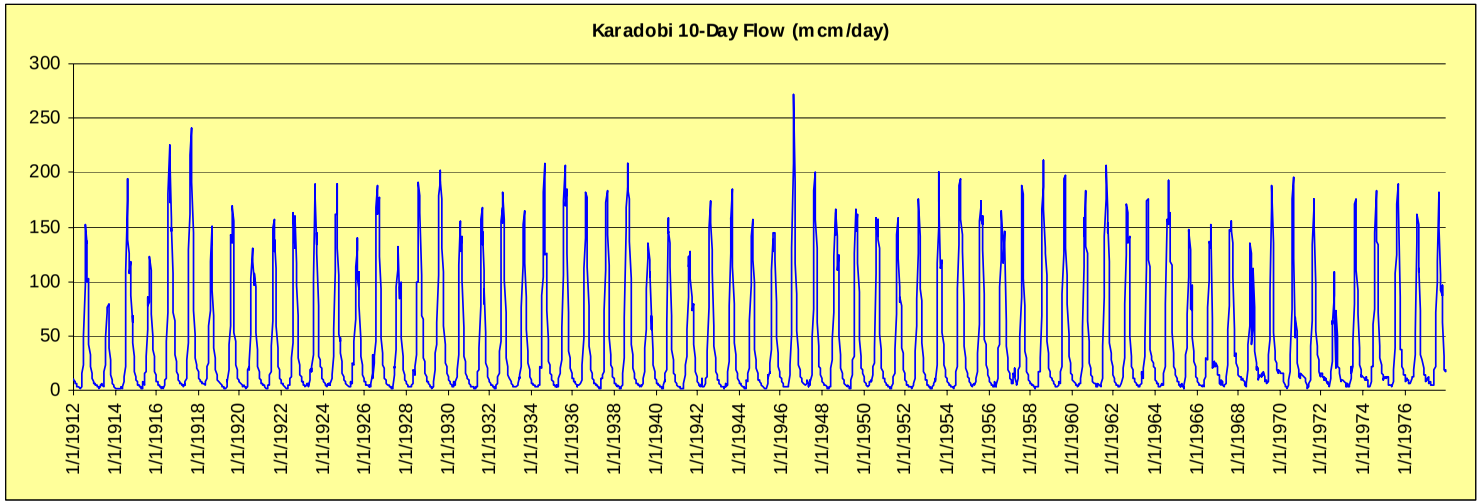
Karadobi 10-Day Flow (mcm/day)
300
250
200
150
100
50
0
1/1/1912
1/1/1914
1/1/1916
1/1/1918
1/1/1920
1/1/1922
1/1/1924
1/1/1926
1/1/1928
1/1/1930
1/1/1932
1/1/1934
1/1/1936
1/1/1938
1/1/1940
1/1/1942
1/1/1944
1/1/1946
1/1/1948
1/1/1950
1/1/1952
1/1/1954
1/1/1956
1/1/1958
1/1/1960
1/1/1962
1/1/1964
1/1/1966
1/1/1968
1/1/1970
1/1/1972
1/1/1974
1/1/1976

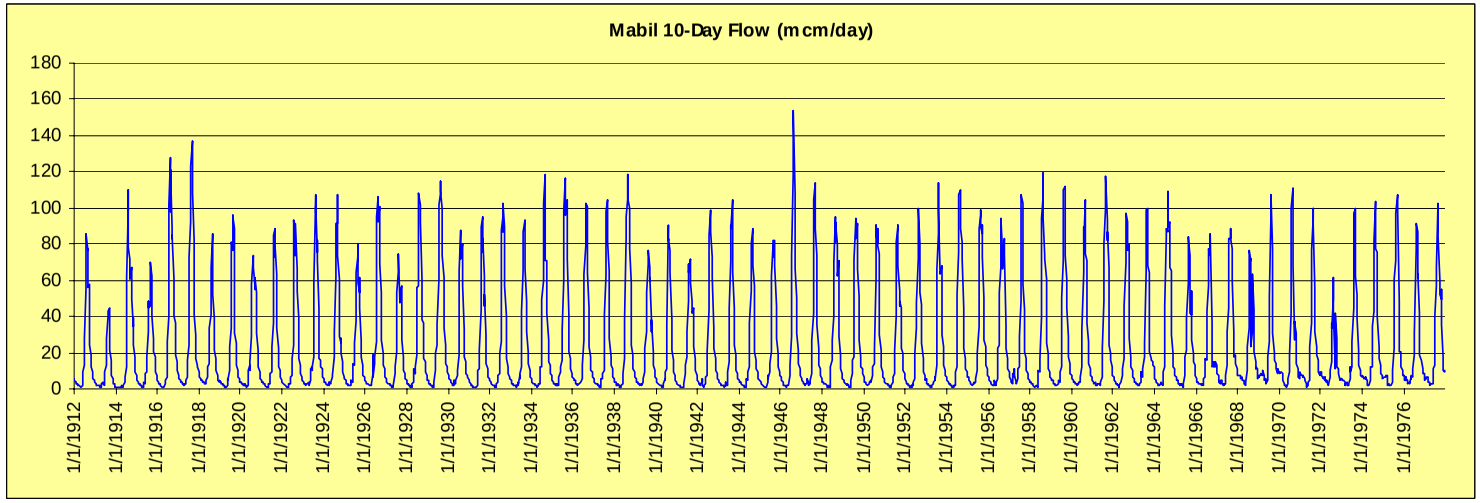
Mabil 10-Day Flow (mcm/day)
180
160
140
120
100
80
60
40
20
0
1/1/1912
1/1/1914
1/1/1916
1/1/1918
1/1/1920
1/1/1922
1/1/1924
1/1/1926
1/1/1928
1/1/1930
1/1/1932
1/1/1934
1/1/1936
1/1/1938
1/1/1940
1/1/1942
1/1/1944
1/1/1946
1/1/1948
1/1/1950
1/1/1952
1/1/1954
1/1/1956
1/1/1958
1/1/1960
1/1/1962
1/1/1964
1/1/1966
1/1/1968
1/1/1970
1/1/1972
1/1/1974
1/1/1976

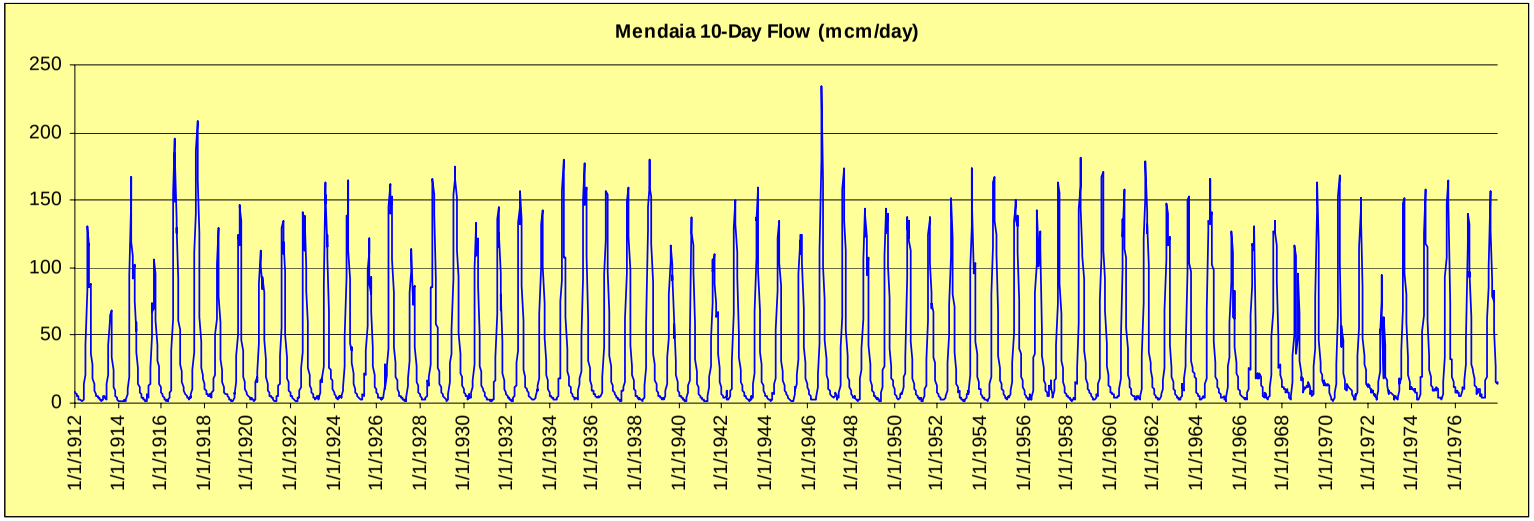
Mendaia 10-Day Flow (mcm/day)
250
200
150
100
50
0
1/1/1912
1/1/1914
1/1/1916
1/1/1918
1/1/1920
1/1/1922
1/1/1924
1/1/1926
1/1/1928
1/1/1930
1/1/1932
1/1/1934
1/1/1936
1/1/1938
1/1/1940
1/1/1942
1/1/1944
1/1/1946
1/1/1948
1/1/1950
1/1/1952
1/1/1954
1/1/1956
1/1/1958
1/1/1960
1/1/1962
1/1/1964
1/1/1966
1/1/1968
1/1/1970
1/1/1972
1/1/1974
1/1/1976

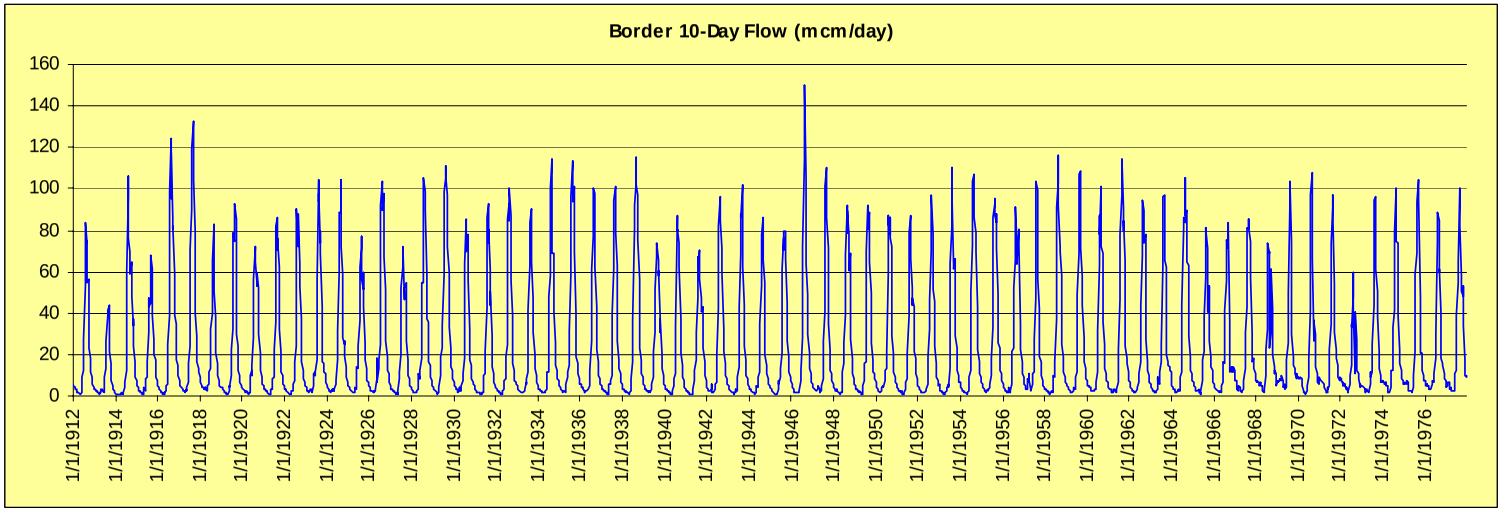
Border 10-Day Flow (mcm/day)
160
140
120
100
80
60
40
20
0
1/1/1912
1/1/1914
1/1/1916
1/1/1918
1/1/1920
1/1/1922
1/1/1924
1/1/1926
1/1/1928
1/1/1930
1/1/1932
1/1/1934
1/1/1936
1/1/1938
1/1/1940
1/1/1942
1/1/1944
1/1/1946
1/1/1948
1/1/1950
1/1/1952
1/1/1954
1/1/1956
1/1/1958
1/1/1960
1/1/1962
1/1/1964
1/1/1966
1/1/1968
1/1/1970
1/1/1972
1/1/1974
1/1/1976

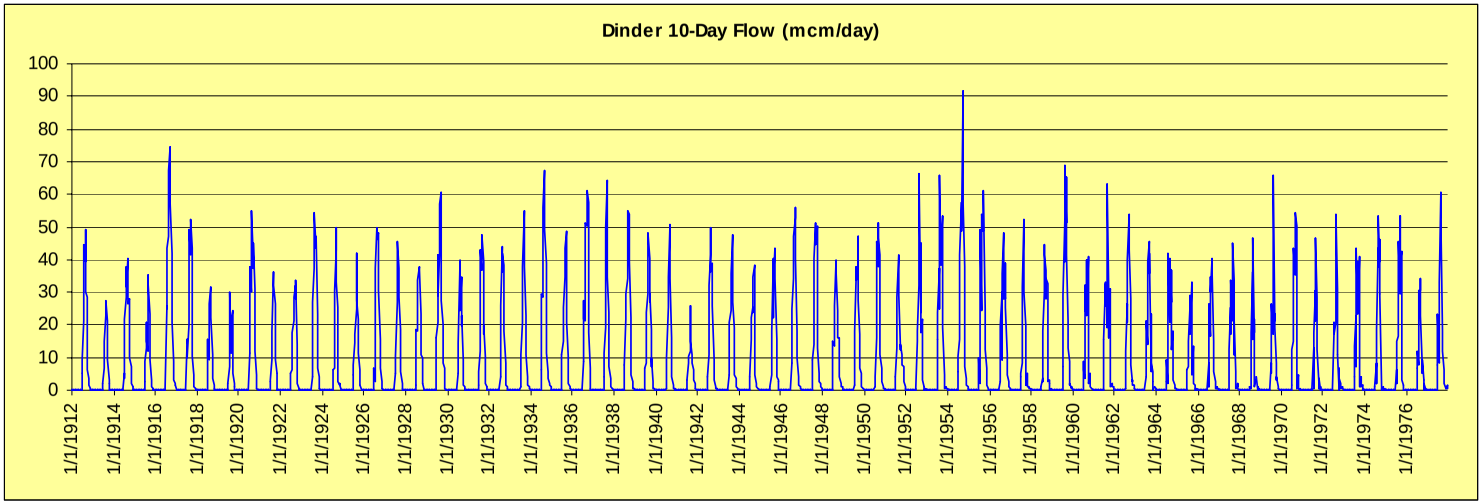
Dinder 10-Day Flow (mcm/day)
100
90
80
70
60
50
40
30
20
10
0
1/1/1912
1/1/1914
1/1/1916
1/1/1918
1/1/1920
1/1/1922
1/1/1924
1/1/1926
1/1/1928
1/1/1930
1/1/1932
1/1/1934
1/1/1936
1/1/1938
1/1/1940
1/1/1942
1/1/1944
1/1/1946
1/1/1948
1/1/1950
1/1/1952
1/1/1954
1/1/1956
1/1/1958
1/1/1960
1/1/1962
1/1/1964
1/1/1966
1/1/1968
1/1/1970
1/1/1972
1/1/1974
1/1/1976

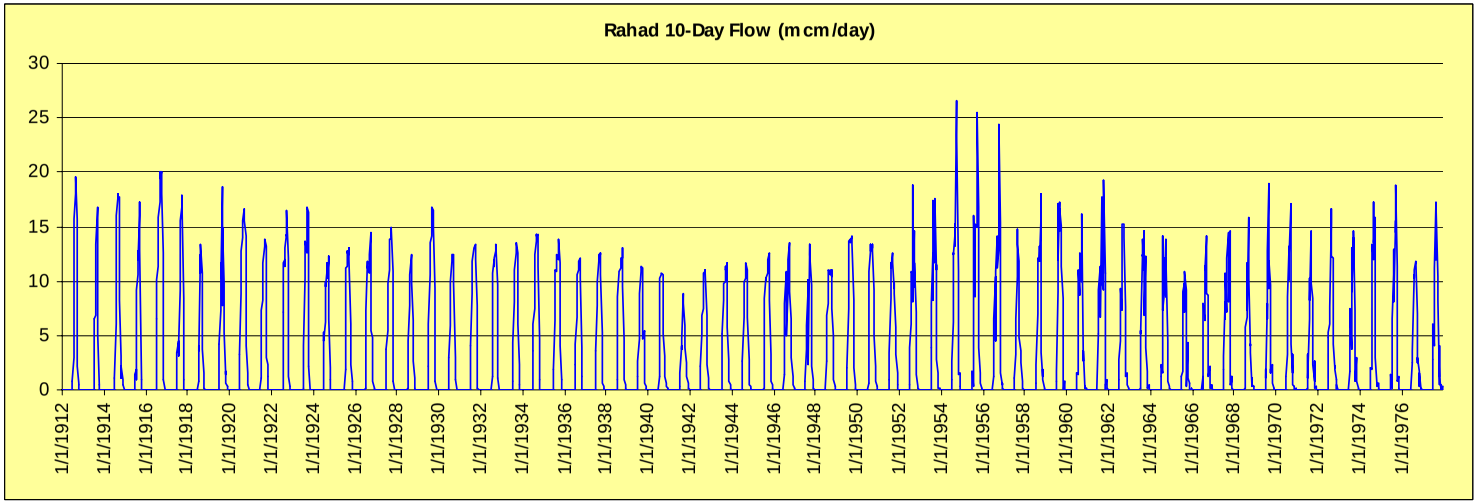
Rahad 10-Day Flow (mcm/day)
30
25
20
15
10
5
0
1/1/1912
1/1/1914
1/1/1916
1/1/1918
1/1/1920
1/1/1922
1/1/1924
1/1/1926
1/1/1928
1/1/1930
1/1/1932
1/1/1934
1/1/1936
1/1/1938
1/1/1940
1/1/1942
1/1/1944
1/1/1946
1/1/1948
1/1/1950
1/1/1952
1/1/1954
1/1/1956
1/1/1958
1/1/1960
1/1/1962
1/1/1964
1/1/1966
1/1/1968
1/1/1970
1/1/1972
1/1/1974
1/1/1976

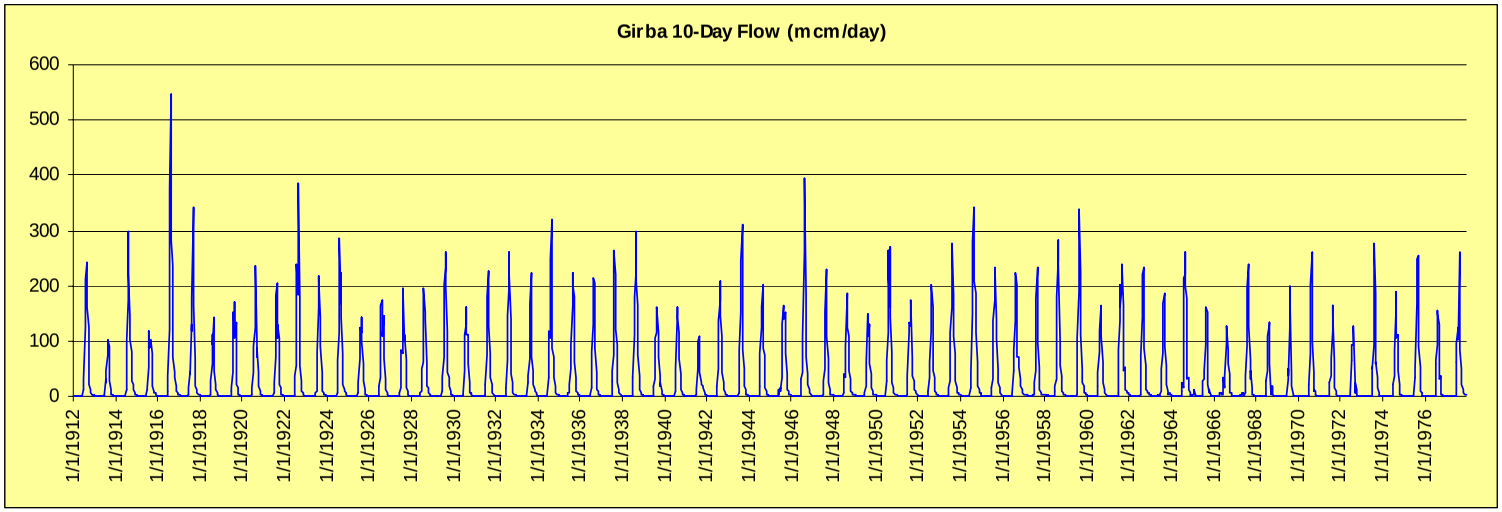
Girba 10-Day Flow (mcm/day)
600
500
400
300
200
100
0
1/1/1912
1/1/1914
1/1/1916
1/1/1918
1/1/1920
1/1/1922
1/1/1924
1/1/1926
1/1/1928
1/1/1930
1/1/1932
1/1/1934
1/1/1936
1/1/1938
1/1/1940
1/1/1942
1/1/1944
1/1/1946
1/1/1948
1/1/1950
1/1/1952
1/1/1954
1/1/1956
1/1/1958
1/1/1960
1/1/1962
1/1/1964
1/1/1966
1/1/1968
1/1/1970
1/1/1972
1/1/1974
1/1/1976

C.3. Annual Historical Average Inflow Sequences

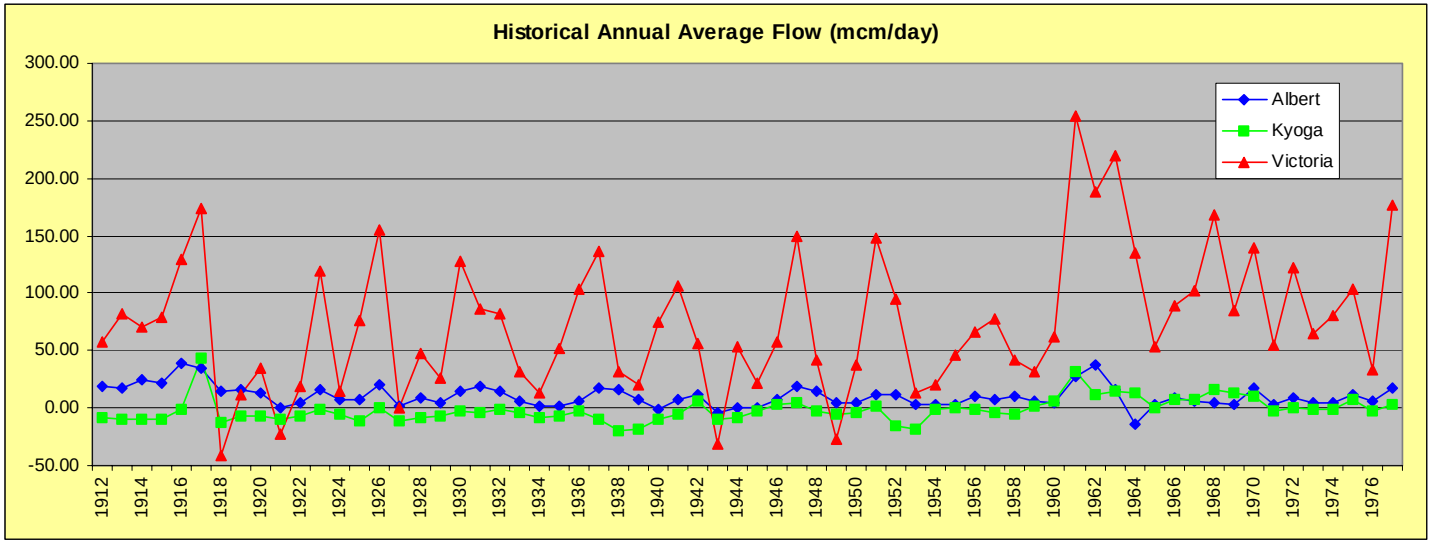

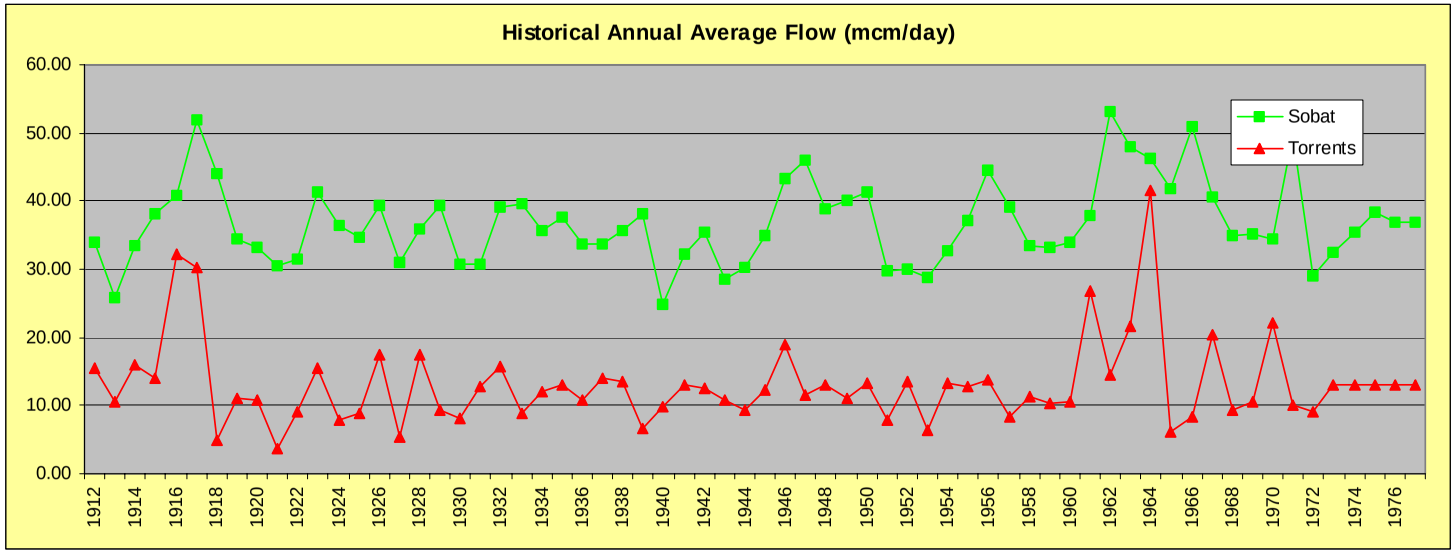
Historical Annual Average Flow (mcm/day)
60.00
50.00
40.00
30.00
20.00
10.00
0.00
1912
1914
1916
1918
1920
1922
1924
1926
1928
1930
1932
1934
1936
1938
1940
1942
1944
1946
1948
1950
1952
1954
1956
1958
1960
1962
1964
1966
1968
1970
1972
1974
1976
Sobat
Torrents

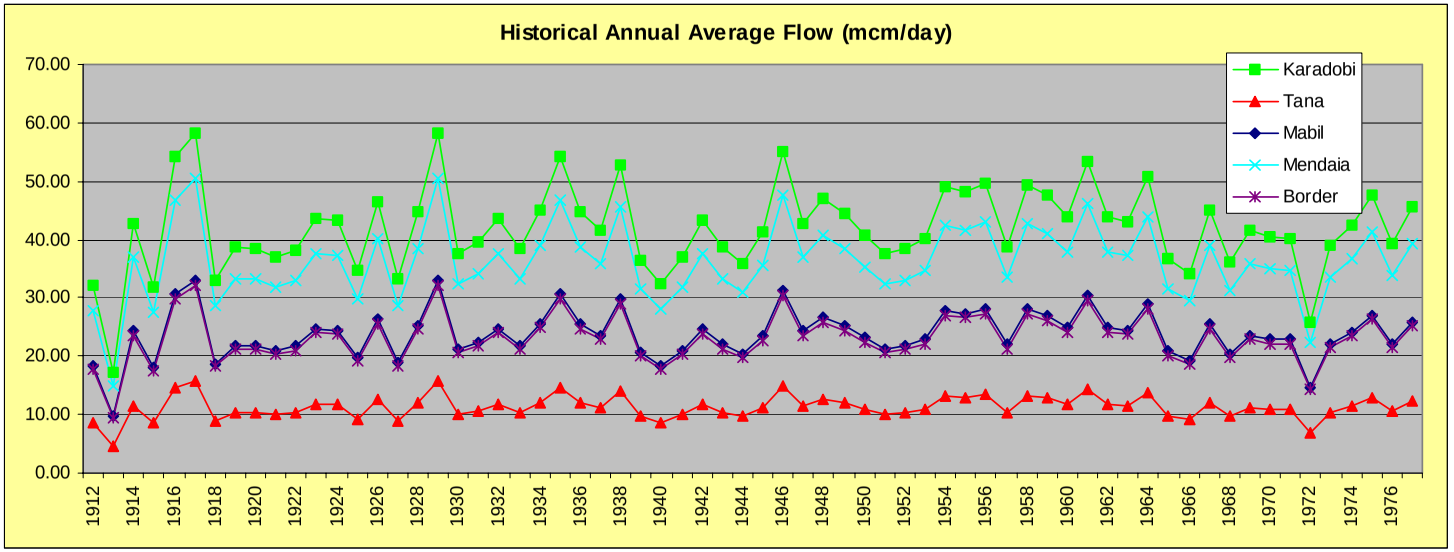
Historical Annual Average Flow (mcm/day)
70.00
60.00
50.00
40.00
30.00
20.00
10.00
0.00
1912
1914
1916
1918
1920
1922
1924
1926
1928
1930
1932
1934
1936
1938
1940
1942
1944
1946
1948
1950
1952
1954
1956
1958
1960
1962
1964
1966
1968
1970
1972
1974
1976
Karadobi
Tana
Mabil
Mendaia
Border

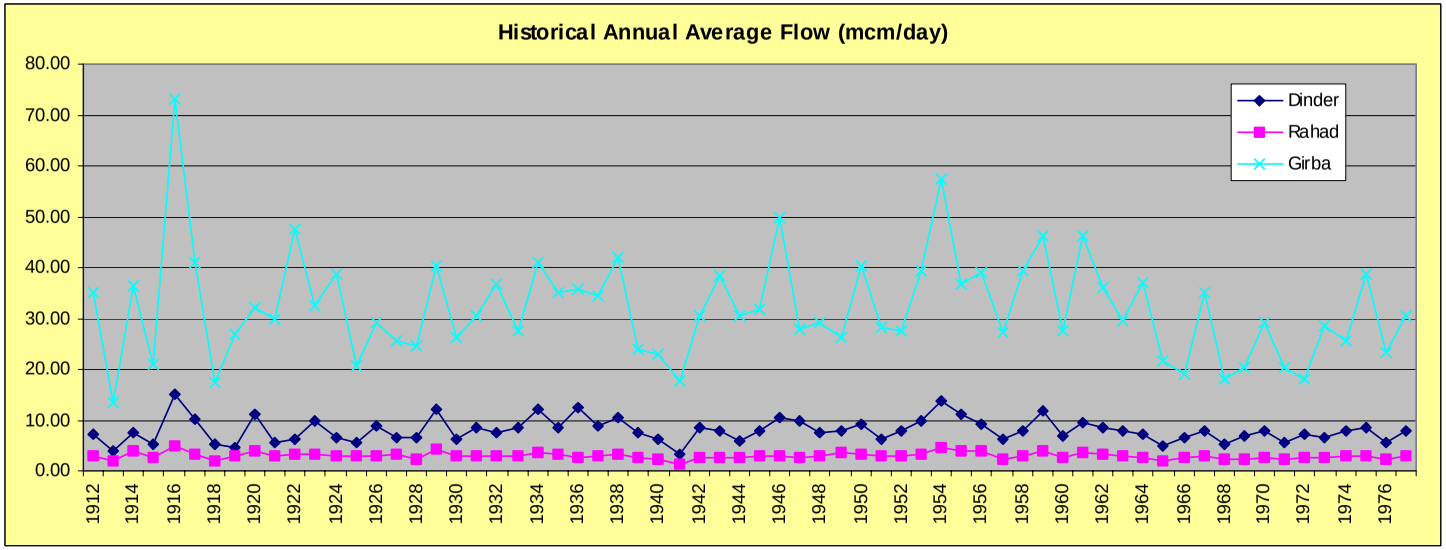
Historical Annual Average Flow (mcm/day)
80.00
70.00
60.00
50.00
40.00
30.00
20.00
10.00
0.00
1912
1914
1916
1918
1920
1922
1924
1926
1928
1930
1932
1934
1936
1938
1940
1942
1944
1946
1948
1950
1952
1954
1956
1958
1960
1962
1964
1966
1968
1970
1972
1974
1976
Dinder
Rahad
Girba

Appendix D

Mathematical Background

D.1. ELQG Control Method

The long range control problem formulated in this report are solved using the Extended Linear Quadratic Gaussian (ELQG) control method which was originally introduced by *Georgakakos and Marks, 1987*, and further developed by *Georgakakos 1989, 1991, 1993, Georgakakos et al., 1995a, Georgakakos and Yao, 1995,* and *Georgakakos et al., 1997a,b,c*. ELQG is an iterative optimization procedure starting from an initial control sequence {**u**(k); k = 0, 1, 2, .., N-1} and subsequently generating increasingly better sequences until convergence. Convergence is achieved when the value of the performance index cannot be reduced any further. ELQG is reliable, computationally efficient, and especially suited for uncertain, multi-reservoir systems. A short account of the ELQG optimization procedure and features follows next.

The optimal control problem includes three elements: system dynamics, constraints, and performance index. These can be expressed in the following general form:

$ System Dynamics:

$$S(k+1) = f\,[\,S(k)\,,\,u(k)\,,\,\xi(k)\,,\,k\,]$$

$$k = 0\,,1\,,\ldots,\,N-1 \quad ,$$

$ Constraints:

$$Prob[\; H_i^{\min}(k) \le H_i(\,S_i(k))\;] \ge \pi_i^{\min}(k)$$

$$Prob[\; H_i(\,S_i(k)) \le H_i^{\max}(k)\;] \ge \pi_i^{\max}(k)$$

$$u_i^{\min}(k) \le u_i(k) \le u_i^{\max}(k) \quad ,$$

$$i \in \textit{reservoirs},\;\; k = 0\,,1\,,\ldots,N\,,$$

These are associated with the system reservoirs and should be expressed in a probabilistic form due to the uncertain system nature.

$ Performance Index:

$$\underset{u(k),\;k=0,1,\ldots,N-1}{\text{Minimize}}\; J = E\left\{\sum_{k=0}^{N-1} g_k\,[\,S(k)\,,\,u(k)\,] + g_N[S(N)]\right\},$$

where **S**(k), **u**(k), and $\boldsymbol{\xi}$(k) are the state, control, and uncertain input vectors defined in Section 5.3, π_i^{min} and π_i^{max} are reliability parameters, g_k is a function including all performance index terms associated with period k, and g_N is a function including terms associated with the terminal time N. (As before, bold type indicates vector or matrix quantities.)

The Extended Linear Quadratic Gaussian (ELQG) solution procedure starts with an initial control sequence $\{ u^0(k) , \quad k = 0, 1, \ldots, N-1 \}$ and the corresponding mean state

$$\bar{S}^0(k+1) = f [\bar{S}^0(k), u^0(k), \bar{\xi}(k), k]$$

$$\bar{S}^0(0) = S(0) = \text{known} \quad ,$$

$$k = 0, 1, \ldots, N-1 \quad ,$$

sequence $\{ \bar{S}^0(k) , \quad k = 0, 1, \ldots, N \}$:

where $\bar{\xi}(k)$ represents the mean of the random processes. The next step is to define a perturbation model valid around these nominal state and control sequences:

$$\Delta S(k) = S(k) - \bar{S}^0(k), \quad k = 0, 1, \ldots, N,$$

$$\Delta u(k) = u(k) - u^0(k), \quad k = 0, 1, \ldots, N-1,$$

$$\Delta \xi(k) = \xi(k) - \bar{\xi}(k), \quad k = 0, 1, \ldots, N-1,$$

This model describes the dynamic relationship of the state, control, and input vector perturbations, and has the following form:

$$\Delta S(k+1) = A(k) \ \Delta S(k) + B(k) \ \Delta u(k) + C(k) \ \Delta \xi(k) \ ,$$

$$\Delta S(0) = 0 \ ,$$

$$k = 0, 1, \ldots, N-1 \ ,$$

where the matrices **A**(k), **B**(k), and **C**(k) represent the gradient matrices of the state transition function with respect to the state, control, and input vectors respectively:

$$A(k) = \nabla_{S(k)}\ f(k) = \begin{bmatrix} \frac{df_1(k)}{dS(k)} \\ \frac{df_2(k)}{dS(k)} \\ \vdots \\ \frac{df_{10}(k)}{dS(k)} \end{bmatrix}, B(k) = \nabla_{u(k)}\ f(k) = \begin{bmatrix} \frac{df_1(k)}{du(k)} \\ \frac{df_2(k)}{du(k)} \\ \vdots \\ \frac{df_{10}(k)}{du(k)} \end{bmatrix}, C(k) = \nabla_{\xi(k)}\ f(k) = \begin{bmatrix} \frac{df_1(k)}{d\xi(k)} \\ \frac{df_2(k)}{d\xi(k)} \\ \vdots \\ \frac{df_{10}(k)}{d\xi(k)} \end{bmatrix} .$$

The performance index is also expressed in terms of the perturbation variables as follows:

$$J = E\ \{\sum_{k=0}^{N1} [\ \frac{1}{2}\ \ \Delta S^T(k)\ \ Q_{SS}(k)\ \ \Delta S(k) + q_S{}^T(k)\ \ \Delta S(k)$$

$$+\ \frac{1}{2}\ \ \Delta u^T(k)\ \ R_{uu}(k)\ \ \Delta u(k) + r_u{}^T(k)\ \ \Delta u(k) + \Delta u^T(k)\ \ Q_{uS}(k)\ \ \Delta S(k)\ ]$$

$$+\ \frac{1}{2}\ \ \Delta S^T(N)\ \ Q_{SS}(N)\ \ \Delta S(N) + q_S{}^T(N)\ \ \Delta S(N)\ \}\ \ ,$$

where $\mathbf{Q}_{ss}(k)$, $\mathbf{q}_s(k)$, $\mathbf{R}_{uu}(k)$, $\mathbf{r}_u(k)$, $\mathbf{Q}_{us}(k)$ are coefficient matrices defining a quadratic approximation of the original performance index. These matrices include the first and second partial derivatives of the $g_k[\ ]$ and $g_N[\ ]$ functions with respect to the state and control variables evaluated at the nominal sequences.

The perturbation control problem defined above is next solved to generate an optimal control sequence $\{\Delta\mathbf{u}^*(k), k=0,1, ..., N-1\}$. This constitutes the optimization direction which defines the new nominal control sequence according to the following relationship:

$$u^{new}(k) = u^0(k) + \alpha\ \ \Delta u^*(k)\ \ ,$$

$$k = 0, 1, \ldots, N-1\ ,$$

where α is the optimization step size. Some important features of the ELQG solution process are summarized below:

$ The ELQG iterations are (**1**) analytically-based (the optimization directions are obtained by Riccati-like equations), (**2**) reliable (the iteration process is guaranteed to converge if the problem has a feasible solution), and (**3**) computationally efficient (convergence is fast). In fact, in the neighborhood of the optimum, it can be theoretically shown that the method converges at a quadratic rate.

$ Control constraints are not included in the performance index as penalty terms but are handled *explicitly* through a Projected-Newton procedure. This has important computational efficiency implications as it allows for many constraints to enter or exit the binding control set at the same iteration. The optimization direction is then obtained in the space of the binding constraints.

One last complication is that in order to compute the control gains {D(k), L(k), Λ(k), k=0,1,...,N} one must already have the storage probability distribution. This, however, is resolved by adopting an iterative approach. Namely, the algorithm is first initiated with the Gaussian approximation approach described above, and a set of control gains is computed. Then, the storage traces are generated, and the process is repeated. Based on our experience, in two to three iterations, the probability distributions converge to their true forms and the procedure can terminate.

$ State (or, equivalently, elevation) constraints are handled through the barrier penalty functions discussed in the previous section. This approach has proven to be reliable and computationally efficient. Handling of the state constraints requires the characterization of the state probability density. A two-phase process is used for the state density computation. In the first phase, this density is approximated by its mean and covariance vector, respectively obtained by:

$$P_S(k+1) = F(k)\ \ P_S(k)\ F^T(k) + C(k)\, P_\xi(k)\ C^T(k)\ \ ,$$

$$F(k) = A(k) - B(k)\ \ D(k)\ \ L(k)\ \ ,$$

$$k = 0, 1, \ldots, N-1\ \ ,$$

where $\mathbf{P}_S(k)$ and $\mathbf{P}_\xi(k)$ are the state and input covariance matrices and {$\mathbf{D}(k)$, $\mathbf{L}(k)$, k=0,1,...,N-1} are control gains generated by the ELQG solution process. These gains represent a linear approximation of the true feedback laws and are used in the covariance computation to indicate that future decisions will take into consideration measurements of reservoir storage (feedback). The state mean and covariance are then used to construct a normal approximation of the state probability density and convert constraints into deterministic equivalents on the elevation mean:

$$Prob[\ H_i^{\min}(k) \le H_i(S_i(k))\ ] = \pi_i^{\min}(k)\ \ ,$$

$$Prob[\ H_i(S_i(k)) \le H_i^{\max}(k)\ ] = \pi_i^{\max}(k)\ \ ,$$

$$i \in reservoirs\ ,\ \ k = 0, 1, \ldots, N\ \ .$$

$$\Phi_i^{\min}(k) \le \overline{H}_i(S_i(k)) \le \Phi_i^{\max}(k)\ \ ,$$

$$i \in reservoirs,\ \ k = 0, 1, \ldots, N\ \ ,$$

where $\{\Phi_i^{\min}\ \ ,\ \ \Phi_i^{\max}\}$ are the mean reservoir elevations such that

After the convergence of the first step, the generated control law is then applied to each inflow trace to generate the corresponding storage trace. With the generated storage traces, the probabilistic characteristics of the state variable are fully defined. The constraints and are updated. The second phase starts using the recalculated constraints until convergence.

The ELQG iterations continue until the value of the performance index can not be reduced any further. At this point the process terminates, and the current nominal control sequence becomes the problem solution. Under convexity conditions (which are valid in this formulation), this solution is globally optimal. (Convexity can be tested by starting the

optimization process from different initial control sequences and verifying that the process converges at the same optimal sequence.)

As mentioned earlier, the control model is applied sequentially, where only the first element of the control sequence is actually applied. The system is then monitored, the new values of the state variables are recorded, and the optimization cycle is repeated at the beginning of the next (decadal) time period. In this way, the model always uses the most updated information regarding the system and continually Atunes@ its optimal policies to the current needs and conditions.

More details on the ELQG features can be found in the above-cited references.

D.2. Artificial Neural Networks

D.2.1. Background

An Artificial Neural Network (ANN) is a group of processing elements called nodes arranged in layers - where each layer receives input from the layer below, makes independent computations, and passes its output to the layer above. In this structure, the very first layer is the input layer and the last is the output layer.

Different layouts and configurations of neural networks have been constructed for solving particular problems (Rumelhart, 1986). However, the layered feedforward network (Figure 2-1) is most general and easy to implement. In this configuration, information is passed only between the nodes of two adjacent layers, as it propagates from the bottom to the top.

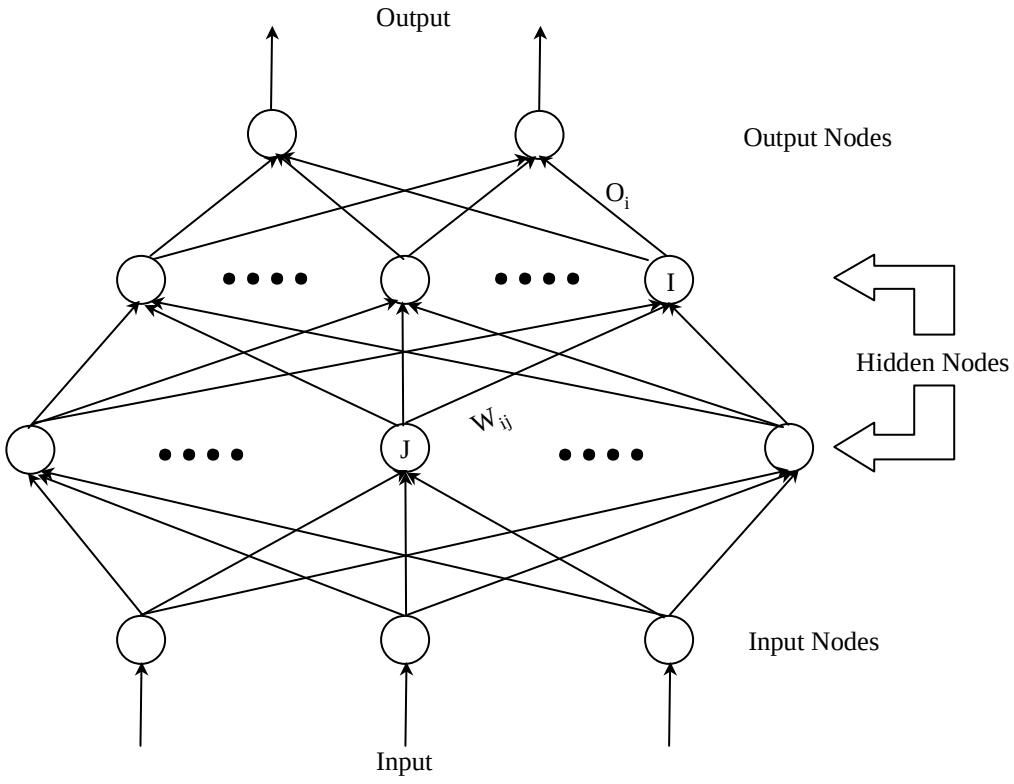

Figure 2-1: Multilayer Feedforward Network

Basic elements of ANN are the nodes (also called processing units) and the arcs. Each arc is assigned a real number called weight (W_{ij}). This weight W_{ij} specifies the strength of information that node i receives from node j. Each node receives information from the other nodes of the layer below (or in the form of data input if it is part of the input layer) and produces an output after passing all its inputs through an activation function associated with it. A node of the input layer is called an input node, while a node of the output layer is called an output node. The layers and nodes between the input and output layers are called hidden layers and nodes. Figure 2-2 shows the basic elements of a node.

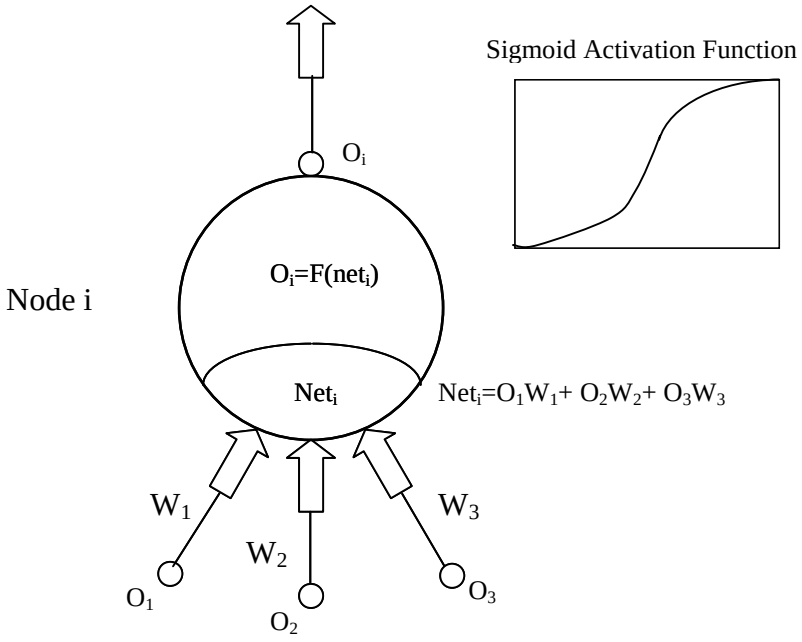

Figure 2-2: Basic elements of Node i

The ANN used in this work is structured as shown in the previous figures except that the output layer includes only one output node.

D.2.2. The Training Process and the Weight Updating Rule

A network with fixed weights and activation functions determines a relationship between inputs and outputs. This relationship can be simple or complicated depending on the network structure and the activation function forms. For a layered feedforward network, the activation functions play a crucial role in identifying the correct relations. Usually, the sigmoidal function is selected as the activation function. Sigmoidal functions are those with limits 1 at positive infinity and 0 at negative infinity. Jones (1990) demonstrated the existence of uniform approximations of any continuous function using continuous sigmoidal functions. Some other functions such as the hard limited, threshold logic, and sigma-pi have also been used successfully in other fields.

After selecting the structure of the neural network, the next step is to determine the weights such that the network can best re-construct the relationship of input and output. In practice, the best weights are obtained based on the observed input and output data pairs through an estimation process called "training". The training process begins with some initial weight estimates that are used to produce an output for certain inputs. This output is subsequently compared with the desired output of the training data set and the weights are adjusted to minimize the discrepancy. This procedure is repeated many times until weight convergence, and it can be fast or slow depending on the method used for weight adjustment after each iteration. Many weight updating rules have been proposed (Ho, 1992; Rumelhart, 1986; Parker, 1986). In this work, we experimented with several rules including a Gaussian-Newton method, and the Delta Rule. The Delta Rule was implemented in two versions, one updating the weights after presenting all training data pairs, and a second updating the weights after presenting each input-output pair. Among all updating rules, the Delta Rule with weight updating after each input-output pair proved to be the most efficient with respect to convergence rate and computational time required for our applications.

The Delta Rule essentially implements a gradient descent parameter estimation procedure. The objective function for the training process is

$$E = \frac{1}{2} \min \sum_{p}^{N} \sum_{j}^{M} \left(t_{pj} - O_{pj} \right)^2 , \qquad (2\text{-}1)$$

where N is the number of training data pairs, M is the output node number, t_{pj} is the desired value of the j^{th} output node for input pattern p, and O_{pj} is the j^{th} element of the actual output associated with input p. Every node, except the input nodes on the first layer, receives data from the nodes of the previous layers. The total input of node j is called the net of node j and is denoted by net_{pj}:

$$net_{pj} = \sum_i W_{ji} O_{pi} \tag{2-2}$$

where W_{ji} is node j's weight of the node i input. Thus, the output of node j is given by

$$O_{pj} = f_j\left(net_{pj}\right) = \frac{1}{1 + e^{-\left(\sum_i W_{ji} O_{pi} + \theta_j\right)}} \tag{2-3}$$

where θ_j is the coefficient of the sigmoidal function.

The weight adjustment is based on the Delta Rule after presenting each data pair, and it is given by

$$\Delta_p W_{ji} = \eta \delta_{pj} O_{pi} \tag{2-4}$$

where η is called the learning rate, taking values between 0 and 1, and δ_{pj} is called the error term of node j given by

$$\delta_{pj} = \begin{bmatrix} \left(t_{pj} - O_{pj}\right) f_j'\left(net_{pj}\right) & if \quad j \quad is \quad an \quad output \quad node \\ f_j'\left(net_{pj}\right) \sum_k \delta_{pk} W_{kj} & otherwise \end{bmatrix} \tag{2-5}$$

For presentational completeness, the derivation of the Delta Rule is included below (Ho, 1992; Rumelhart, 1986; Parker, 1986).

Let the measure of the error on input/output pattern p be

$$E_p = \frac{1}{2}\sum_j \left(t_{pj} - o_{pj}\right)^2 \tag{2-6}$$

and let

$$E = \sum_N E_p \tag{2-7}$$

be the overall measure of the error. We first show that the Delta Rule implements a gradient decent in E when the nodes are linear. We will proceed by simply showing that

$$-\frac{\partial E_p}{\partial W_{ji}} = \delta_{pj} i_{pi} \tag{2-8}$$

is proportional to $\Delta_p W_{ji}$. When there are no hidden nodes it is straightforward to compute the relevant derivative. For this purpose we use the chain rule to write the derivatives as the product of two parts: the derivative of the error with respect to the output of the unit ties the derivative of the output with respect to the weight.

$$\frac{\partial E_p}{\partial W_{ji}} = \frac{\partial E_p}{\partial o_{pj}} \frac{\partial o_{pj}}{\partial W_{ji}} \tag{2-9}$$

The first part shows how the error changes with the output of the j^{th} node and the second part indicates how much W_{ji} changes that output. The derivatives are computed as follows.

$$\frac{\partial E_p}{\partial o_{pj}} = -\left(t_{pj} - o_{pj}\right) = -\delta_{pj} \tag{2-10}$$

The contribution of node j to the error is simply proportional to δ_{pj}. Since we have linear units,

$$o_{pj} = \sum_i W_{ji} i_{pi} \tag{2-11}$$

from which we have

$$\frac{\partial o_{pj}}{\partial W_{ji}} = i_{pi} \tag{2-12}$$

Thus,

$$-\frac{\partial E_p}{\partial W_{ji}} = \delta_{pj} i_{pi} \tag{2-13}$$

Now, combining this with the observation that

$$\frac{\partial E}{\partial W_{ji}} = \sum_p \frac{\partial E_p}{\partial W_{ji}} \tag{2-14}$$

leads us to conclude that the net change in W_{ji} after one complete cycle of pattern presentations is proportional to this derivative and hence that the Delta Rule implements a gradient descent in E. Actually, this is strictly true only if the values of the weights are not changed during this cycle. By changing the weights after each pattern is presented we depart to some extent from a true gradient descent in E. Nevertheless, provided the learning rate is sufficiently small, this departure will be negligible and the Delta Rule will implement a very close approximation to a gradient descent in E.

For layered feedforward network, a generalized Delta Rule can be derived. The derivation is given below:

To get the correct generalization of the Delta Rule, we must set

$$\Delta_p W_{ji} \propto -\frac{\partial \mathrm{E}_p}{\partial W_{ji}} \tag{2-15}$$

where E is the same sum-squared error function defined earlier. Using the chain rule, we have

$$\frac{\partial E_p}{\partial W_{ji}} = \frac{\partial E_p}{\partial net_{pj}} \frac{\partial net_{pj}}{\partial W_{ji}} \tag{2-16}$$

The second factor is

$$\frac{\partial net_{pj}}{\partial W_{ji}} = o_{pi} \tag{2-17}$$

Now, let us define

$$\delta_{pj} = -\frac{\partial E_p}{\partial net_{pj}} \tag{2-18}$$

Then, to implement a gradient descent in E weight changes should be performed according to

$$\Delta_p W_{ji} = \eta \delta_{pj} o_{pi} \tag{2-19}$$

just as in the standard Delta Rule. The issue is to figure out what δ_{pj} should be for each node in the network. The interesting result is that there is a simple recursive computation of these δ's which can be implemented by propagating error signals backward to the network. Using the chain rule, we have

$$\delta_{pj} = -\frac{\partial E_p}{\partial net_{pj}} = -\frac{\partial E_p}{\partial o_{pj}} \frac{\partial o_{pj}}{\partial net_{pj}} \tag{2-20}$$

The second factor is given by

$$\frac{\partial o_{pj}}{\partial net_{pj}} = f_j^{/}\left(net_{pj}\right) \tag{2-21}$$

which is simply the derivative of the activation function f_j for the j^{th} unit (node), evaluated at the net input net_{pj} to that unit.

To compute the first factor, we consider two cases. First, assume that node j is an output unit. In this case, it follows the definition of E_p that

$$\frac{\partial E_p}{\partial o_{pj}} = -\left(t_{pj} - o_{pj}\right) \tag{2-22}$$

which is the same result as the one obtained with the standard Delta Rule. Substituting for the two factors in Equation (2-20), we have

$$\delta_{pj} = \left(t_{pj} - o_{pj}\right) f_j^{/}\left(net_{pj}\right) \tag{2-23}$$

for any output node j. If a node j is not an output node we use the chain rule to write

$$\sum_k \frac{\partial E_p}{\partial net_{pk}} \frac{\partial net_{pk}}{\partial o_{pj}} = \sum_k \frac{\partial E_p}{\partial net_{pk}} \frac{\partial}{\partial o_{pj}} \sum_i W_{ki} o_{pi} = \sum_k \frac{\partial E_p}{\partial net_{pk}} W_{kj} = -\sum_k \delta_{pk} W_{kj} \tag{2-24}$$

In this case, substituting for the two factors in Equation (2-20) yields

$$\delta_{pj} = f_j^{/}\left(net_{pj}\right) \sum_k \delta_{pk} W_{kj} \tag{2-25}$$

whenever node j is not an output unit. Equation (2-23) and (2-25) give a recursive procedure for computing the δ's for all nodes in the network, which are then used to compute the weight changes. This procedure constitutes the generalized Delta Rule for a feedforward network.

The learning process involves two phases: during the first phase, the input is presented and propagated forward through the network to compute the output value O_{pj}. This output is then compared with the desired value t_{pj}, resulting in the error δ_{pj} for each output node. The second phase involves a backward pass through the network during which the error is passed to each node and the appropriate weight changes are made.

The above weight updating rule is the generalized Delta Rule for the multilayer feedforward network. The larger the learning rate, the larger the changes of the weights. One should select a constant as large as possible without causing oscillations during the training process. Several papers (Ho et al, 1992; Rumelhart, 1986; Tollenaere, 1990) include discussions on selecting this constant. However, the conclusions are quite diverse. There is no one unique number applicable to all cases. Instead, one should try different numbers between 0 and 1 and select the one that performs best.

There are many ways to improve the learning process. One such way that avoids oscillations is to incorporate a momentum term in the Delta Rule, i.e.

$$\Delta W_{ji}(n+1) = \eta \delta_{pj} O_{pi} + \alpha \Delta W_{ji}(n) \tag{2-26}$$

where n is the iteration index, and α is a constant reflecting the effect of the past weight changes on the current direction in the weight space. Though this approach helps to improve the convergence rate of the learning procedure, it creates new problems. The question is how to select the value of α and what should be the best combination of the two constants η and α. Regarding the adjustment of α, in the case study we use an adaptive learning algorithm proposed by Ho et al (1992). According to this algorithm, the constant α is modified after each iteration based on

$$\alpha(n+1) = \begin{cases} 1.01\alpha(n), & \Delta E_n \rangle 0 \\ 0.99\alpha(n), & otherwise \end{cases} \tag{2-27}$$

where $\alpha(n)$ is the momentum constant at iteration n, and $\Delta E_n = E(n-1) - E(n)$ with E(n) being the objective value at the n^{th} iteration.

The activation function used for each node is shown by equation (2-3) where θ_j is a bias to be learned just like the other weights. The sigmoidal function is continuous and differentiable everywhere. Then, it is easy to show that the error term in the Delta rule is given by

$$\delta_{pj} = \begin{bmatrix} (t_{pj} - O_{pj}) O_{pj}(1 - O_{pj}) & if \quad j \quad is \quad an \quad output \quad node \\ O_{pj}(1 - O_{pj}) \sum_k \delta_{pk} W_{kj} & otherwise \end{bmatrix} \tag{2-28}$$

One should note that the output range of the function is between zero and one. However, time series values are not necessarily within this range. Thus, to utilize this function, appropriate data preprocessing is required. To satisfy the requirement, we first normalize the data by subtracting their mean and dividing by the standard deviation. Then, we use the following linear transformation to bring them into the zero-one range:

$$Q' = A * \frac{Q_{\max} - Q}{Q_{\max} - Q_{\min}} + B * \frac{Q - Q_{\min}}{Q_{\max} - Q_{\min}} \tag{2-29}$$

The above expression is a general linear transformation in which Q is the original value, Q' is the transformed value, Q_{max}, Q_{min} are the maximum and minimum values of the entire series, and A and B are the lower and upper bounds after the transformation. It should be noted that the activation function cannot take the values 1 and 0 without infinitely large weights, implying that the network will never produce Q_{max} and Q_{min}. One way to resolve this problem is to let A be higher than 0 and B lower than 1.

Appendix E

Operating Rules for Reservoirs in Sudan and Ethiopia

E.1. Operating Rules for Roseires

- The first filling starts frm June 20 every year if the U.S. level is less than 467 meter meters;
- The second filling starts between September 1-26 every year according to the flood case, and the filling is done in 45 days to level 480 meters, which is equivalent to storage of 3 billion cubic meters

E.2. Operating Rules for Roseires

- The filling of the reservoir is done is two periods;
- The first filling to level 417.20, and it starts on June 25 every year. The reservoir must reach 417.20 meters in the first half of July;
- The second filling starts with Roseires between September 1 to 26 every year and lasts for 45 days

E.3. Operating Rules for Khashm El Girba

- The filling is done in two stages;
- The first filling is to level 462 meters and is done is July;
- The second filling is to level 473 and it starts after the flood period and the filling is done in September or in the first days of October according to the inflow of Atbara river. The corresponding storage is 1.3 billion cubic meters.

E.4. The Release Rules used in the simulation for the Ethiopia Reservoirs

Tana		Karadobi		Mabil	
Elevation (m)	Discharge (m^3/s)	Elevation (m)	Discharge (m^3/s)	Elevation (m)	Discharge (m^3/s)
1783.5	0	1041	0	837.00	0
1784.5	40	1051	60	847.00	120
1785	56	1061	129	857.00	220
1785.5	80	1071	175	867.00	350
1786	107	1081	220	877.00	540
1786.5	132	1091	268	887.00	780
1787	165	1101	320	897.00	1130
1787.5	204	1111	387	910.40	1750
1788	260	1121	480	917.00	2190
1788.5	397	1131	580		
		1141	724		
		1151	851		
		1161	1014		
Mendaia		Border			
Elevation (m)	Discharge (m^3/s)	Elevation (m)	Discharge (m^3/s)		
724	0	563	0		
727	110	565	310		
730	260	567	910		
733	520	569	1780		
736	930	571	2840		
739	1680	573	4350		
742	2960	575	6110		
745	5290				